Chapter 1

THESIS INTRODUCTION AND AIMS

This research aimed to undertake a multipurpose seismic study of the Amery Ice Shelf (AIS), East Antarctica within the general region 68-74°S 66-74°E, with the goal of expanding glaciological knowledge and measurements of the structure of the AIS. The research was funded under the Australian Antarctic Division (AAD) ASAC Project 2581 as part of a large umbrella project investigating the AIS under the AAD's Ice Ocean Atmosphere and Climate programme. The overall aim of this programme is to answer the question "What is the role of the Antarctic cryosphere in the global climate system and sea level change?".

As the largest ice shelf in East Antarctica, and one of the largest glacier drainage basins in the world (Allison, 2003), the AIS provides a highly suitable research area to investigate the extent to which the Antarctic ice sheet and individual drainage basins are in balance with the present climate; and also whether, and over what time scale, global warming might lead to irreversible change in the ice sheet-ice shelf systems.

1.1 The Amery Ice Shelf

The AIS (Figure 1.1) is the third largest embayed shelf in Antarctica, and the largest in East Antarctica, having a total surface area of ~60,000 km² (Galton-Fenzi et al., 2008). It drains approximately 16% of the grounded Antarctic ice sheet from the interior of the Lambert Glacier drainage basin, through the Lambert Glacier and other tributary glaciers (Allison, 1979; Allison, 2003). The valley formed by the Lambert Glacier opens out north of the Mawson Escarpment into the AIS, which then extends for approximately 550 km north from its grounding zone.

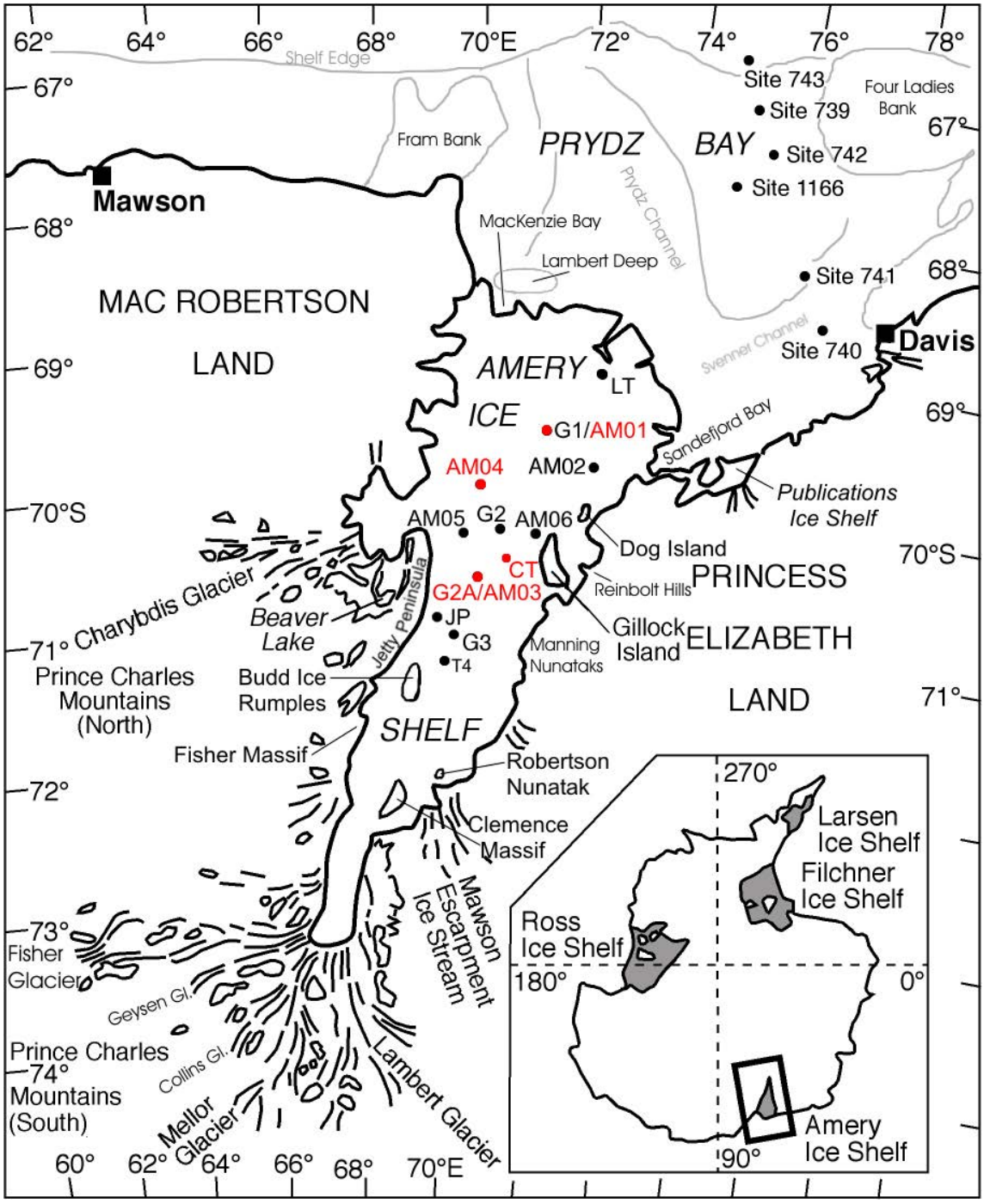

Figure 1.1 – A location map of the Amery Ice Shelf, including the main tributary glaciers, surrounding rock formations, and other sites of interest to this study. (Gl.= Glacier). Red text denotes major seismic sites related to this thesis. Inset: Map of Antarctica showing the location of the major ice shelves.

The AIS is bounded in the west by the Prince Charles Mountains (PCMs) – which can be subdivided into two main groups, the North PCMs and South PCMs – and the Jetty Peninsula including Beaver Lake (an ice-free area where a small branch of the Charybdis Glacier flows south into a valley ending in the lake), with the western ice shelf front sitting in MacKenzie Bay at ~68.5°S. To the east, the AIS is bounded by the Mawson Escarpment, Manning Nunataks and Reinbolt Hills, ending in Sandefjord Bay at ~69.5°S. Compared to the other major ice shelves in Antarctica, such as the Ross Ice Shelf and the Filchner Ice Shelf, the AIS is relatively narrow with an ice shelf front only ~200 km wide.

Meteoric ice is fed into the AIS via four major ice streams: the Lambert, Fisher, and Mellor Glaciers in the south and the Charybdis Glacier in the west. Other smaller glacial additions include the Scylla Glacier adjacent to the Charybdis, and the Geysen and Collins Glaciers in the southern catchment area (Treverrow et al., 2010). Smaller streams also supply ice to the shelf from the east, including the Mawson Escarpment Ice Stream which is formed by over eleven smaller glaciers entering the AIS from the Mawson Escarpment. This meteoric ice sourced from the southern entrances to the AIS equates to an ice thickness of ~2,500 m (Fricker et al., 2000; Galton-Fenzi et al., 2008). As the floating ice travels downstream (northwards) to Prydz Bay, some meteoric ice is added at the surface due to the compaction of accumulated snow, and some ice is also removed as it melts from the base of the shelf. Even with accretion of marine ice at the base of the shelf (frozen saline cavity water), by the time the shelf has reached its northern-most point basal melting and spreading of the shelf has caused the total ice shelf thickness to be reduced from ~2,500 m to ~400 m.

1.2 The seismic technique

Shallow refraction surveys were used on the AIS to model the snow-firn-ice transition and ice fabric properties in the top few hundred metres of the ice shelf, while reflection surveys were employed to gain information to a greater depth – total ice thickness, meteoric and marine ice boundaries, intra-ocean boundaries, sedimentary structure and seafloor depths. These reflection surveys were carried out using the common depth

point (CDP) stacking method, with a fold coverage maximum of six. This method resulted in detailed seismic profiles imaging through the entire ice shelf-ocean water-seafloor system.

1.3 Why study the AIS using the seismic technique?

Prior to the seismic project discussed in this thesis, during the 1970s the Soviet Antarctic Expedition (SAE) collected the only other seismic data in the AIS area. The available output of these data is a collection of depths to the base of ice and to the ocean floor for a number of locations across the AIS, with very few in the southern area of the AIS and none around the grounding zone (Allison, 2003). The validity of these data is in question, since access to the data is difficult and its quality, survey methodology and how it was processed is unknown. It did however provide the first broad image of the basic structure of the AIS, which oceanographers and glaciologists still use as a starting point for their models. However, there are still improvements to be made:

> *"…the lack of sea-floor bathymetry for the southern part of the Amery cavity remains a deficiency in defining the model domain."*
> *(Allison, 2003)*

The need for a more current, detailed and less ambiguous seismic dataset became apparent, leading to the formation of this project. Besides the general aim of producing an improved map of the ice thicknesses and seafloor depths of the AIS, the seismic technique was also to investigate other glaciological questions.

For example, all previous remotely sensed data from the AIS and other ice shelves has not been able to delineate meteoric (freshwater) ice from marine (saline) ice at the base of ice shelves. Ice radar soundings give good results for meteoric ice thicknesses with a clear definition between ice and bedrock, but radar will not penetrate into marine ice, due to the presence of conductive brine within the ice (Allison, 2003), hence the true total thickness of ice shelves cannot be measured with this method. The seismic technique was proposed as the means to define the marine ice thickness, concentrating

on the AIS. This technique, its methods and the initial results have been discussed by McMahon (2003) and McMahon & Lackie (2006) (Appendix A).

Seismics was also used to explore the upper 200 m of the ice shelf – the section where accumulated snow first undergoes compaction to become firn, and then with increasing pressure due to further burial becomes ice. Seismic refraction is a relatively quick method for modelling this change in density caused by compaction. The same type of surveys can be used to explore the residual effect of strain upon ice, by measuring the azimuthal anisotropy of seismic velocities resulting from an alignment of ice crystal *c*-axis orientations. The seismic method can provide initial information regarding ice fabric, and can begin to elucidate this information more rapidly than an extensive, large area program of time-intensive ice drilling and ice core analysis.

The seismic method can also assist in providing answers for oceanographers. Access to the ocean cavity beneath an ice shelf is a localised and lengthy process. Ocean water property measurements have so far been confined to those collected from several moorings in Prydz Bay off the front of the ice shelf, and seven individual hot-water bores through the AIS to access the ocean cavity to collect conductivity-temperature-depth (CTD), ocean current speed and current direction data. These sites, although each representative of a general region of the AIS, are isolated one dimensional data points (in terms of thickness measurements) and give a sparse coverage of the northern and central region of the AIS. The seismic technique can provide further information about the size and shape of the ocean cavity, with the ability to display 2D images of water properties/features beneath the ice shelf. This expands upon the 1D view given by drilling, and can also cover a much greater area in the time it takes to drill a hole and run downhole surveys. In areas where physical water property measurements have not been taken or are difficult to obtain, seismic surveying can fill in the gap in knowledge.

This research will lead to a better understanding of the ice shelf mechanics and to improved glaciological and oceanographic models of the AIS. These in turn will help us understand the ice shelf's role in the global climate system, and what effects modern day changes are having on the ice shelf.

1.4 Thesis aims and structure

The aims of this thesis are as follows:

- ***Chapter 4*** *– To investigate changes in the AIS over time, and to discuss what processes may be the cause*.
  The site G2A (Figure 1.1), the location of study for McMahon & Lackie (2006), is to be re-surveyed after a significant lapse in time (approximately three years) from the first survey of this site in January 2003, with the aim to quantify differences and propose possible explanations for any changes that have occurred over this time period. The two seismic reflection surveys are to be compared and contrasted to define any changes in total ice thickness and/or marine ice thickness, and also to be compared to physical property measurements taken at the same location and time as the 2005/06 survey by the Amery Ice Shelf Ocean Research Program's (AMISOR) hot-water drilling project (G2A is named AM03 by AMISOR).

- ***Chapter 5*** *– To compare and contrast seismic reflection results with physical water and ice properties collected by the AMISOR and the Chinese Antarctic Research Expedition (CHINARE) drilling programs*.
  Discussion is to be made on similarities and differences between the seismic and physical property models, possible reasons for these differences, and what improvements physical property measurements can make to constraining seismic modelling.

- ***Chapter 6*** *– To undertake and discuss visible features present in a ~3 km seismic reflection profile surveyed over a convergence of two AIS ice stream units*.
  The aims are to determine if there is a visible subsurface distinction between the separate ice stream units in terms of ice properties, ice thicknesses, or intra-ice features. (Can the seismic technique view the vertical foliation through the ice shelf, akin to the seismic imaging of a fault?) Also, to discover, describe and

discuss any other features present at this location, such as water column and seafloor features, and the possible explanations for these.

❄ ***Chapter 7*** *– To explore seismic methodologies for the measurement of azimuthal anisotropy within ice shelf ice – the remnants/evidence of previous strain applied to the ice during the merging of ice streams in the formation of the ice shelf.*

Discuss the effectiveness of the seismic method employed to measure azimuthal anisotropy in terms of efficient and effective field data collection, and whether the results are meaningful and/or significant.

Chapter 2

THE AMERY ICE SHELF

2.1 The Amery Ice Shelf, East Antarctic: introduction and location

The AIS, located at approximately (70°S, 70°E) and having a total surface area of ~60,000 km^2 (Galton-Fenzi et al., 2008), is the third largest embayed shelf in Antarctica after the Ross and Ronne ice shelves, and the largest entirely in East Antarctica (Allison, 2003) (Figure 2.1). The Amery Ice Shelf-Lambert Glacier (AIS-LG) system is one of the largest glacier drainage basins in the world, draining approximately 16% of the East Antarctic ice sheet through the AIS-LG Drainage Basin (AIS-LGB) (Allison, 2003); an area equivalent to more than one million square kilometres (Janssen & Hurd, 2008) draining through a section of coastline that represents only 1.7% of Antarctica's total continental circumference (Budd et al., 1967; Fricker et al., 2000b).

Floating ice shelves are the main pathway for ice loss from the Antarctic ice sheet, either via iceberg calving from their outer margins or from basal melting in the ocean cavities beneath them (Allison, 2001). The AIS catchment area along with 23 other major catchment areas within Antarctica (shown in Figure 2.2) are defined by Vaughan et al (1999) based on analysis of an elevation model derived from ERS-1 satellite altimetry supplemented with conventional ground-based elevation data. (A more

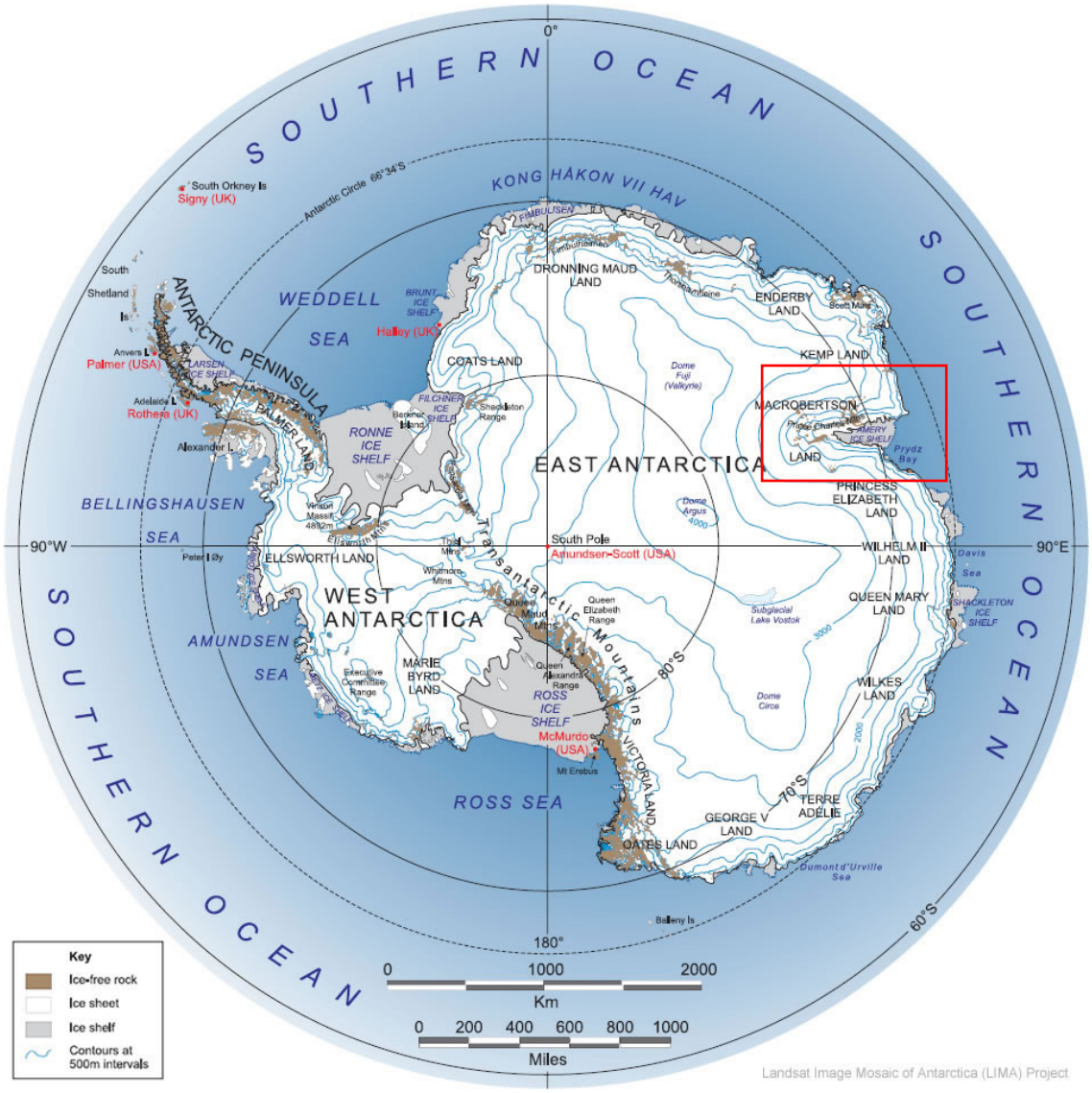

Figure 2.1 – Map of Antarctica, showing the location of the Amery Ice Shelf and other major Antarctic ice shelves (LIMA, 2010).

detailed outline of the AIS catchment area is shown in Figure 2.3.) Being the only major ice shelf in East Antarctica, the AIS is therefore of extreme importance to the mass balance in the East Antarctic ice sheet.

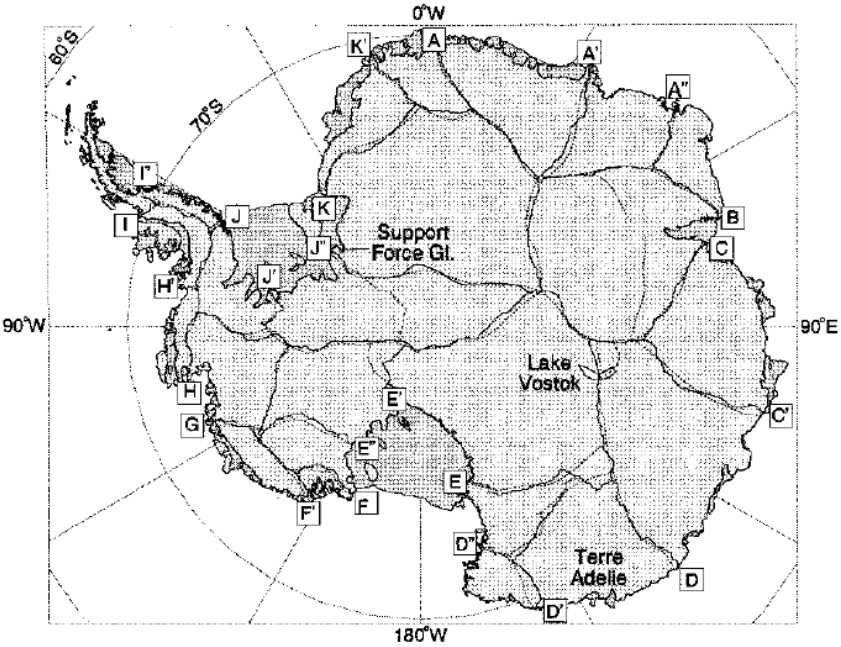

Figure 2.2 – Delineation of drainage basins according to coastline sectors between marked locations given by Giovinetto and Bentley (1985). The Amery Ice Shelf is between marker B and C. Dotted lines indicate those drawn by Giovinetto and Bentley (1985). Solid lines indicate the drainage basins derived from the Observed DEM but with manual intervention from the light dotted line upstream of Support Force Glacier and upstream of Lake Vostok (shaded white) (Vaughan et al., 1999, Fig 3).

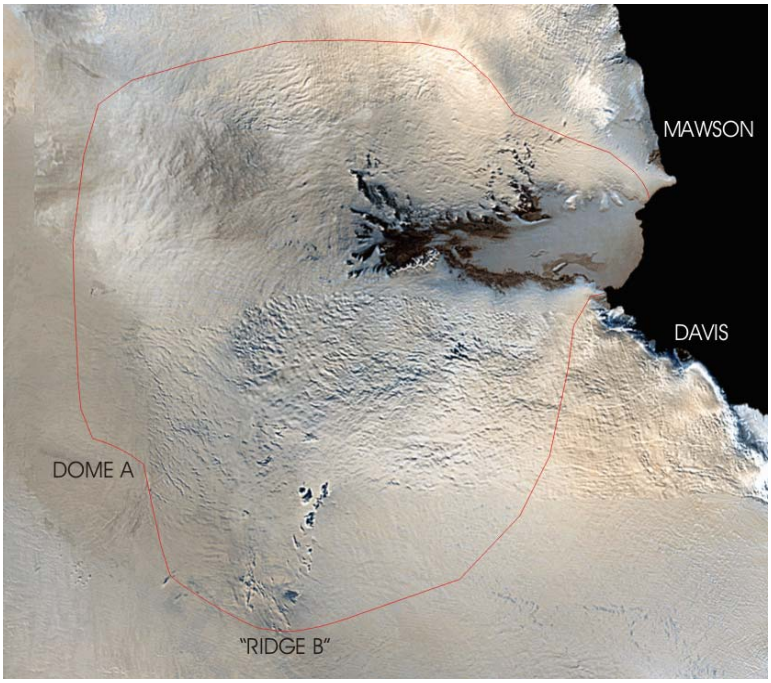

Figure 2.3 – The Amery Ice Shelf catchment area (outlined in red) (adapted from USGS Colour AVHRR image).

2.1.1 Ice sheets, ice shelves and sea ice: definitions

Ice in Antarctica can be grouped into three main categories: grounded ice (ice sheets and ice streams), ice shelves and sea ice.

An **ice sheet** (also known as an ice mantle) is defined as a continental mass of thick glacial ice more than 50 000 km^2 in area (Armstrong, 2011) forming a continuous cover over a land surface and moving outward in all directions (Dictionary of Earth Science, 2003). The ice sheet of Antarctica is more the 4,200 m thick in some areas, and covers all but small areas of exposed rock, these areas amounting to only 2.4% of the total continental area. An **ice stream** is a channelised glacier that flows significantly faster than the surrounding ice sheet, providing an avenue for ice removal from the continent (Armstrong, 2011).

An **ice shelf** is a thick sheet of ice with a fairly level or undulating surface, formed along a polar coast and in shallow bays and inlets, fastened to the shore along one side but afloat and nourished by annual accumulation of snow and by the seaward extension of land glaciers (Dictionary of Earth Science, 2003). In thickness they range from a few hundred meters to over 1000 metres (Armstrong, 2011). Ice shelves link continental ice to the ocean, allowing for interaction, but they are also affected by atmospheric processes. Ice shelves are important environmental change indicators as they are the primary means of mass loss from the continent via either iceberg calving (production of icebergs due to break-off from the ice shelf) or basal melt (melting of ice at the bottom of the ice shelf due to warmer ocean temperatures or increased pressure) (Janssen & Hurd, 2008). As such it is important to understand their processes and monitor changes.

Sea ice is frozen ocean water – it forms, grows, and melts in the ocean. In contrast, icebergs, glaciers, and ice shelves float in the ocean but originate on land (Meier, 2011). The amount of sea ice surrounding Antarctica varies between 18 million km^2 in the winter to 3 million km^2 in summer (Meier, 2011).

The interaction of these ice bodies can be seen in Figure 2.4. The ice sheet flows towards the ocean via a glacier to an ice shelf. In the open ocean, near freezing water sinks to the bottom and flows under the ice shelf. In the case of the AIS, high pressure

causes a lowering of the local freezing point, meaning the incoming water is warmer than the ice above, so basal melting occurs (Allison, 2002). This melting lowers the water temperature and salinity, making the water less dense causing it to rise along the base of the ice shelf until it reaches a point where it is colder than the local freezing point (Allison, 2002). Here ice crystals form and accrete to the underside of the ice shelf, enclosing brine within the new ice layer. Some of this supercooled water flows out from under the AIS into Prydz Bay, where it interacts with ocean water and ice, influencing the ocean circulation and the local ecosystem in Prydz Bay. It also contributes to formation of dense Antarctic Bottom Water which ventilates (i.e. provides oxygen and other dissolved atmospheric gases to) the deep ocean (Allison, 2002).

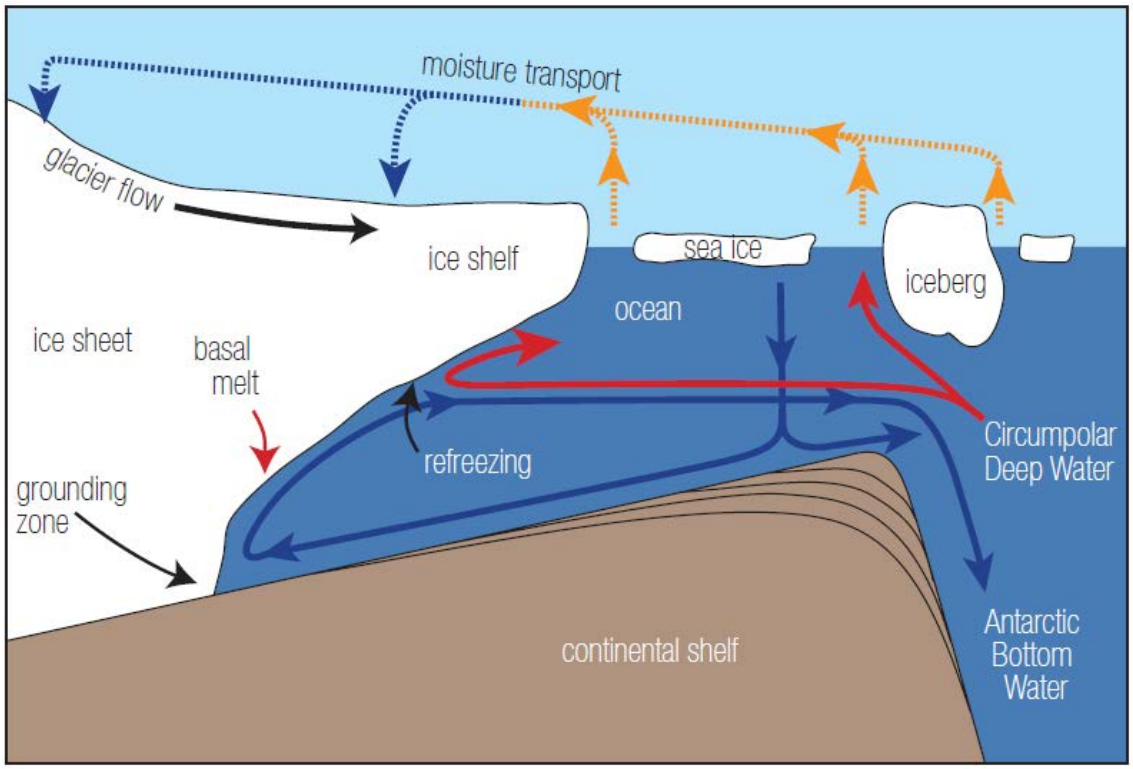

Figure 2.4 – Schematic representation of the Amery Ice Shelf and its interactions with the ocean and atmosphere (Allison, 2002). Salt rejected by winter sea ice growth forms dense, high salinity water, which sinks and flows under the ice shelf. This causes melt when it comes into contact with deep ice. The freshened plume rises under the base of the ice shelf and can either refreeze as marine ice or mix with warm salty Circumpolar Deep Water to form Antarctic Bottom Water.

2.1.2 Previous work on the AIS

The AIS has been the focus of considerable study by the Australian National Antarctic Research Expedition (ANARE) since the 1950s (Allison, 2003). Studies previously carried out on the shelf (and some still currently running) have included but are not limited to traverses (Kiernan, 2001), glaciological surveys (Budd, 1966; Budd et al., 1982; Budd et al., 1967), drilling and ice core analyses (Allison, 2003; Craven & others, 2004; Morgan, 1972; Treverrow et al., 2010; Wakahama & Budd, 1976), ice thickness measurements using airborne radio echo soundings (Manson et al., 2000; Morgan & Budd, 1975), Global Positioning System (GPS) surveys (Fricker et al., 2002a; Manson et al., 2000), satellite image investigations (Partington et al., 1987; Young & Hyland, 2002), rift propagation and iceberg calving investigations (Bassis et al., 2005; Fricker et al., 2002b; Fricker et al., 2005), stress and strain modelling (Budd & Jacka, 1989; Janssen, 2009; Young & Hyland, 2002), seismic surveying (McMahon, 2003; McMahon & Lackie, 2006; Tassell, 2004), marine ice investigations (Craven et al., 2009; Craven & others, 2005; Fricker et al., 2001; McMahon & Lackie, 2006) and oceanographic studies (Galton-Fenzi et al., 2008; Hunter et al., 2004; Leffanue & Craven, 2004). Russian surveys conducted under the Soviet Antarctic Expedition (SAE) in the 1970s have also completed traverses over the ice shelf and performed seismic studies looking for ice thickness (Federov et al., 1982; Kurinin & Grikurov, 1977). The Chinese Antarctic Expedition (CHINARE) completed a 301.8 m ice core during the 2002/2003 summer at the location AIS01 at the front of the ice shelf (Dong, 2003) – a complete core through the AIS.

Previous research sites on the AIS (shown in Figure 1.1) of relevance to this thesis are G1 (69.5°S, 71.5°E) about 60 km from the shelf front, which was the site of a bore hole study of the ice in 1968 (Budd et al., 1982), and other sites studied for surface ice velocity G2, G3, T4 (71.2°S), and G2A – situated along the flowline between G2 and G3 (McMahon & Lackie, 2006), JP (named for its proximity to Jetty Peninsula) and LT (for a location near “Loose Tooth” situated along the same flowline as JP, AM04 and AM01) (as defined by Craven et al., 2009), and the drill sites AM01, AM02, AM03, and AM04. These sites were drilled under the AMISOR project, and correlate closely with the seismic program as discussed in this thesis.

2.2 The AMISOR project

Due to its significance to the research presented in this thesis, the following is an outline of the AMISOR project; its aims, methodologies, site locations and results to-date.

The Amery Ice Shelf Ocean Research (AMISOR) project (ASAC Project 1168) is a multi-year joint project of the Australian Antarctic Division (AAD) and the Antarctic Climate and Ecosystems CRC (ACE CRC) (as part of their Sea Level Rise programme). Its all encompassing aim is to investigate the interaction between the AIS and the ocean. The project also aims to provide an assessment of the role of the AIS in the ice sheet mass budget and in driving deep ocean circulation (Allison, 2001). It forms part of a broad umbrella study of the Lambert Glacier Basin-Amery Ice Shelf system with the aim to understand both the climatic history of the region and its probable response to global warming.

The AMISOR project aims to better quantify ice shelf processes through both an oceanographic component and a shore component (Allison, 2001). The oceanographic component entailed measurements across the front of the AIS of the properties and flow of seawater entering and leaving the ocean cavity beneath the ice shelf. These were carried out in the 2000/01 season from onboard the RSV Aurora Australis Voyage 6. Moored instruments were left over the winter and retrieved the following summer (Allison, 2003; Leffanue & Craven, 2004).

The shore component of the AMISOR project, involving deployment on the AIS, involves in situ measurements of the processes beneath the shelf through a series of access holes drilled through the ice shelf (Allison, 2001). These holes are made with a hot water drill, designed and constructed by the AAD. The first season's fieldwork occurred during the 2000/2001 summer, while the most recent fieldwork was conducted in the 2009/2010 summer season.

AMISOR brings together glaciological fieldwork, marine science and oceanographic surveys, sedimentation history and seafloor biology, airborne and satellite remote sensing, and numerical modelling of the past and future behaviour of the ice-ocean

system (Craven et al., 2007). The seismic program – a major part of what makes up this thesis – is another area of science that can contribute to and be tied in with work carried out by AMISOR. Data gained from seismic surveying is fed into “coupled” ice shelf ocean models that predict patterns of melting and freezing at the base of the shelf, and the modification to water masses circulating below the shelf (Craven et al., 2007).

The measurements and samples collected at the AMISOR borehole sites have provided information such as ice shelf elevation, ice thickness, surface weather, ice shelf temperature profiles, and annual variability in salinity and temperature in the water cavity below the ice shelf (Craven et al., 2007). Further measurements of the boreholes and new sites, with the oceanographic data from the ice shelf front, will provide estimates of the melt and freezing rates under the ice shelf (Allison, 2001). These can be used to validate numerical models of the ocean circulation in the cavity (Galton-Fenzi et al., 2008).

2.2.1 AMISOR equipment

The AMISOR hot-water drill setup is outlined in Figure 2.5. The drill is first assembled, after which ~380 m of ice can be bored approximately every 24 hours. The 300 mm borehole is made through the ice using a high-pressure jet of hot water (which is produced by melting and heating in-situ snow in the flubber). The hole is subsequently reamed to a 400 mm diameter, and then a series of measurements are made in the ocean beneath the ice shelf. Moorings of Seabird SBE 37-IM inductive modern MicroCATs are left suspended underneath the ice shelf, with the mooring wire frozen into the borehole. The SBE 37-IM MicroCAT is a high-accuracy conductivity and temperature sensor/recorder (Sea-Bird Electronics, 2011). These instruments continue to measure conductivity and temperature of sub-AIS water over several years, and the data is downloaded annually via conductive coupling with the top of the mooring wire (Rosenberg, 2005).

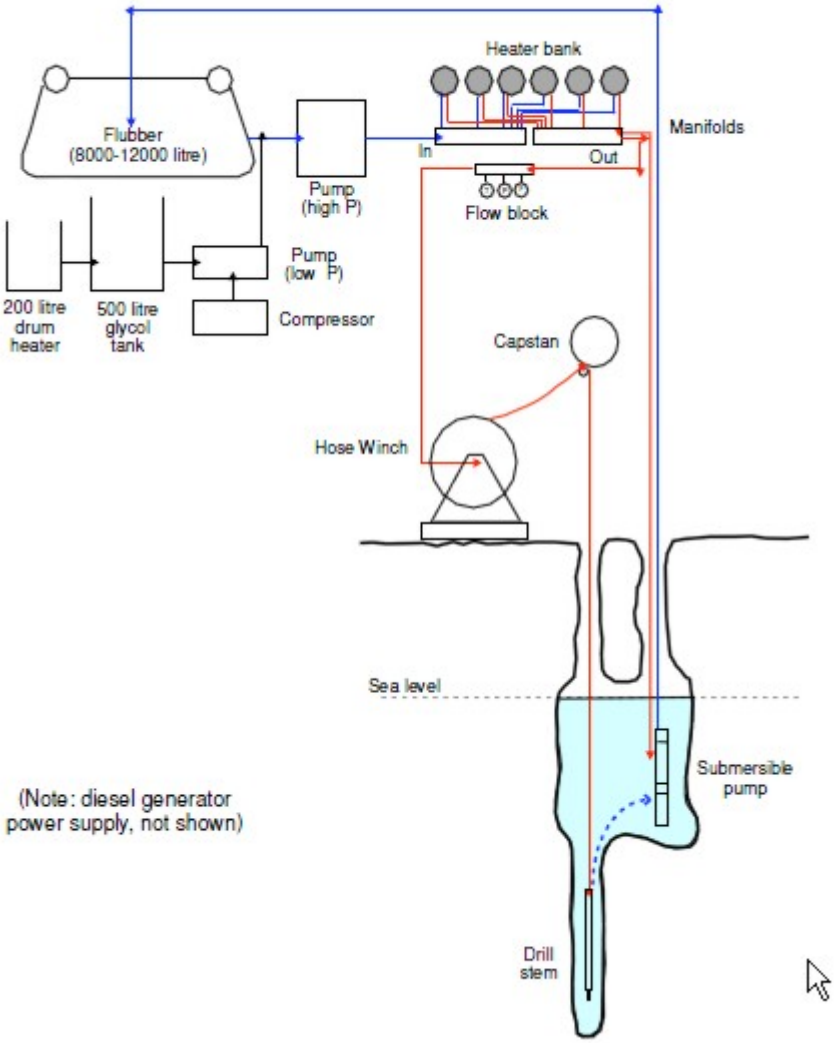

Figure 2.5 – Diagram of AMISOR's hot-water drill equipment, showing the reservoir of water in the flubber and pumps at the surface and below sea level down-hole; the flow of water is indicated with cold (blue) water and hot (red) water which is used to melt the hole through the ice shelf. (Treverrow & Donoghue, 2010)

2.2.2 The AMISOR drill sites

Six sites and seven boreholes on the AIS have been hot-water drilled to the base of the ice between the summer seasons 2000/2001 and 2009/2010, all as part of the AMISOR project. AM01 and AM02 were drilled prior to this seismic project (ASAC Project 2581) and the previous seismic surveys of the 2002/2003 season carried out under ASAC Project 2542 (McMahon, 2003; McMahon & Lackie, 2006). Concurrent to this

seismic project, AM01b (a repeat hole at AM01), AM03 (at the G2A 2002/03 seismic site) and AM04 were drilled. Recently in the 2009/2010 season two new sites AM05 and AM06 were drilled; AM06 was reported to have no marine ice and AM05 had marine ice reported as being present (see Figure 1.1 for these locations). Table 2.1 gives a summary of measured ice thicknesses from the AMISOR sites (AM05 marine ice status is currently unknown).

Table 2.1 – AMISOR borehole results for ice thicknesses and seafloor depths below the ice shelf surface (* value calculated from AM06 borehole profile caliper run (Treverrow & Donoghue, 2010))

Drill name	Year surveyed	Location		Surface velocity (m a^{-1})	Azimuth of ice flow (°)	Total ice thickness (m)	Marine ice thickness (m)	Seafloor depth below surface (m)
		Latitude	Longitude					
AM01	2001-02 & 2002-03 (as AM01b)	-69.4051	71.5191	840	43.8	479	203	841
AM02	2000-01	-69.6825	72.7315	650	44.7	373	0	841
AM03	2005-06	-70.5511	70.3381	390	11.4	722	0	1339
AM04	2005-06	-69.8872	70.3152	600	35.8	603	207	1002
AM05	2009-10	-70.2278	69.6784	402	25.7	624	?	979
AM06	2009-10	-70.25	71.35	386	29	607	0	902

2.3 Structure and dynamics of the Amery Ice Shelf System

In general the entirety of the Amery Ice Shelf system can be broken into three parts: the interior basin (the inland boundary is shown in Figure 2.3), the glaciers and tributaries that feed into the AIS (including the Lambert, Mellor, Fisher, Charybdis and Scylla Glaciers and the Mawson Escarpment Ice Stream, as shown in Figure 1.1), and the ice shelf itself. The following is an introduction to the features and structure of the AIS.

2.3.1 Ice dynamics: merging glaciers, foliation and fracturing

The Lambert Glacier-AIS system is made up of several confluent ice streams (refer to Figure 1.1 for locations.) The Lambert, Mellor and Fisher glaciers originate the farthest inland, forming the main trunk glacier, dwarfing the input from the Collins and Geysen glaciers. Although the Collins and Geysen glaciers enter the AIS beside the Lambert,

Fisher and Mellor, they soon form only a narrow indistinguishable strip of the AIS. However, by the time the ice from these southern glaciers reaches the ice front these **flow units** (as the ice from each major tributary can be defined as) are not the largest. This is due to several other glaciers joining the main trunk glacier and others joining the ice shelf itself during its northward journey. The major contributor of ice at the ice shelf front is the Charybdis Glacier, which joins the AIS from the west. The Mawson Escarpment Ice Stream also contributes a significant amount of ice from the east margin of the AIS.

Satellite images, such as the one shown in Figure 2.6, reveal complex structural detail which can be interpreted in terms of flow dynamics and the flow direction, or path. Linear longitudinal features, called **flowlines**, are a surface manifestation of the 3D structure of the ice (Hambrey, 1991), i.e. where ice streams have merged together and yet still maintain a structural boundary. Commonly this foliation forms parallel to and in association with medial moraines (Hambrey et al., 1991). Such boundaries may divide ices that have undergone rather different histories of accumulation and deformation, and they provide an interesting site to investigate subsurface structure and ice properties. Tracing these flowlines can reveal the path the ice has travelled, and interpreting the history of a section of ice at depth can be a matter of following the flow unit back upstream and interpreting the present day situation of ice at the surface. Knowing the surface ice velocity and the rate of accumulation can lead to a 3D understanding of the ice shelf itself.

Figure 2.6 shows the flowline traces of the boundaries of the eight major flow units that make up the AIS. These reveal a change in the direction of flow downstream as more ice enters from the margins and diverts the ice in the older flow units, first changing to a slightly west of north bearing, then changing to a slightly easterly bearing as large amounts of ice enter from the Charybdis and Scylla glaciers and other smaller NW ice streams. It can also be observed that although the ice units narrow as they pass through the confined central AIS, once the margins open towards the ice shelf front, the surface width of each flow unit increases slightly as the ice expands and spreads out.

The second major structural feature that can be seen in satellite images are crevasses. Crevasses occur where glaciers converge and where ice streams diverge – i.e. where

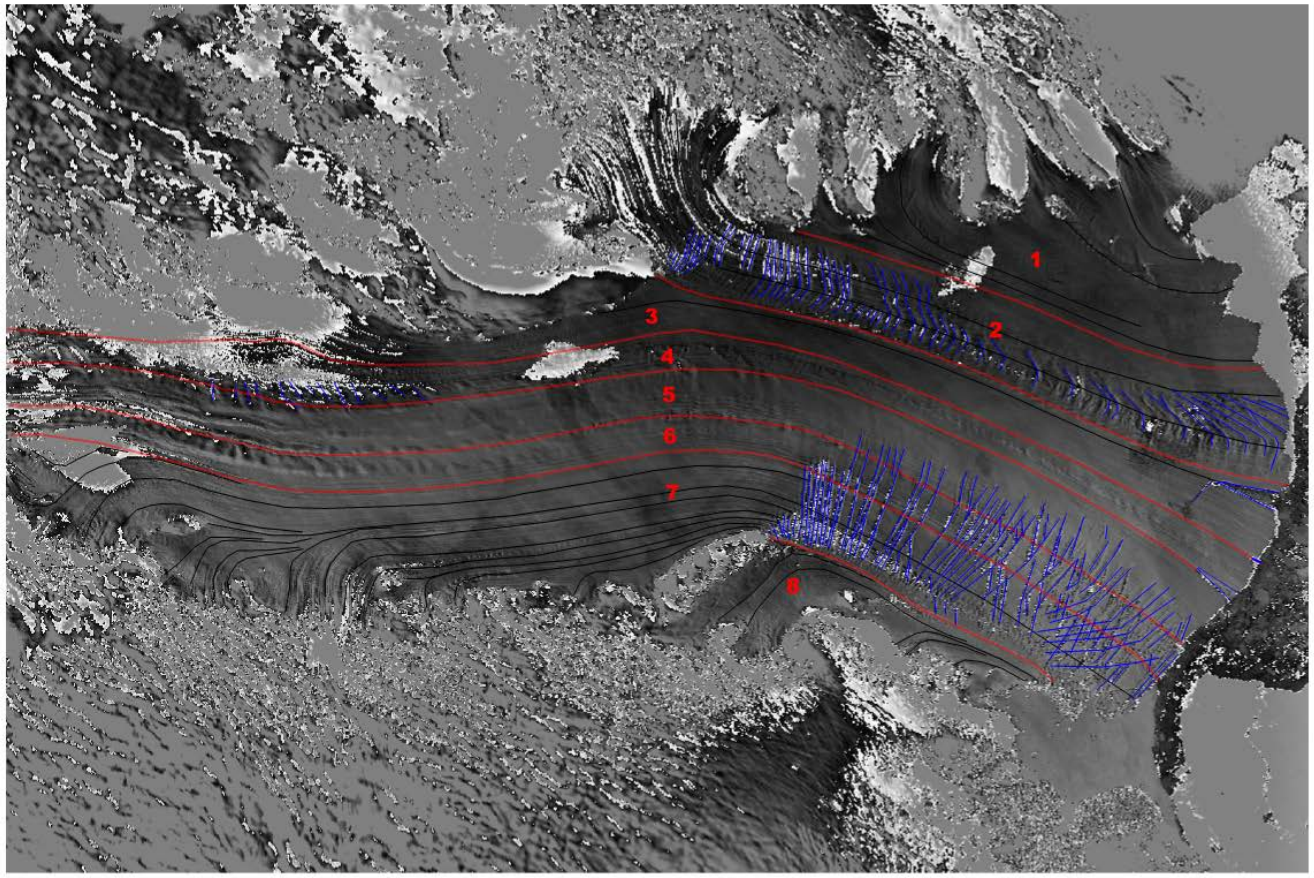

Figure 2.6 – Satellite image of the AIS (taken 2002) showing the path of glacial ice units (North is to the right). Black lines indicate flowline traces; Red lines define major flow unit boundaries: 1 = NW AIS, 2 = Charybdis Glacier, 3 = Eastern PCMs, 4 = Fisher Glacier, 5 = Mellor Glacier, 6 = Lambert Glacier, 7 = Mawson Escarpment, 8 = NE AIS; Blue lines indicate crevasses and rifts. (Image: Neal Young, Richard Coleman, Pers. Comm.)

there is a change in the stress field. The major visible crevasses are highlighted in blue in Figure 2.6. There are two major areas of crevassing in the north of the AIS – associated with the Charybdis Glacier Unit (hereafter referred to as the Charybdis Unit) in the west and the AIS bending around Gillock Island in the east – and there is another visible area of crevassing in the central south AIS, at the Budd Ice Rumples.

The Charybdis Unit crevasse field is mainly due to expansion crevassing as the ice entering the AIS is released from the strain within the glacier and accelerates forward to the ice front. The effect of varying ice velocities across the smaller ice streams that make up the Charybdis Unit can be seen in the crevasses here. The western most component of the Charybdis Unit is travelling relatively slow compared to the eastern components, and the crevasses are deformed - the east sections of crevasses are located closer to the ice shelf front while the west end of the crevasse is being dragged. This has led to the bent and curved crevasses visible towards the front of the shelf, getting more offset the further north the ice travels.

In the east, the major crevasses form as the AIS changes direction around the north tip of Gillock Island. Crevasses are initially short in length, occurring in the Mawson Escarpment Unit, but they quickly extend to cut across the Lambert Unit and into the Mellor Unit. As the AIS continues to gradually turn east, secondary and tertiary crevasse systems crosscut the older crevasses. At the very front of the ice shelf in the east, there is crevassing parallel to the ice shelf front, where sheets of the AIS would eventually break off and enter Prydz Bay as icebergs. Different to the Charybdis Unit, crevasses here are offset by newer crevasses rather than by the ductile dragging and stretching of the crevasses in the west.

Another major fracture feature present is what is known as the Loose Tooth, a 30 km by 30 km block at the front of the AIS. Two major rifts have opened up: one along a flowline within the Eastern PCM Unit where the glacial ice sourced north of the Jetty Peninsula (east of the Charybdis Unit) spilts from the rest of the Unit (shown in Figure 2.6); and the other where the Fisher Unit and Mellor Unit boundary meets the ice shelf front. A perpendicular rift is also opening eastwards into the Eastern PCM Unit. Eventually these rifts will meet up, leading to a calving event and an enormous iceberg entering Prydz Bay from the AIS (Bassis et al., 2005; Fricker et al., 2005; Janssen,

2009). There is also a much smaller rift present at the ice shelf front at the boundary between the Eastern PCM Unit and the Fisher Unit – a “chip” in the Loose Tooth, so to speak. It is interesting to note that these major units are so distinct that their boundaries are the locations for rifting at the ice shelf front, even after hundreds of years of being joined as part of the AIS.

The last feature of note from this satellite image is the minor crevasse field in the western part of the AIS in the vicinity of Fisher Massif and Jetty Peninsula. This feature is known as the Budd Ice Rumples, a large area where the AIS passes over a subsurface feature that causes the ice to rumple up and for crevasses to form. The Fisher Unit’s western boundary shows how this feature locally disturbs the otherwise smooth path downstream.

2.3.2 Surface velocity

Budd et al. (1982) produced a velocity vector map of the AIS (shown in Figure 2.7), which also displays the idealized flowlines drawn from satellite images and their measured velocity vectors. These data and other Lambert Glacier catchment velocity data (shown in Figure 2.8) were acquired in the field using a combination of standard surveying techniques (electronic distance measurement and theodolites, and GPS). Figure 2.8 shows ice flows into the AIS from the catchment area at a maximum of 60 m a^{-1} in both the southern grounding zone and at the very northeast (perhaps due to the steepness of the coast here), while ice flows into the AIS around the rest of the catchment at an average rate of less than 20 m a^{-1} (Manson et al., 2000; Ren et al., 2002). Data from the AIS itself shows the centre of the ice shelf (adjacent to Beaver Lake) flows north at around 350 m a^{-1}. By the time the ice nears the ice shelf front, the middle of the ice shelf is flowing at a velocity of 1350 m a^{-1} while ice nearer the shelf margins flows at a slower rate (approximately 300 m a^{-1}) due to friction at the ice shelf margins.

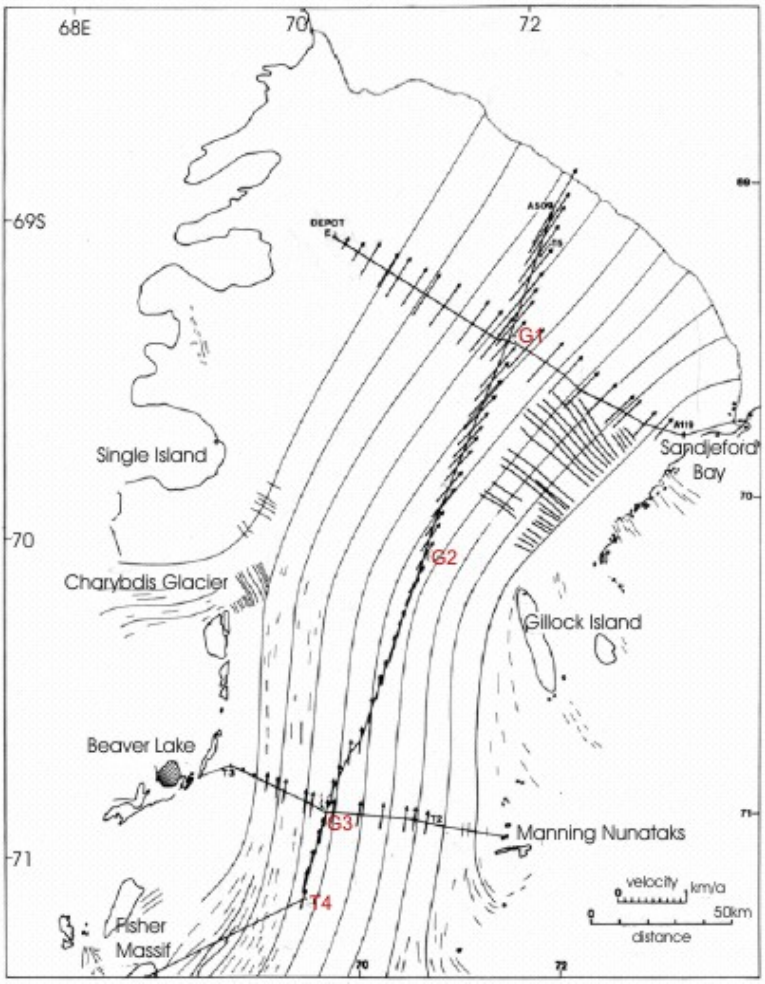

Figure 2.7 – Traverse routes surveyed during the 1968 AIS Project, showing measured ice movement vectors and flowlines derived from vectors and Landsat imagery (after Budd et al., 1982, Figure 1)

Using interferometric analysis of RADARSAT SAR data, Young & Hyland (2002) generated a dense network of surface velocity vectors over the AIS (shown in Figure 2.9). This image shows ice velocities decreasing downstream from the grounding zone, located at 73.2°S (Fricker et al., 2002a), where surface velocity is about 800 m a^{-1}, to less than 350 m a^{-1} near location T4 (71.2 °S, shown in Figure 1.1). Swithinbank (1988) found that the ice velocity around T4 reached 327 m a^{-1}. North of T4, the surface velocity increases to almost 1400 m a^{-1} at the centre of the calving front of the AIS. Fricker et al. (2002b) have used RADARSAT imagery to show the front of the ice shelf is advancing seaward at a rate of 1300 m a^{-1}.

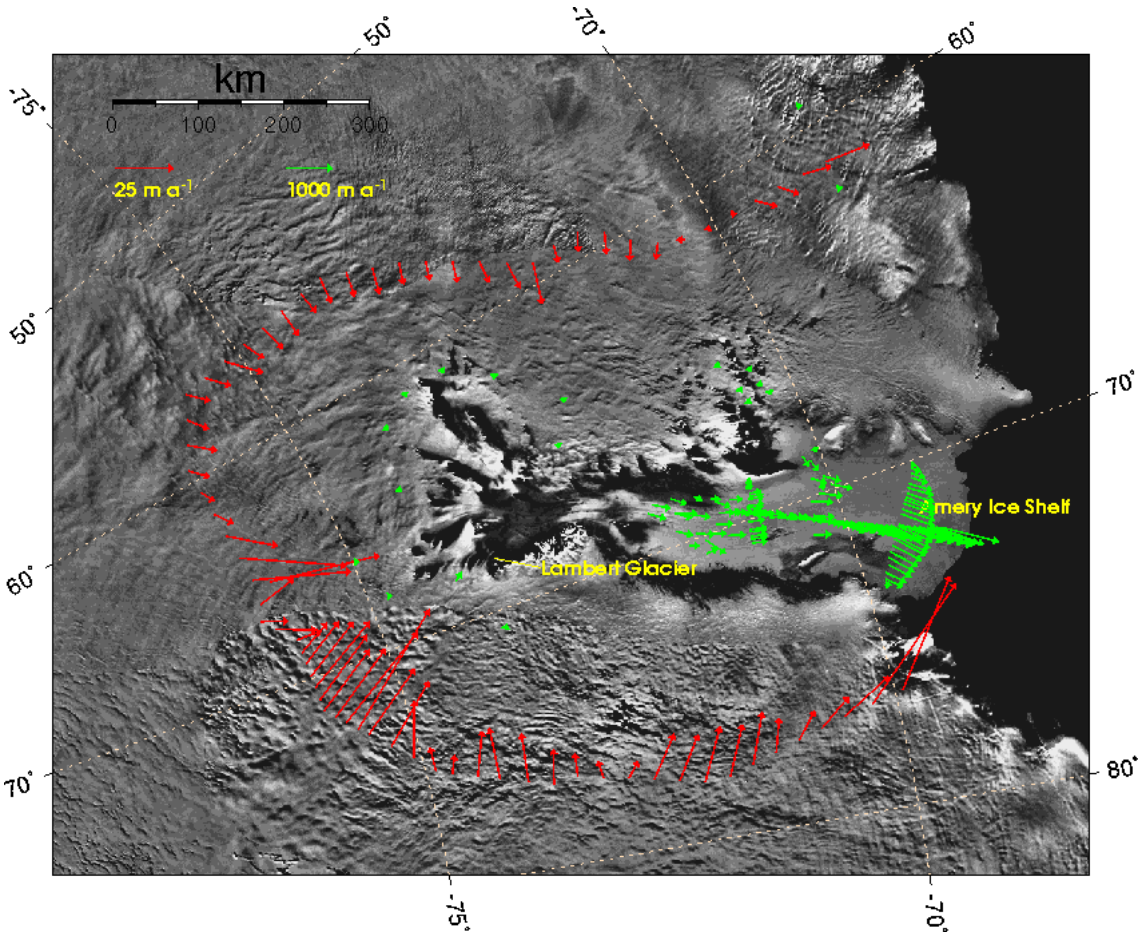

Figure 2.8 - AIS ice velocity image with survey points on the AIS and catchment area. (Note the order of magnitude difference for green and red velocity scale.) The map is a subscene from the USGS 1 km AVHRR mosaic (Ferrigno et al., 1996) (National Snow and Ice Data Center).

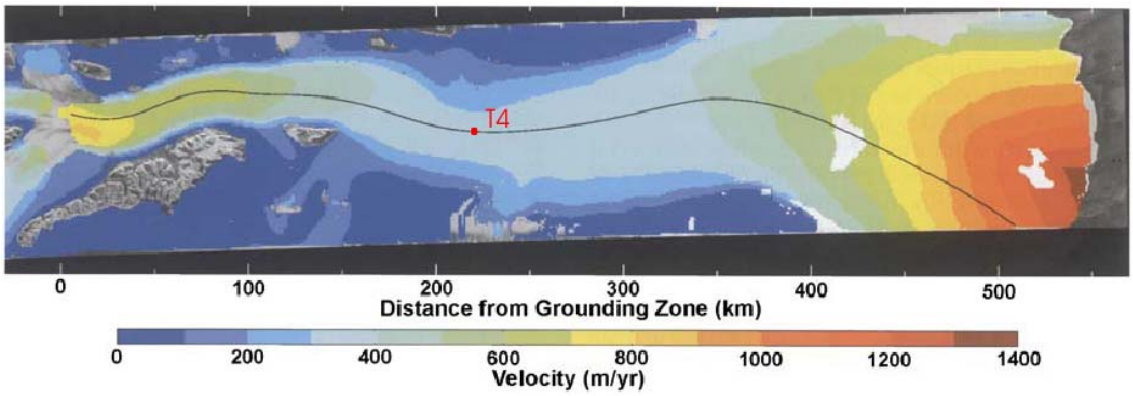

Figure 2.9 – Smoothed distribution of surface ice velocity over the AIS derived from interferometric analysis of Landsat SAR data (Young & Hyland, 2002). T4 location marked; black line = Fisher-Mellor boundary. Scale: less than 100 m a^{-1} (dark blue) to almost 1400 m a^{-1} (dark red) (adapted from Janssen & Hurd, 2008, Plate 8).

2.3.3 Mass balance

The Antarctic ice sheet is the largest solid water reservoir with an area $13.5x10^6$ km² and a volume nearly $30x10^6$ km^3, containing approximately 90% of the total ice and more than 70% of the fresh water on the earth (Ren et al., 2002). Since even a tiny variation in Antarctica's volume will cause a significant environmental effect (e.g. a change in 1% of total volume will result in a global sea level change of 0.7-0.8 m) the ability to measure whether the ice sheet is growing or shrinking has taken on global import and mass balance has become an important climatic variable (Fricker et al., 2000b; Ren et al., 2002).

Almost all of the precipitation that falls on the Antarctic ice sheet becomes ice. **Mass balance** as defined by Fricker et al. (2000b) describes the budget between mass income (precipitation – mainly snow) and mass loss (due to evaporation, wind redistribution, surface hoar frost deposition, melting and run-off, and iceberg calving) and is used to express the volume change of the ice sheet. A positive mass balance means mass income exceeds mass loss and net volume will increase; a negative mass balance, conversely, means a net volume decrease (Ren et al., 2002).

Fricker et al. (2000b) describes the AIS-LG system as covering the area 68.5-81°S, 40-95°E – an area approximately 1,550,000 km² with a floating ice area of 69,000 km². In the past decades some attempts have been made to estimate the mass balance of the AIS-LGB from observations of limited areas on long distance traverses. Since 1990 ANARE have carried out five inland traverses (1990-1994) following routes at about 2,500 m elevation for a maximum distance 2014 km (Fricker et al., 2000b; Ren et al., 2002), but the emphasis was placed on the west side of the basin with the traverses starting at Mawson Station and only two of the traverses completing the entire route around to the other side of the AIS-LGB. CHINARE carried out three inland traverses from Zhong Shan Station to Dome A in the east part of the basin between 1997-1999 (Ren et al., 2002). Snow accumulation was measured using bamboo canes at 2 km spacing for both programs, and 24 shallow cores were taken for analysis. Surface velocity, magnitude and azimuth were determined using GPS observations over two or more years.

In general the accumulation rate is higher near the coast and decreases gradually inland. Averages of 124-171 kg $m^{-2}a^{-1}$ snow accumulation in the east and 94 kg $m^{-2}a^{-1}$ in the west suggest more moisture reaches the east side than the west side of the AIS-LGB, which is consistent with moisture transport models (Ren et al., 2002). The results from core analysis show accumulation on the east side of the AIS-LGB is higher on average and has increased in the past 250 years, whereas the opposite is true on the west side of the AIS-LGB where accumulation rates have dropped in the last 30-60 years (Ren et al., 2002). Fricker et al. (2000b) calculated the following ice flow fluxes (using ice velocities and thickness) of 13.6 Gt a^{-1} in the west, 21.8 Gt a^{-1} in the Lambert Glacier area and 8.6 Gt a^{-1} in the east.

If ice flux over a section is equal to net accumulation upstream over a period of time, then the area is in a balanced state and thickness remains constant. The calculated accumulations in each area (as defined by Ren et al. (2002)) are shown in Table 2.2. From this Ren et al (2002) suggest the system is in a state of positive mass balance budget of 13%, however there are some uncertainties due to the sparse nature of observed data near the ice divide.

Table 2.2 Calculated accumulations and outflow fluxes (Gt a^{-1}) over upstream area of ANARE traverse (Ren et al., 2002, Table 1).

	East			Stream	West			Total
	I	II	Sum		I	II	Sum	
Area×10^4/km^2	6.2	10.7	16.9	41.8	7.8	13.9	21.7	80.4
Accumulation	6.3	6.4	12.7	21.6	7.3	8.1	15.4	49.7
Outflow flux			8.6	21.8			13.6	44.0
Imbalance (%)			47.7	–0.9			13.2	13.0

.

Comparing these more recent results to older studies, for the interior basin Allison (1979) estimated the total mass flux to be 60 Gt a^{-1} and calculated the outflow from the interior to the Lambert Glacier system to be 30 Gt a^{-1}. This is suggestive of a positive mass balance. For the mass flux through a section of the boundary between Lambert Glacier and Amery Ice Shelf, with the input of 30 Gt a^{-1}, was calculated to be 11 Gt a^{-1}. Adding a 7 Gt a^{-1} loss due to ablation leaves an excess mass of 12 Gt a^{-1}, a 40% positive mass balance (Allison, 1979).

Robin (1983) has suggested that the apparent mass imbalance, as noted by Allison (1979), may be due to strong basal melting but only partial replacement by basal freeze-on of marine ice, hence the accumulation rate may have been underestimated. Evidence for strong basal melting includes oxygen isotope profiling (Morgan, 1972). This shows that approximately 40% of the ice thickness of the Lambert Glacier is absent at the outer edge of the AIS, and must have melted near the grounding line. However, McIntyre (1985) used remote sensing techniques to conclude there was no significant imbalance in the system. Redefinition of the interior basin using Landsat imagery gave a reduced area of 902,000 km^2, as opposed to the value of 1,090,000 km^2 as given by Allison (1979). This resulted in a calculated mass flux of 30 Gt a^{-1}, which almost balances an input of 32 Gt a^{-1}.

All these studies show varied results for mass balance of the AIS-LGB system, from positive balances of <+1% up to +40%, with the results from traverse measurements coming to +13%. If this is correct, then the Lambert Glacier-Amery Ice Shelf system would appear to be in positive balance overall, but this could vary on a local scale.

Newer studies use this same traverse data to validate and calibrate satellite measurements of the ice sheet, and assist in developing numerical models (Stoddart, 2008). An example of this is shown in Figure 2.10 below. Where the balance flux is greater than the measured flux, the interior ice sheet is growing and vice versa. Much of East Antarctica is nearly in balance, although gains in the AIS-LGB (LGB in Figure 2.10) and Wilkes Land lead to an overall gain for this section of the ice sheet that is equivalent to a drop in sea level of 0.1 mm yr^{-1} (Stoddart, 2008). Different balance conditions in other parts of Antarctica and between the 2,000 m elevation contour and the coastline also impact sea level, and overall Antarctica is probably contributing to a net sea level rise (Stoddart, 2008).

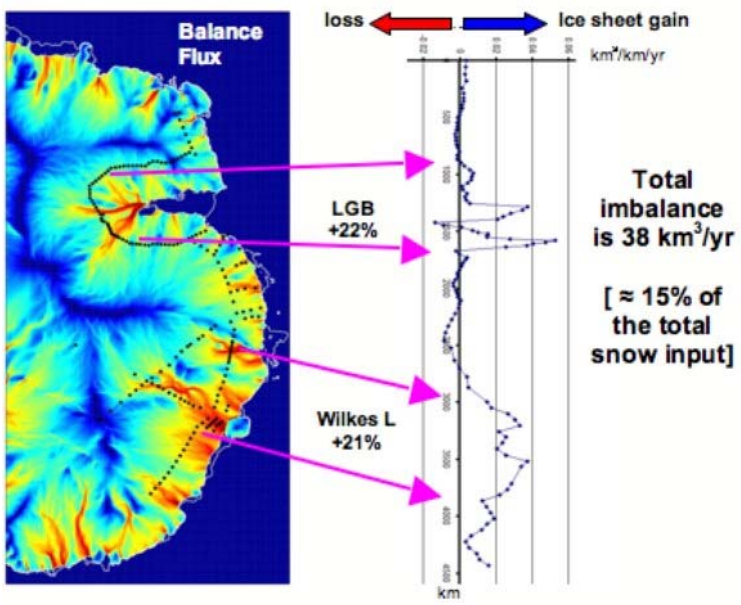

Figure 2.10 – The map shows the balance flux - the volume of ice that must be discharged to balance the annual snow fall onto the ice sheet. This is derived by a computer model (Budd & Warner, 1996) for a given snow fall distribution: the blue areas are low ice discharge rates and the red are high rates, on a logarithmic scale. The plot compares the modelled mass flux across the 2000 metre surface elevation contour with the discharge derived from ice velocity and the ice thicknesses measured by Australians over snow traverses between 40-130ºE (black dots). LGB = Lambert Glacier Basin; Wilkes L = Wilkes Land.

2.4 Geology of the AIS region

In MacRobertson Land (west of the AIS) and Princess Elizabeth Land (east of the AIS), exposed rocks extend about 600 km inland from the coast and are most widespread in the Prince Charles Mountains (PCMs) (which includes the Mawson Escarpment bordering the east of the AIS) and in the Vestfold Hills near Davis Station. These areas have been studied by both Soviet and Australian geologists since the 1970s, and there have been varying interpretations. The Soviets considered the rocks to become increasingly more metamorphosed as they became older (Ravich et al., 1984), whereas Australians, using geochronological investigations, suggested lower grade rocks

exposed in the southern PCMs to be Archaean in age and the highest grade rocks to be of late Proterozoic age (Tingey, 1982).

A recent Australian geological map is shown in Figure 2.11. A structural interpretation of the region made from aerial magnetic data is shown in Figure 2.12. The major area of study for this thesis lies over the area defined as the Amery Group (unit 2g in Figure 2.12).

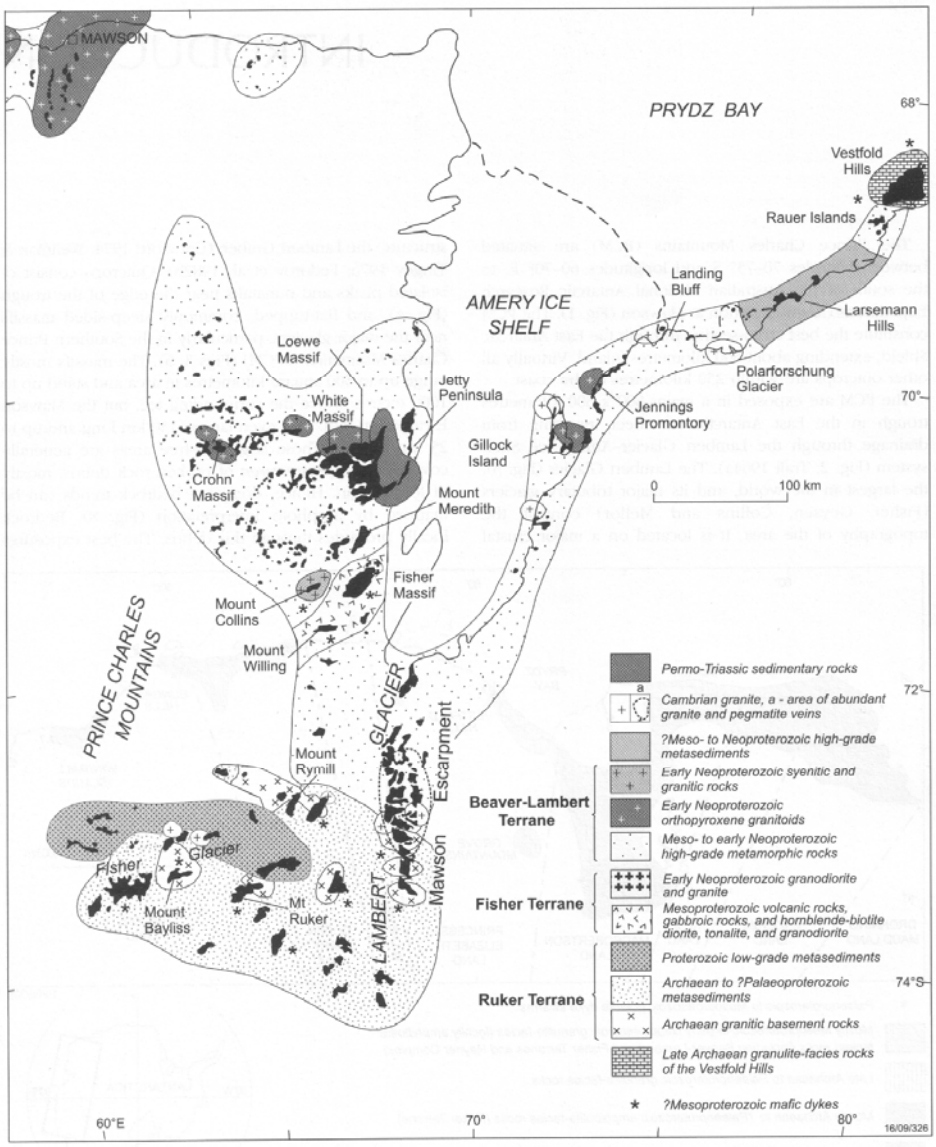

Figure 2.11 – Generalised geologic map of PCM-AIS area, showing terranes (as defined by Mikhalsky et al., 2001) and main granitoids intrusions. Solid black lines show outcrop; boundaries away from outcrop are only diagrammatic (Mikhalsky et al., 2001, Fig 2).

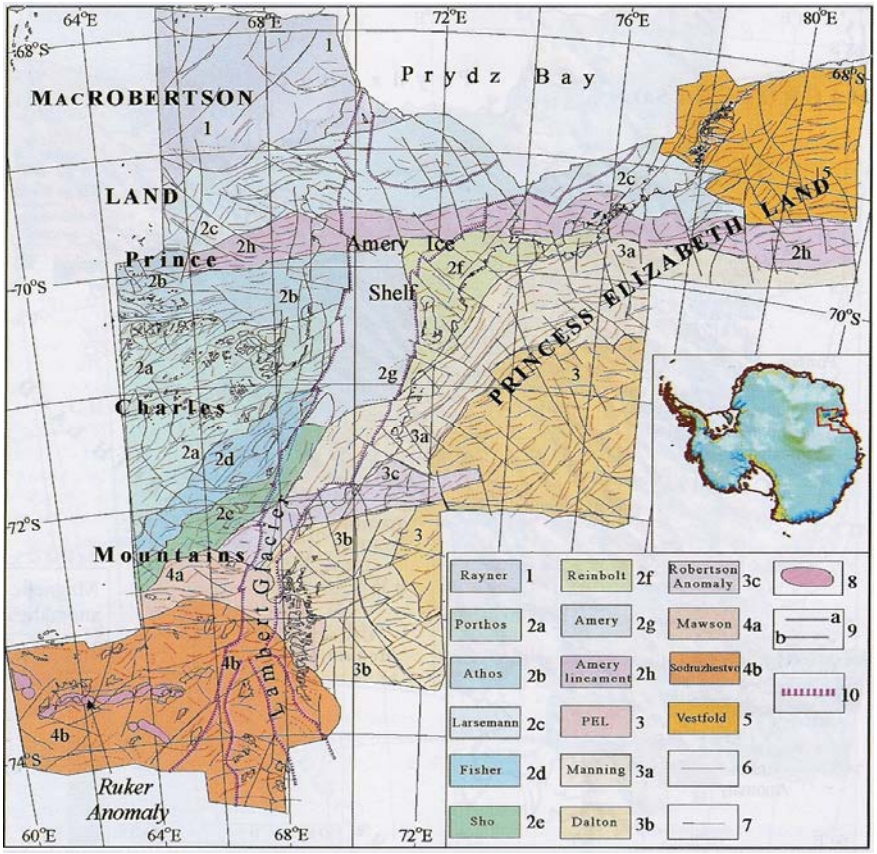

Fig 2.12 – Structural map of the PCMs and surrounding areas based on aeromagnetic data interpretation. Note: Structural subdivision (10) = Lambert Graben rift boundary (Golynsky et al., 2006).

The AIS-LG Drainage Basin is quite well defined by ice surface contouring (Figure 2.3, Figure 2.13), showing the area that drains through to the AIS. Underlying this area is a deep rift valley, the Lambert Graben (Hambrey & McKelvey, 2000; Ren et al., 2002). The graben has been defined by gravity, seismic (Federov et al., 1982; Stagg, 1985) and magnetic data (Federov et al., 1982), showing a major graben structure underlying the Lambert Glacier and AIS, extending 700 km inland. Inland magnetic surveys show bedrock depressions of up to 5 km filled with non-magnetic units, and offshore magnetic surveys have shown the structure may extend out into Prydz Bay (Stagg et al., 1983; Stagg, 1985). These surveys indicate a crustal structure of deep N-S trending fractures (Figure 2.12), marked in the bedrock topography as escarpments bounding the Lambert Glacier and AIS, that offset two major seismic boundaries, one being the Moho (Stagg, 1985), and indicate the Lambert Graben is the failed rift arm of a triple junction.

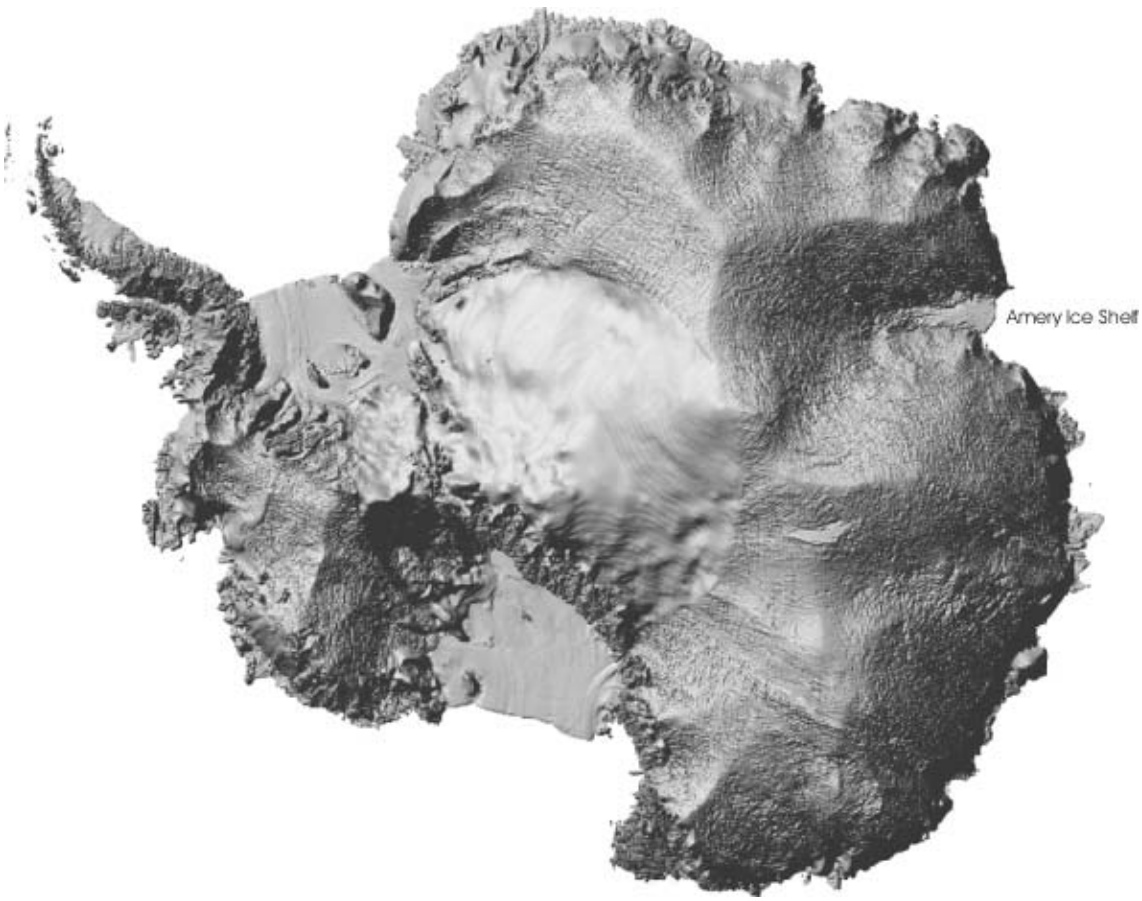

Fig 2.13 – Relative ice elevation (exaggerated), AVHRR image (Advanced Very High Resolution Radiometer) (USGS).

2.5 Ice thickness and ice properties

In the 1969/1970 summer, the Australian National Antarctic Research Expedition (ANARE) made the first measurements of ice thickness using a radar system, and performed the first of many thermal ice drilling programs, resulting in a deep ice core from G1 that reached a depth of 315 m (Allison, 2003; Morgan & Budd, 1975). Oxygen isotope and salinity analysis of the G1 ice core revealed a three-layer structure to the AIS: meteoric ice formed from accumulated snowfall accounted for the top 70 m, with glacial ice at 70-270 m and accumulated marine ice below that (Allison, 2003; Morgan, 1972). Most importantly, that season succeeded in mapping the bedrock below the ice and determining ice thickness values in the AIS region, finding a maximum ice

thickness of 2,500 m (Janssen & Hurd, 2008; Morgan & Budd, 1975). The ice draft in the AIS region varies from > 2500 m in the southern grounding zone to 200-250 m at the ice shelf front (Treverrow & Donoghue, 2010). Various techniques have been used to investigate and measure ice thickness and various ice properties, from ice temperature, salinity, and density, to stress and strain, anisotropy and ice crystal fabric.

2.5.1 Ice cover in the Amery Ice Shelf-Lambert Glacier system

The ice cover thickness is variable and tends to smooth the underlying topography (Hambrey, 1991). Ice is thinnest at the coast, with small coastal areas of bare rock displayed in the Vestfold Hills and other localities between Davis and the Amery Ice Shelf. Otherwise, in coastal areas, the ice thickness is less than 500 m. Figure 2.14 shows the blanket of thick ice in the AIS-LGB with the AIS being relatively thin in comparison and only small pockets of exposed rock.

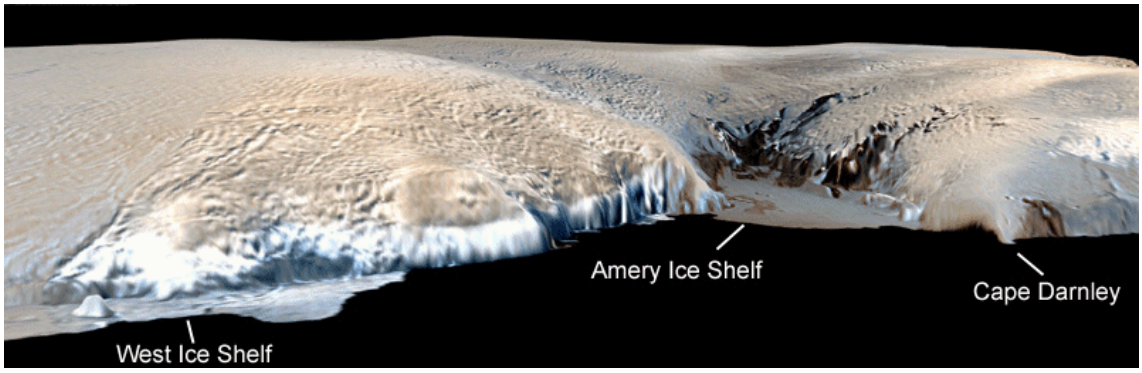

Figure 2.14 – Multispectral Composite Image over DEM to give a perspective view of the AIS (looking south), showing the relative ice (exaggerated) accumulation behind and around the AIS (USGS).

Ice reaches 2,500 m in thickness in the Lambert Graben, decreasing with distance north to about 900 m at the grounding line and 270 m at the shelf front. In all other areas, the ice becomes thicker inland to a maximum of about 3,000-3,500 m at the margins of the drainage basin near the Ice Divide. Figure 2.15 displays both surface elevation contours and ice thicknesses.

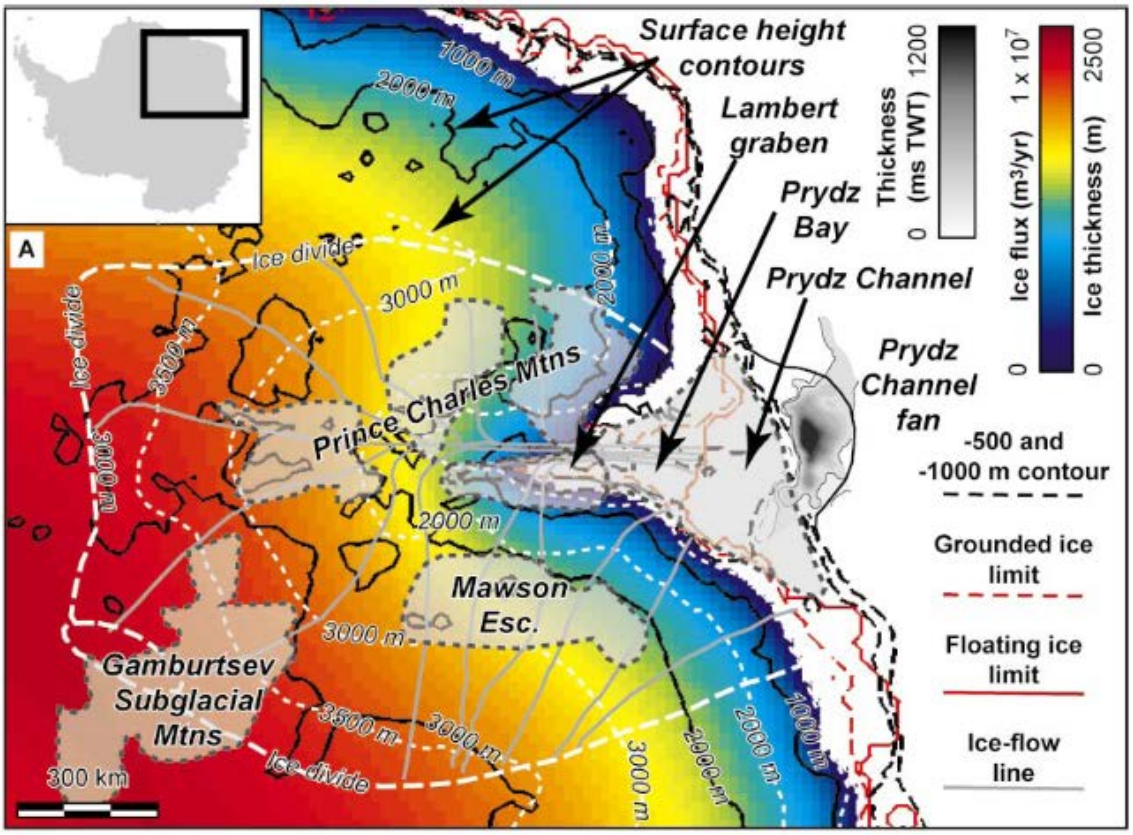

Figure 2.15 – A two dimensional model representation of present ice extent and thickness (Taylor et al., 2004, Fig 1a). Limits and offshore contours are from Lythe et al. (2000); ice flowlines, ice divide, and white height contours are adapted from Hambrey et al. (1991). Also shown are post–late Miocene isopachs from O'Brien et al. (2001), based on surface A of Mizukoshi et al. (1986). Thickness refers to two-way traveltime of seismic waves through sediment in milliseconds (ms TWT). Inset shows location of study area.

The Lambert Glacier has a freeboard of ~90 m above sea level (asl) as it crosses the southern grounding line and joins the AIS. The Lambert Glacier decreases gradually from 1,000 m to 800 m thickness over the southern grounding zone where it begins to float (Morgan & Budd, 1975). The ice then thins quickly to 450 m thickness by the time it reaches G1, 62 km inland from the ice shelf front, and decreases further to 270 m by the ice shelf front (Morgan, 1972; Morgan & Budd, 1975).

2.5.2 Ice draft of the Amery Ice Shelf

Surface elevations and ice thicknesses have been measured over much of the AIS area using satellite radar altimeter and radio-echo sounding (Fricker et al., 2002a; Fricker et al., 2000a). The ice draft of the AIS was calculated by Galton-Fenzi (2008) by subtracting the elevation of the surface of the ice shelf from the ice thickness data of Fricker et al. (2002a; 2000a). This resulted in the continuous ice draft map that is shown in Figure 2.16. As part of his study of the ice draft, Galton-Fenzi (2008) found that the southernmost grounding line of the AIS is deeper than previous BEDMAP estimates by approximately 450 m (Lythe et al., 2000), making it one of the deepest grounding lines of any ice shelf. Galton-Fenzi (2008) states the ice draft in the southern grounding zone is 1,600 m deeper than that used in studies by Williams et al. (2001), having major implications for the amount of melting that is possible in this region. Figure 2.16 shows the ice draft in the central region of the AIS that is relevant to this thesis lies within the range 400-800 m thick.

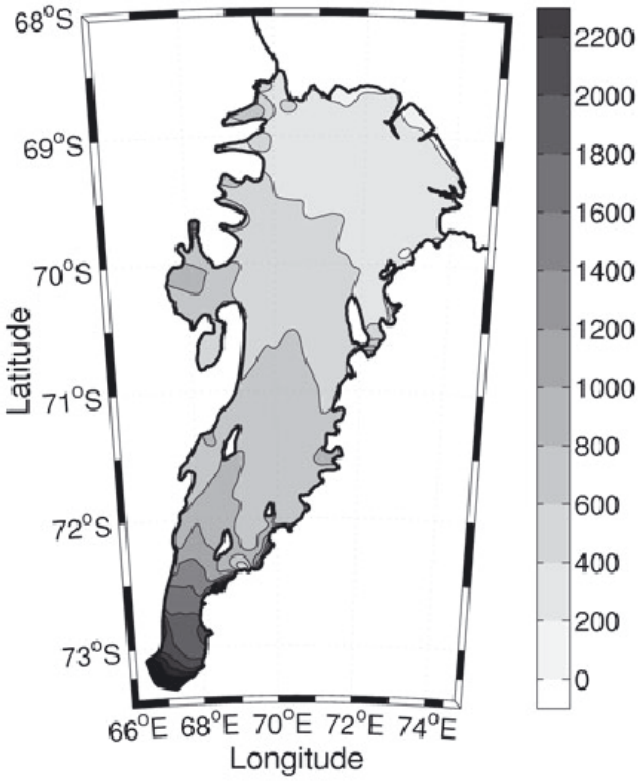

Figure 2.16 – Ice draft of the AIS showing 200 m contour intervals (Galton-Fenzi et al., 2008, Fig 2)..

2.5.3 Marine ice thickness

The presence of a significant hydrostatic anomaly in the northwest quadrant of the AIS has been attributed to an extensive layer of marine ice (Allison, 2003; Fricker et al., 2001). Radio echo soundings (RES) have been used to measure the thickness of the glacial ice, but this thickness cannot account for the total mass balance of the ice shelf, i.e. “the ratio of surface elevation to the measured thickness is not what is expected for floating ice” (Allison, 2003). RES surveys can only pick up meteoric ice, since the signal cannot penetrate marine ice due to the presence of conductive brine (Blindow, 1994). The likelihood that the marine ice-water interface of an accreting ice shelf may also be gradational at radar wavelengths and rates of attenuation (Blindow, 1994; Englehardt & Determann, 1987) may prevent a sharp reflective interface using RES (Janssen & Hurd, 2008).

Therefore, using only RES data to calculate ice thickness resulted in an unexpected ratio of surface elevation to the measured thickness of the ice. Fricker et al. (2001) calculated the thickness of marine ice from this anomaly. Figure 2.17 displays the distribution of marine ice under the AIS calculated using this method. A maximum thickness of 190 m for the accreted marine ice was predicted (Fricker et al., 2001), occurring in the western part of the shelf under the NW AIS Unit (Figure 2.6). This thickness generally decreases towards the east, with a zero modelled-thickness for most of the eastern half of the AIS.

Since this model was created, marine ice has been observed in ice cores and seen in down-hole video taken at AM01, AM04 and AM05 on the AIS, but it has not been observed at AM02, AM03 and AM05 (Craven et al., 2009; Craven & others, 2005; McMahon & Lackie, 2006; Treverrow & Donoghue, 2010; Treverrow et al., 2010). These physical sightings match the distribution model except at AM03 (G2A on Figure 2.17) where no marine ice was observed in summer 2005/06 despite the model showing a thickness of 20 m at this location and up to 40 m nearby. G2A was surveyed using the seismic technique in 2002/03 with the aim of delineating the marine ice layer, whose presence there had been expected due to Fricker et al.’s (2001) model. A thin <20 m

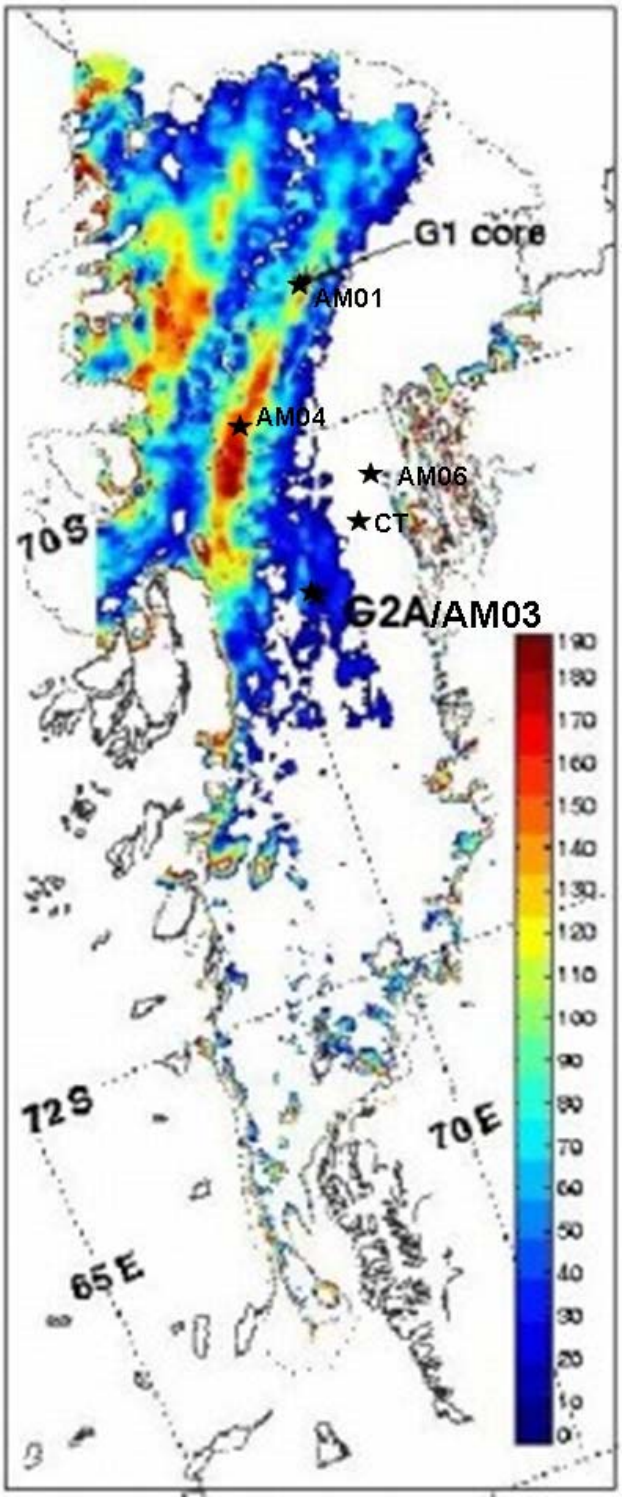

Figure 2.17 – Distribution of thickness of marine ice accreted under the northwestern segment of the AIS (in metres) (after Allison, 2003, Fig 2). The other regions around the margin of the shelf are where hydrostatic equilibrium is not satisfied; this is where the ice is grounded, not an accretion of marine ice, and instead approximates the grounding line location.

layer was observed in the seismic record at the base of the ice shelf and was interpreted as a marine ice layer (McMahon, 2003; McMahon & Lackie, 2006). However the absence of visible or measurable marine ice at the same location three years later tends to indicate that the observed layer was most likely not marine ice. It is unlikely that close to 20 m of ice would melt in three years; however it is possible the seismic response was due to a layer of semi-consolidated frazil ice sitting at the base of the ice shelf (Mike Craven, Pers. Comm.). The marine ice modelled here may be due to a larger area where hydrostatic equilibrium was not satisfied, such as what produced the modelled marine ice thicknesses around the margin of the AIS (Fricker et al., 2001).

2.5.4 Strain, stress and anisotropy

Ice crystals upon deposition and compaction naturally form a layered structure. The molecular bonds in the ice crystal are easy to break when deformed under shear stress. Under a given amount of stress, they will tend to rotate until they can deform in the easiest possible way – by sliding along these pre-formed layers (Pettit et al., 2005). In this way ice crystal *c*-axis orientations become realigned when placed under strain. See Figure 2.18.

In grounded ice sheets the ice undergoes both vertical compression and bed-parallel shear (Pettit et al., 2005). The ice crystals tend to rotate until their *c*-axes become vertically oriented, and due to this vertical nature, the way to describe the degree of anisotropy of the ice is to use a “cone angle” representing a statistical distribution of crystal orientations (Figure 2.19). Ice that is initially isotropic has a cone angle of 90°, as it becomes more strongly anisotropic, its cone angle decreases. The time required for a block of ice to go from isotropic to strongly anisotropic depends on factors such as temperature, strain history, grain size, and impurity content of the ice (Pettit et al., 2005).

In terms of ice streams merging and then forming a floating ice shelf, the ice within narrow marginal zones where two ice streams merged would undergo horizontal compression. This theoretically results in a horizontal alignment of crystals, which should be measurable with the seismic technique (Udías, 1999; Yilmaz, 2001).

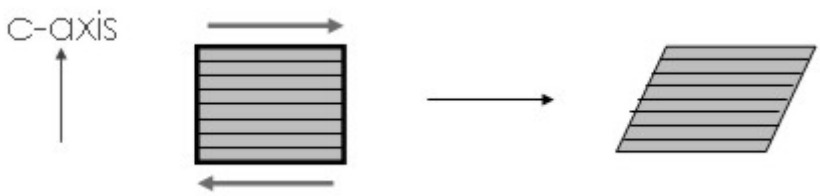

Figure 2.18 – Diagram showing the deformation of an ice crystal under strain (Pettit et al., 2005).

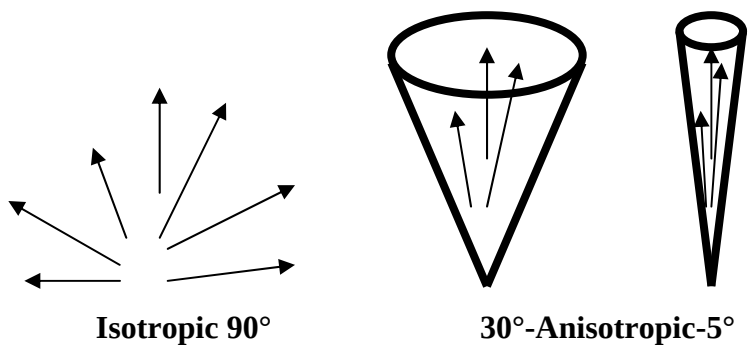

Figure 2.19 – Diagram of the orientation of c-axes of ice crystals becoming aligned (Pettit et al., 2005)

The total strain due to the longitudinal deformation from one position to another can be estimated from the difference in surface velocity (Budd, 1972; Budd & Jacka, 1989).

A map of the strain present in AIS ice has been produced by Young & Hyland (2002), using the analysis of two RADARSAT Synthetic Aperture Radar (SAR) images to first produce a velocity map over the entire surface of the AIS, then converting this to strain rate. Maps of the vertical and shear strain rate over the entire AIS are shown in Figure 2.20. The vertical strain rate varies with distance from the southern grounding line (or conversely, proximity to the ice shelf front), whereas the shear strain rate is closely aligned with flow and has higher values at the ice shelf margins.

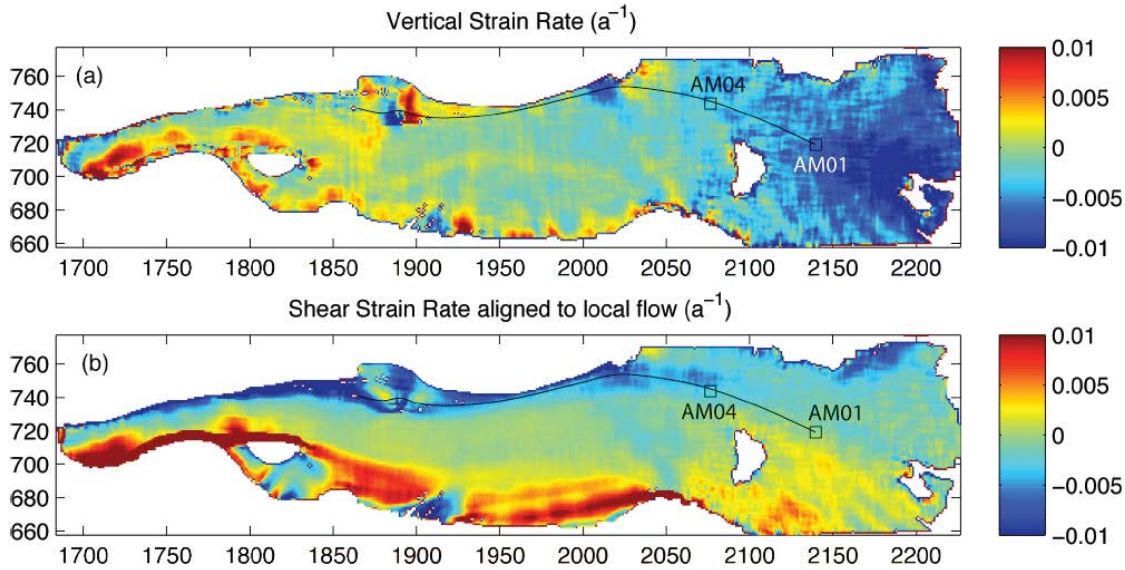

Figure 2.20 – Amery Ice Shelf strain rates calculated using the InSAR-derived surface velocities of Young & Hyland (2002). The AM01 and AM04 boreholes and the approximate flowline passing through the two sites are indicated. (a) Vertical strain rates. Negative values (blue) indicate compression. (b) Shear strain rates, $\dot{E}_{xy}$, are aligned to the local flow direction. As Amery Ice Shelf velocities are highest near the centre of the shelf and decrease towards the margins, the sign of the transverse shear strain rate, $\dot{E}_{xy}$, changes across the shelf. Horizontal and vertical axes indicate distance from the geographic South Pole (Treverrow et al., 2010).

2.5.5 Ice fabric

The northwestern sector of the AIS has a layered structure, due to the presence of both a meteoric ice and marine ice layer resulting from sub-shelf freezing processes (Treverrow et al., 2010). Marine ice found at AM01 and AM04 by AMISOR was discovered to be porous – the discovery was made during drilling when the pressure sensor in the well indicated a hydraulic connection with the ocean cavity whilst the drill head was 70-100 m above the true base of the ice shelf (Craven et al., 2007). This lower 70-100 m of marine ice displayed honeycomb structure, made up of welded ice platelets with interstitial sea water filling progressively larger cavities as the base of the ice was approached. The permeable nature of these sea-water filled pores makes this part of the ice shelf vulnerable to any increases in water temperature, which would more easily

melt this porous ice (Craven et al., 2007). An example of AIS brine included ice is shown in Figure 2.21.

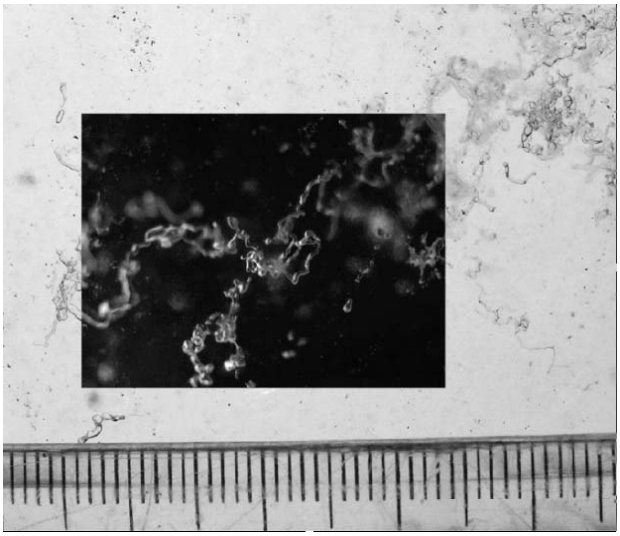

Figure 2.21 – Marine ice sample showing brine inclusions; from AM04 sample AM04-450a, 80 m above the hydraulic connection depth. The image is a composite created from transmitted light and plane-polarised light (the dark inset) through the same core section. Elongated sinuous centimetre length inclusions are evident. Scale: gradations at base of image are mm (Treverrow et al., 2010, Fig 13).

Marine ice accretion is likely to start with the formation of frazil ice within the water column. Frazil ice is a disc-shaped crystal formed during the freezing process, typically 1-4 mm in diameter and 1-100 μm thick (Jenkins & Bombosch, 1995). For initial nucleation of frazil ice, Jenkins and Bombosch (1995) propose a mechanism of mass exchange at the ice-ocean interface. As the cavity water becomes supercooled, freezing commences directly onto the base of the ice shelf, as dendrites (see Figure 2.22 for a laboratory controlled experiment in growing saline ice). These may break off and become the nucleus of other ice crystals, or nucleus material may be provided from fracturing of the ice shelf – so frazil ice forming in that situation is most likely where there is basal crevassing present.

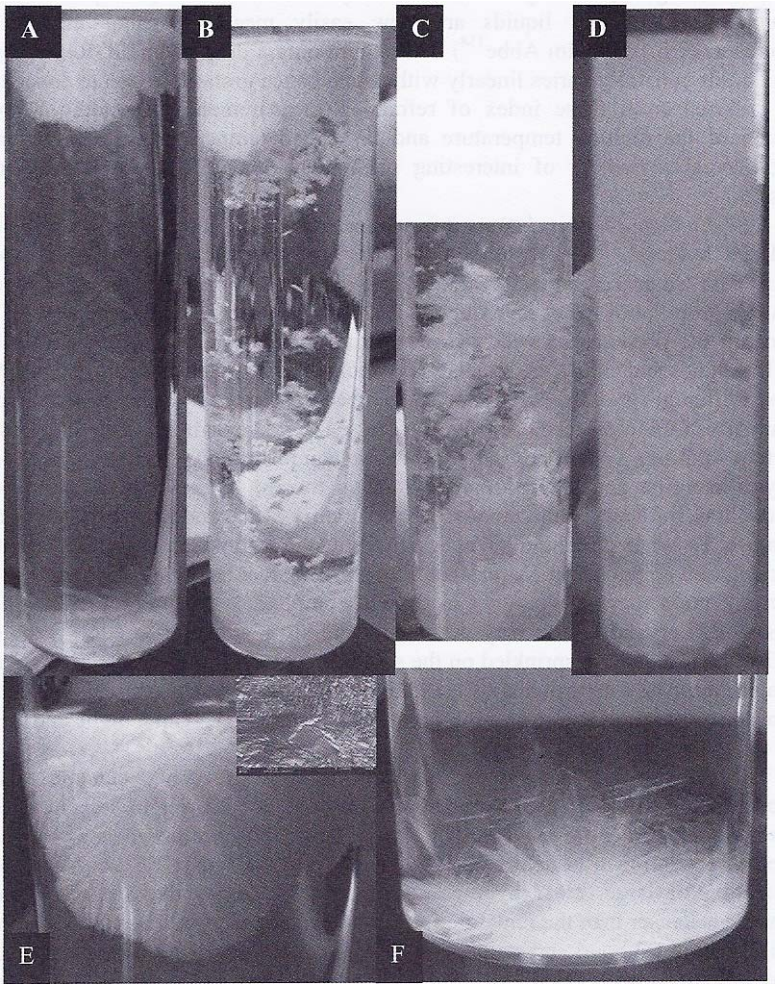

Figure 2.22 – A lab demonstration of the process of freezing saline water: An analogy for frazil ice formation, for the NaCl/H2O system. A saturated salt solution was held at 247 K for about 1.5 hrs before initial crystallization of large, clear hydrohalite began at the bottom of the tube (e-f). (a) At 1.7 hrs: crystallization of eutectic intergrowth of ice and hydrohalite began to occur at the top and tube walls, and (b-d) then grew downward and inward. The intergrowth exhibits radial cellular growth from original point of nucleation (Kirby, 2007, Fig 2).

Marine ice fabric is different from meteoric ice due to differences in deposition, composition and flow history. Interpretation of anisotropic marine ice fabrics is complicated by the combined effects of the accretion mechanism, inclusion content and complex stress configurations. The presence of multiple-maxima crystal orientation fabrics and large mean grain sizes in the meteoric ice indicate stress relaxation and

subsequent grain growth in AIS ice (Treverrow et al., 2010). Strongly anisotropic single-maximum crystal orientation fabrics and rectangular textures near the base of the approximately 200 m thick marine ice layer suggest accretion occurs by the accumulation of frazil ice platelets (Treverrow et al., 2010). In older marine ice (i.e. marine ice no longer at the ice shelf base but higher up in the ice shelf) the crystal orientation fabrics exhibit vertical large circle girdle patterns, influenced by the complex stress configurations that exist towards the margins of the ice shelf. Any subsequent grain growth and fabric development in the marine ice layer is restricted by the high concentration of brine and insoluble particulate inclusions. Differences in the meteoric and marine ice crystallography are indicative of the contrasting rheological properties of these layers, which must be considered in relation to large-scale ice-shelf dynamics (Treverrow et al., 2010).

2.5.6 Melting and freezing: mass gain or loss from the AIS

Melt and refreezing processes on the underside of the floating ice shelves can be significant (Allison, 2001). The AIS undergoes high basal melt rates near the southern limit of its grounding line, and recent estimates have it that 80% of the ice melts within 240 km of becoming afloat (Craven et al., 2009). This is a significant increase to the estimate made by (Allison, 2001) that 50% of the total ice draining from the Lambert Glacier system is lost as melt beneath the AIS.

As mentioned in Section 2.1.1, cold water flows under the AIS and comes into contact with the base of the ice where pressure means it is above the local freezing temperature and basal melting can occur. The water melted from the base of the ice decreases the salinity of the seawater it mixes with, and this new layer of fresher water is more buoyant than the colder more-saline water and it flows upwards under the shelf, travelling northwards towards the ice shelf front. In the NW AIS region, the water reaches a point where it is below the local freezing temperature again and new ice crystals nucleate forming a layer of frazil ice, which may then adhere to the base of the ice shelf as a layer of marine ice (Allison, 2001). As it freezes, this ice traps particles and pockets of brine, and grows with a plate structure, very different from the meteoric ice it adheres to.

The horizontal distribution pattern of melting and freezing under the AIS is controlled by the clockwise ocean circulation. The ocean water from Prydz Bay enters under the AIS in the eastern half of the ice shelf, coming out again at the ice shelf front at the western side of the AIS (Allison, 2002; Williams et al., 2001; Williams et al., 2002).

Figure 2.23 gives an estimation of mass gains or losses in different segments of the AIS-LG system. Inland, the grounded ice sheet has a slight mass gain (blue arrows) until it nears the grounding zone where is begins to undergo a small mass loss (red arrows). Under the AIS there is greater mass loss proximal to the grounding zone where substantial basal melt occurs. This rate of loss decreases then slightly increases again nearer to the front of the shelf. There is an overall net loss from this basal melting but there are also areas in the north-west of the shelf where refreezing onto the base occurs (not shown in the figure).

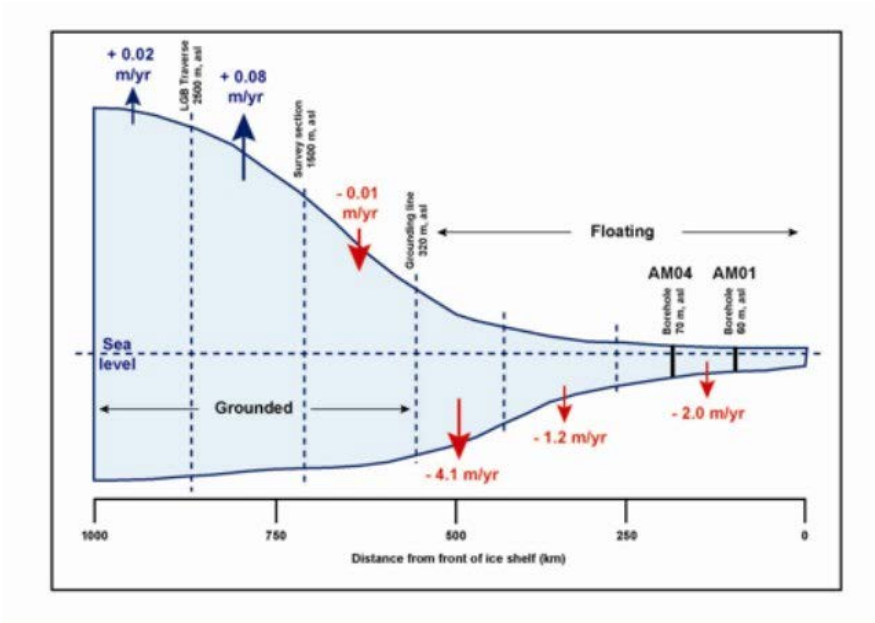

Figure 2.23 – A schematic section through the Lambert Glacier drainage basin from the centre of the ice sheet, including the 550 km of floating ice. The dotted vertical lines are elevations derived from Australian field observations. The state of balance of different parts of the system has been estimated; blue = gain, red = loss. (Stoddart, 2008).

Figure 2.24 is a thickness profile through part of the ice shelf based on physical depth measurements. An analysis of mass balance along the AM04–AM01 flowline by

Craven et al. (2009) indicates that the 207 m marine ice layer at AM04 would be reduced in thickness to 113.9 m by strain thinning as it flowed to AM01. As the measured marine ice thickness at AM01 is 203 m, an additional 89.1 m of ice must be added between AM04 and AM01 (Craven et al., 2009; Treverrow et al., 2010). Because ice accumulated upstream of AM01 is also subject to strain thinning, the total accumulation between AM04 and AM01 is estimated to be 118.1 m, with an average annual accumulation rate of 1.16 m a^{-1} (Craven et al., 2009). Thus, more than half of the marine ice layer present at the AM01 site is accreted downstream from AM04 (Treverrow et al., 2010).

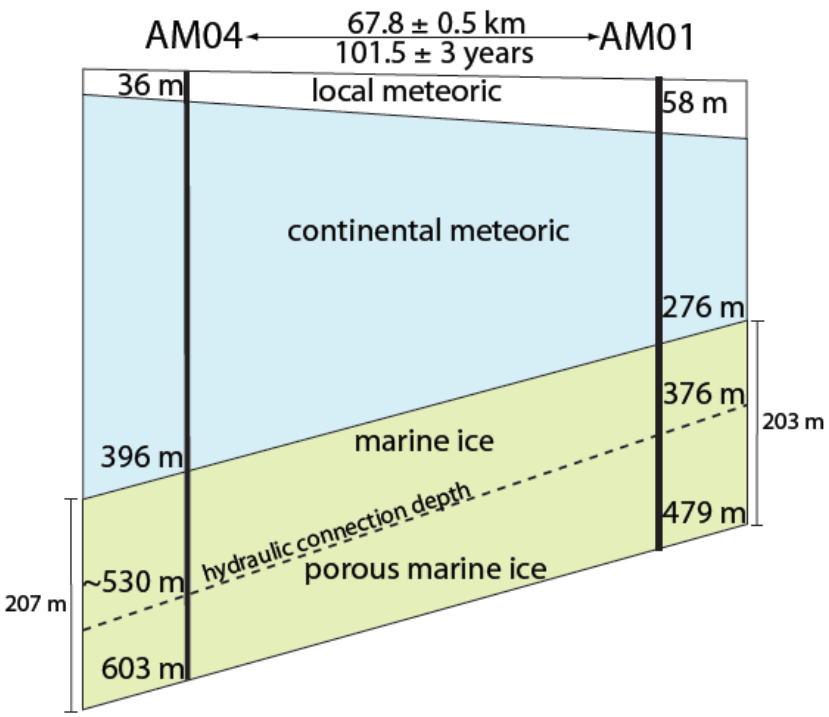

Figure 2.24 – A schematic thickness profile through the AIS following the flowline from the AM04 to AM01 drill hole (North to the right). Depths and thicknesses are as measured in the boreholes; distance is accurate and age difference is calculated from average surface ice velocities (Treverrow et al., 2010).

2.6 The Ocean Cavity

2.6.1 Bedrock topography/bathymetry beneath the Amery Ice Shelf-Lambert Glacier system and Prydz Bay

The bathymetry of Prydz Bay is characterized by a deepening coastward trend from depths of about 500 m at the continental shelf break to over 1000 m in some places near the coast (Hambrey, 1991). This forms what is known as the Amery Basin. In the outer parts of the bay lie a number of banks, of which the most prominent is the Four Ladies Bank, located in the northeast. It rises to within 200 m of sea level and is scoured by icebergs. Prydz Bay is transversed by the Prydz Channel, a broad channel that crosses the bay and reaches the continental shelf edge at the head of a large trough mouth fan. Subglacial topography is known broadly from radio-echo soundings (Drewry, 1983). The deep Lambert Graben is surrounded by high ground to the west, east and south. From the front of the Amery Ice Shelf, the Amery Basin deepens progressively to the south under the ice shelf and the Lambert Glacier, reaching a depth of at least 2500 m below sea level (Hambrey, 1991). Figure 2.25 shows a bathymetry model under the AIS and in Prydz Bay, produced from ocean cavity modelling of the AIS.

The Lambert Graben is bordered to the west by exposed rock of the PCMs, with several tributary trenches cutting through these mountains. The eastern margin is contained by a largely continuous straight escarpment rising to over 1000 m above sea level, and outcrops to the south as the Mawson Escarpment. Taking into account the ice thickness, the true relief of this area is approximately 3000 m. East of the Mawson Escarpment, magnetic data (Federov et al., 1982) indicates the presence of a branch of the main graben. It is mostly sediment filled, acting as a drainage route for ice from the Grove Mountains. The Grove Mountains extend above the ice as nunataks 1000-1500 m high.

At the head of the Lambert Graben, a north-northwest trending subglacial mountain mass, serves as a ridge to either side of which the ice flow is directed. Penetrating the PCMs and the Grove Mountains (72.75ºS, 75ºE) are feeder branches of the Lambert Graben, but apart from a general movement of ice into the Lambert Graben, ice surface flow is not strongly controlled by bedrock irregularities (Hambrey, 1991).

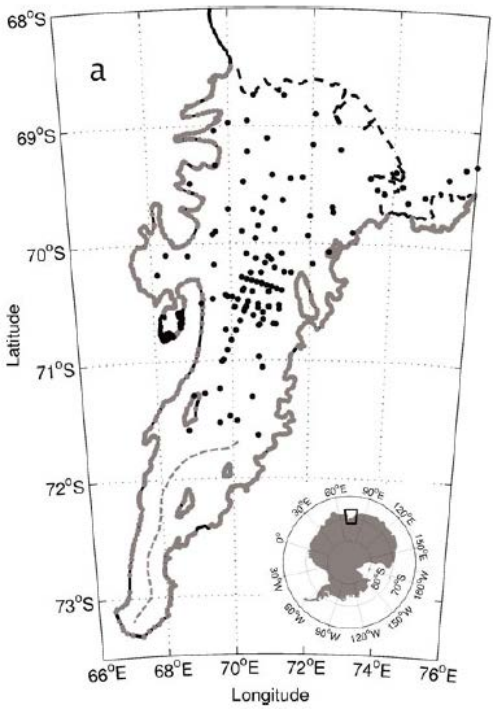

(a)

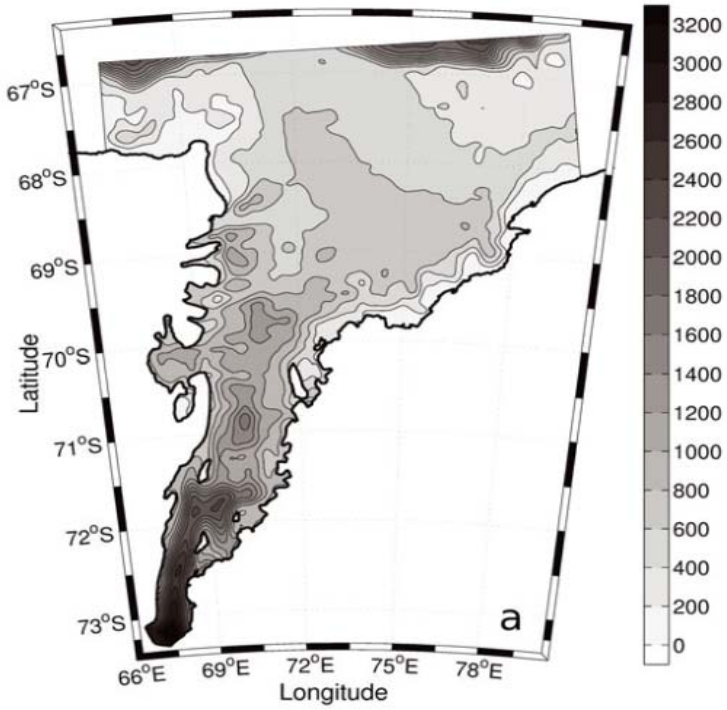

(b)

Figure 2.25 – (a) The bathymetry data used in Galton-Fenzi et al.'s (2008) AIS ocean cavity interpolation (includes seismic locations), (b) Bathymetry of the AIS and Prydz Bay regions showing 200 m contour imtervals (Galton-Fenzi et al., 2008, Fig 1a & Fig 5a).

2.6.2 The Amery Ice Shelf ocean cavity

Depth profiles under the AIS have been produced from ocean circulation models by Hunter et al. (2004), Hemer et al. (2006) and more recently by Galton-Fenzi et al. (2008). Hunter et al. (2004) used the Princeton Ocean Model to model the AIS, since it has a free-surface and can therefore represent tides. According to Hunter et al. (2004) the AIS has a mean draft of 700 m and an average water column thickness of 230 m.

Hemer et al.'s (2006) cross section through the AIS displaying ice draft and bathymetry models is shown in Figure 2.26(a). Galton-Fenzi et al. (2008) updated the depth model using depths gained from recent drilling and seismic results. A profile through the ice shelf was trialled, similar to the Hemer et al. (2006) model as displayed in Figure 2.26(a) – the results of this are shown in Figure 2.26(b). The difference between the bathymetry model of Galton-Fenzi et al. (2008) and Hemer et al. (2006) is shown in Figure 2.27. The major areas of difference between the models are in the centre of the AIS between the Budd Ice Rumples and Clemence Massif and in the southern grounding zone, where the differences are up to 1100 m. Figure 2.27 displays a bathymetry model difference between the Hemer et al. (2006) model and Galton-Fenzi et al. (2008) model of approximately 100-300 m over the majority of the ice shelf.

Figure 2.26 (opposite) – (a) Zonally averaged bed elevation for the cavity of the four model topographies. Dashed line = topography A; solid line = topography B; dash-dotted line = topography C; dotted line = topography "CADA". Filled section represents the zonally averaged ice draft. (Hemer et al., 2006, Fig 2). (b) Vertical sections along North-South transect as shown in the inset in (b) (Galton-Fenzi et al., 2008, Fig 3a) – Ten possible bathymetries are shown, with black dashed line indicating the best estimate. Each estimate was created by varying the thickness of the water column in the southern sector of the AIS. The vertical black line in (b) and (c) shows the intersection of the two transects

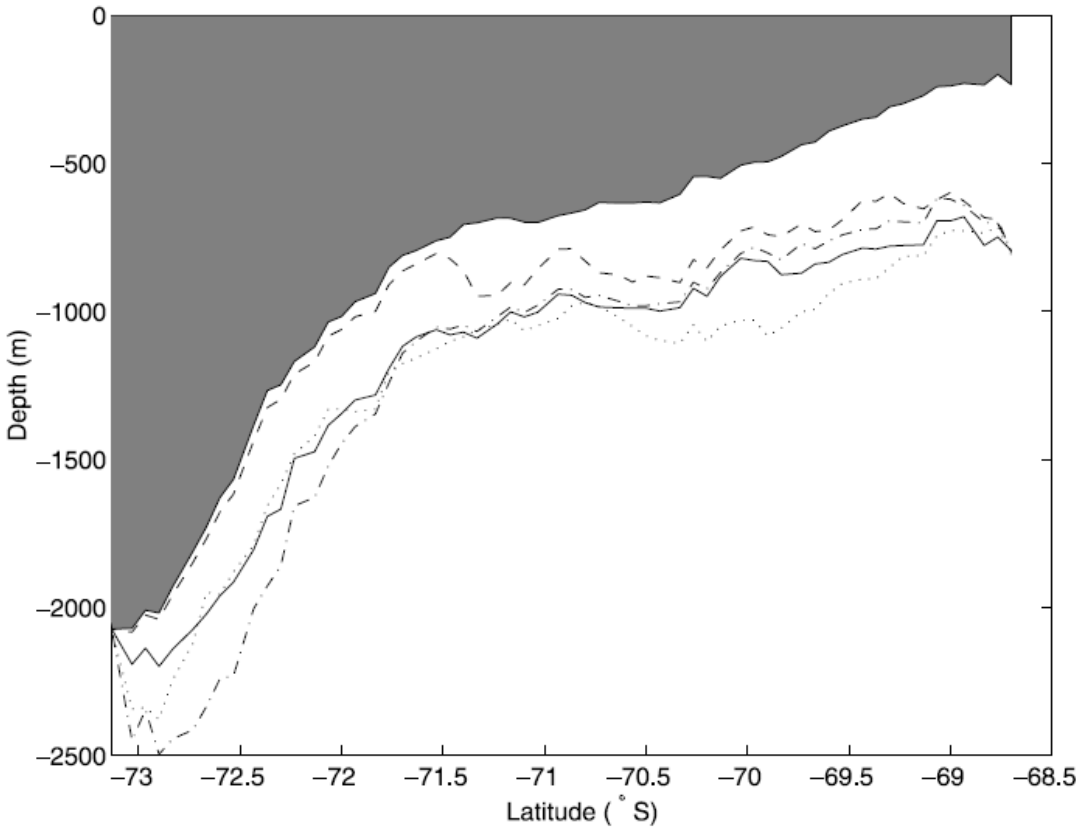
0
−500
−1000
−1500
−2000
−2500
Depth (m)
−73
−72.5
−72
−71.5
−71
−70.5
−70
−69.5
−69
−68.5
Latitude (˚ S)

(a)

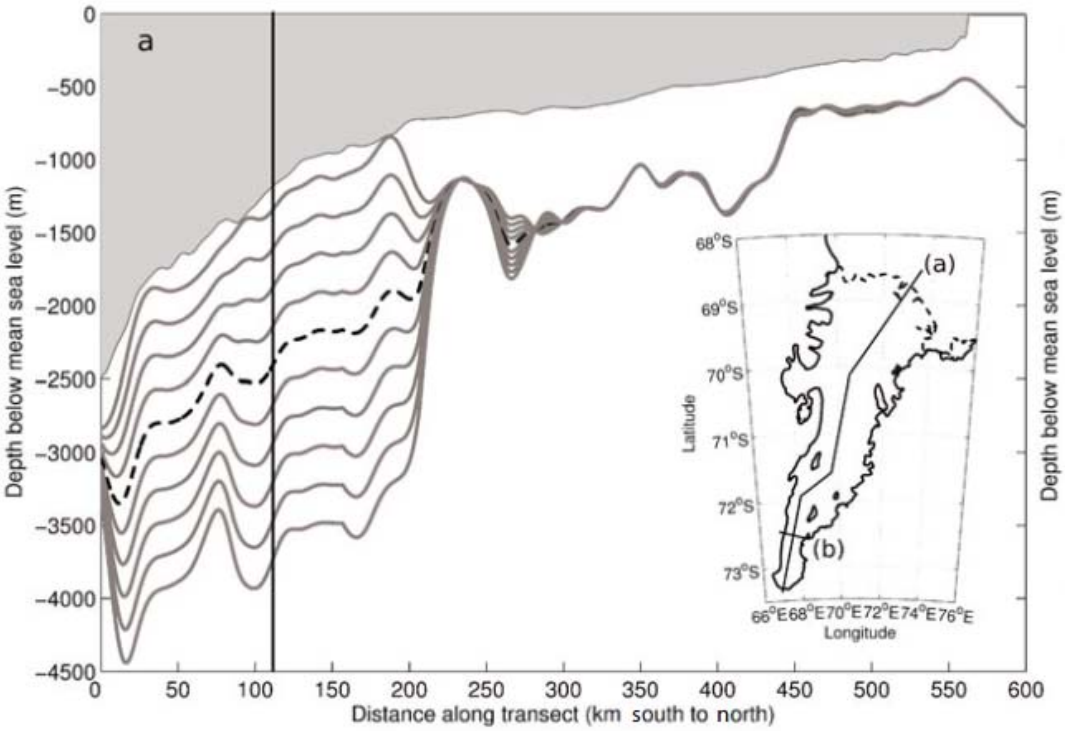
a
Depth below mean sea level (m)
0
−500
−1000
−1500
−2000
−2500
−3000
−3500
−4000
−4500
0
50
100
150
200
250
300
350
400
450
500
550
600
Distance along transect (km south to north)
68°S
69°S
70°S
71°S
72°S
73°S
Latitude
(a)
(b)
66°E68°E70°E72°E74°E76°E
Longitude

(b)

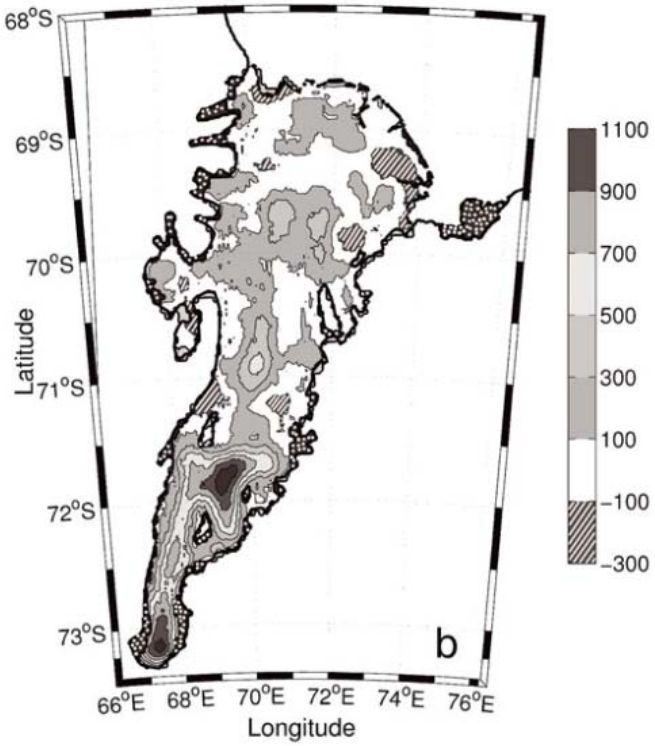

Figure 2.27 – The difference between Galton-Fenzi's 200 m contoured bathymetry model (Figure 2.26(b)) and Hemer et al.'s (2006) bathymetry model. The area used by Galton-Fenzi et al.'s (2008) model alone is shown in spotted dark grey; the area used by Hemer et al.'s(2006) model alone is shown as light grey (e.g. some regions near the grounding line such as in Beaver Lake) (Galton-Fenzi et al., 2008, Fig 5b).

Directly comparing the cross sections of Hemer et al. (2006) and Galton-Fenzi et al. (2008), the ice draft at the southern grounding line is deeper in Galton Fenzi et al.'s (2008) model by ~400 m, although it decreases in thickness over 0-150 km more quickly than Hemer et al's (2006) model. The ice shelf base from this point forward is of similar thickness in both models. North of 150 km from the southern grounding line the best-fit bathymetry of Galton-Fenzi et al. (2008) is smoother and more detailed, and is shallower in the northern part of the AIS. Galton-Fenzi et al.'s (2008) modelled bathymetries from ~275 km northwards all plot in approximately the same depths, and display more bathymetric variation than Hemer et al.'s (2006) model. Both models display ~200 m deepening just north of the southern grounding line. Hemer et al.'s (2006) ocean cavity thickness model based on the modelled "topography B" bathymetry is shown in Figure 2.28.

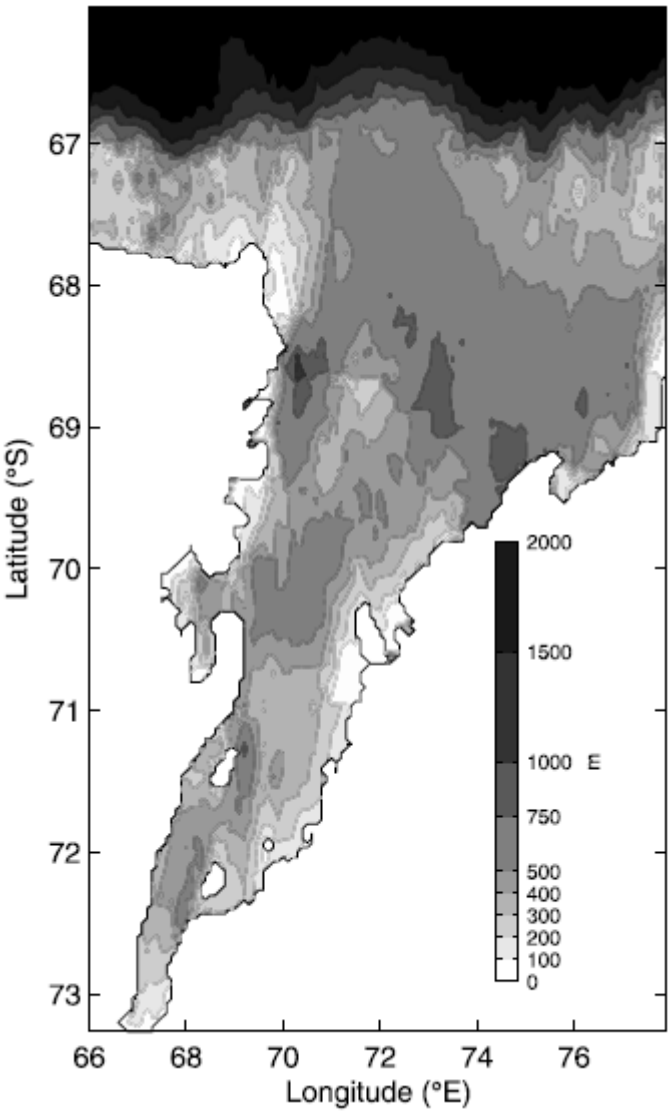

Figure 2.28 – AIS water column thickness (m) for Topography B (Hemer et al., 2006, Fig 3)

2.7 Ocean Circulation and Sediment Deposition

2.7.1 Prydz Bay

It is possible to make inferences concerning the origin and nature of sediments on the continental shelf off the front of the Amery Ice Shelf by looking at glaciological parameters (Hambrey, 1991). The most important flow units in this situation are those of the Charybdis and Mellor glaciers, and the Mawson Escarpment ice stream. Each represents about 20% of the mass flux of the AIS if measured through a profile perpendicular to the ice shelf front. Ice from the southern PCMs and the interior basin

only makes up about 42% in total. Therefore the dominant sources of ice that reach Prydz Bay are from the northern areas, which reflects a greater deposition of sediment towards the coast and erosion further south in the Lambert Glacier system (Hambrey, 1991).

According to Hambrey (1991) depositional processes are basically influenced by the thermal nature of the shelf. Although there is a considerable amount of basal melting at the grounding zone, marine ice also begins to freeze onto the base of the ice shelf. At the calving limit of the ice shelf, marine ice makes up about 40% of the thickness of the ice (Hambrey, 1991; Morgan, 1972). Thus, englacial debris that is not melted out at the grounding zone will not be released until icebergs break off from the front of the shelf, disintegrate and release their sediment load. Icebergs drift west along the Antarctic coast; hence much of the debris from the Lambert Glacier system is probably deposited anywhere up to hundreds of kilometres west of Prydz Bay. By the same token, the sediment being deposited in Prydz Bay today may have originated further east (Hambrey, 1991).

The sediments of the continental shelf beyond the Amery Ice Shelf are mainly of continental provenance in the inner region and terrestrial-marine glaciogenic in the outer regions (Hambrey, 1991). These sediments would have been derived from the hinterland of Prydz Bay. The sedimentary clasts and matrix of Prydz Bay diamictite units originate from a sequence that must have been much more extensive than the presently small outcrop of Permian rocks at Beaver Lake (Hambrey, 1991). The over-deepened Lambert Glacier trough (now ice filled) was the main source of sediment.

Drilling programs have been run in Prydz Bay to determine sediment thickness and sediment type. This includes the Ocean Drilling Program (ODP) Legs 119 and 188 (location of ODP Sites are shown in Figure 1.1). At Site 740 of Leg 119, seismic studies show the basement rock occurs at ~1880 ms, and this is likely to be eroded metamorphic rocks (Cooper et al., 1991). A core was drilled 225.5 m deep, finding sandstones and siltstones overlain by diatom ooze (Hambrey, 1991). Sediments in Prydz Bay have been dated to as far back as the Oligocene (Ehrmann, 1991).

Surface sediment grabs were taken from immediately in front of the Amery Ice Shelf during AMISOR voyages undertaken in 2000/2001 and 2001/2002. The locations for these are shown in Figure 2.29. From sediment properties collected at these sites – including grain-size, biogenic opal, and total organic carbon (TOC) – coupled with horizontal transport perpendicular to the ice front, it was observed that there must be a large ocean inflow east of 74°E in the eastern AIS cavity and there exists a return outflow between 72.8°E and 74°E (Hemer & Harris, 2003). On the western side, a broader but smaller inflow occurs between 71°E and 72.8°E, and a larger outflow west of 71°E is observed.

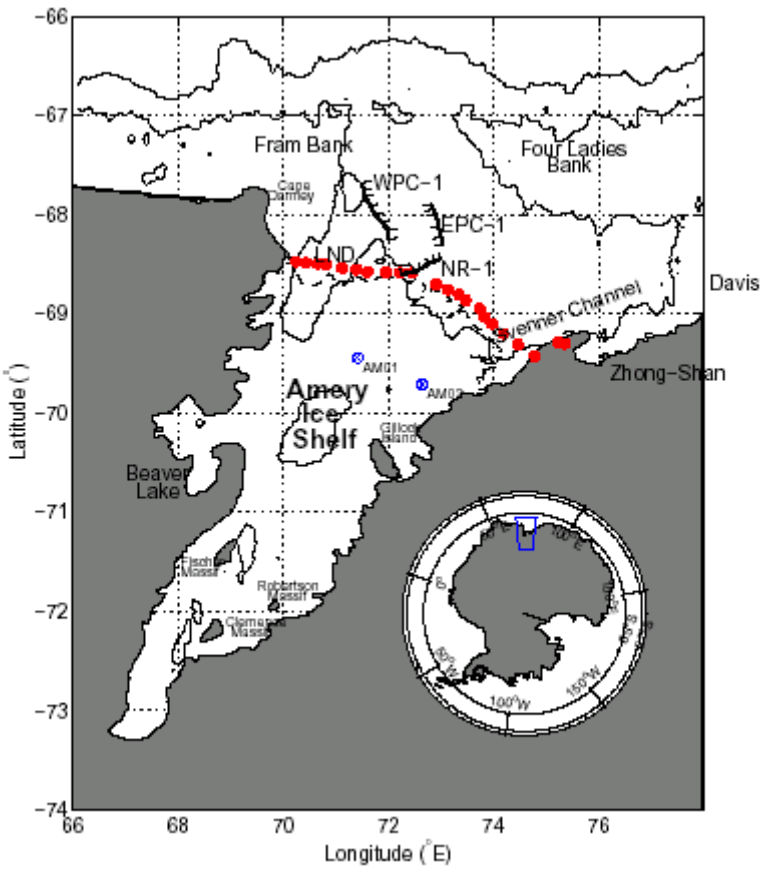

Figure 2.29 – The location of 23 surface grabs from adjacent to the ice shelf front (•) and location of the AM02 and AM01 sub-ice-shelf core sites (⊗) (Hemer & Harris, 2003, Fig 1)

2.7.2 The Amery Ice Shelf cavity

AMISOR drilled two holes through the AIS to collect sediments; at AM02 and AM01. From AM02, a 144 cm sediment core was retrieved (core log displayed in Figure 2.30), and at AM01, a surface sediment grab sample was obtained.

The AM02 core contains a continuous record of glacial retreat (Hemer & Harris, 2003). The surface unit is a 50 cm thick Holocene layer of siliceous mud and diatom ooze (SMO) of marine origin. This is underlain by a rapidly lain diamicton and waterlain till. The SMO unit gives evidence for Holocene deposition beneath the ice shelf, and so implies transport of marine sediments landward. From the numerical ocean model results of Hunter et al. (2004), AM02 is thought to be in an area of inflow and basal melt, and AM01 is thought to be in an area of outflow and basal freeze. This would suggest there is a clockwise circulation of waters under the AIS.

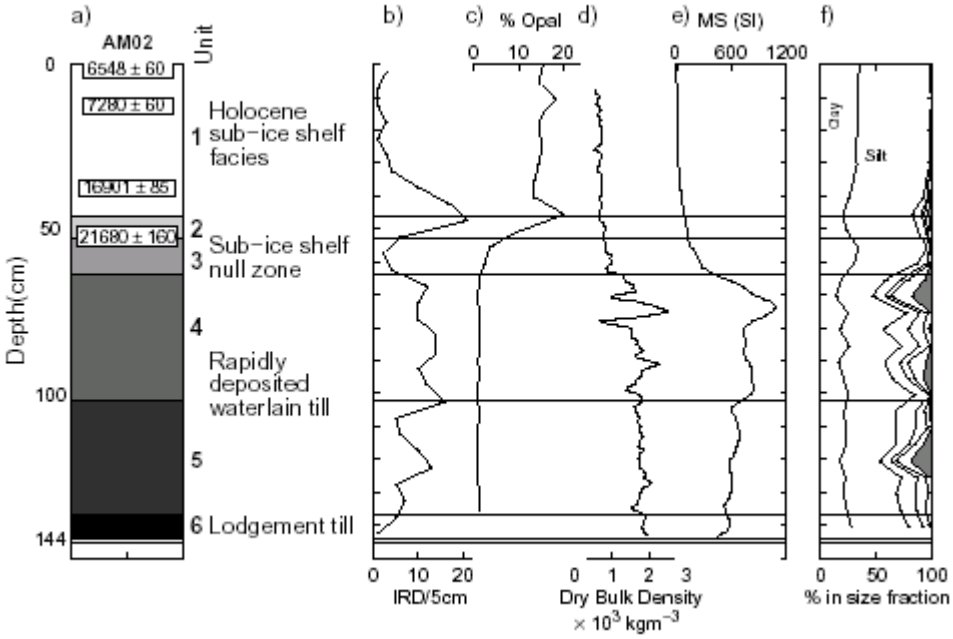

Figure 2.30 – Visual AM02 core log and down core profiles. (a) Core log. Numbers are uncorrected radiocarbon dates with errors. (b) Ice-rafted (gravel) debris count. (c) % Biogenic opal per dry weight sediment. (d) Dry Bulk Density (kgm^{-3}). (e) Magnetic Susceptibility (MS). (f) Grain size distribution of mud and sand fraction. Contours at 3.9, 62.5, 125, 250, and 500μm; component larger than 500μm shaded. (Hemer & Harris, 2003, Fig 2)

Chapter 3 METHODOLOGY

Numerous seismic surveys of varying types were carried out on the Amery Ice Shelf during the 2002/03, 2004/05, and 2005/06 Antarctic summer seasons as part of this project. All survey locations and some other sites of importance are shown in Figure 3.1. The survey type, geometry and methodology used to survey each location varied depending on the aims and purpose of investigation for each particular site. The acquisition values and line bearings of these seismic lines are detailed in Table 3.1.

The seismic program was led in the intermediary 2003/04 summer season by Hugh Tassell (then of the University of Tasmania); that work formed the basis of his honours thesis (Tassell, 2004). The data from the 2003/04 season will not be discussed or used in this thesis except in the context of previous work on the AIS, and in terms of observations made by Tassell (2004) in his thesis.

The surveys undertaken can be divided into the two main types used – refraction and reflection surveys. They can also be further subdivided into surveys undertaken to investigate different aspects of the AIS. For example, refraction surveys for the measurement of near surface ice properties (including P wave velocity, snow to ice transition and crystal fabric) and reflection surveys used for either ice shelf thickness measurements, structural investigations and mapping, or for comparison of changes over time. This chapter will explain the methodology used at the various sites surveyed on the AIS and separate data into the groups they will be discussed in later in this thesis.

3.1 Reflection CDP profile surveys

3.1.1 G2A – 2002/03 and 2005/06

A series of common-depth point (CDP) reflection surveys were carried out, the first in 2002/03 located halfway between the historical survey points G2 and G3, at a site

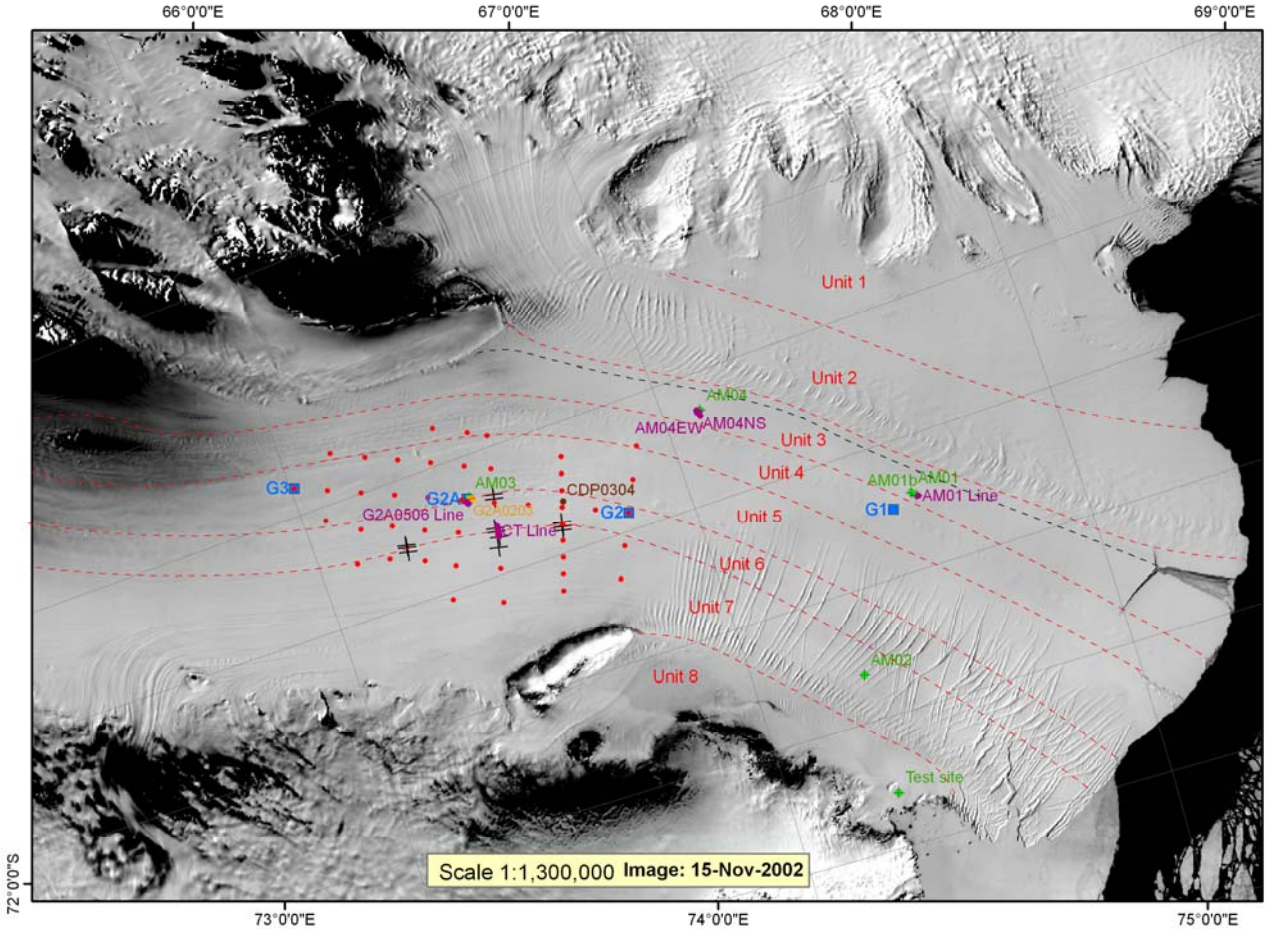

Figure 3.1 – Satellite MODIS image with flowline units outlined (labelled as per Figure 2.6) and locations of all sites and seismic surveys. Key: ■ G locations; ✚ AMISOR drillsites; ● Regional surveys; — G2A0203 Line; — G2A0506 Line, AM04 Lines, AM01 line, CT Line; ● CDP0304 (Tassell); ┼ Anisotropy surveys

Year Surveyed	2002/03			2004/05					2005/06			
Line Name	**G2A**	**Regional**	**Regional**	**AM01**	**AM01**	**Anisotropy**	**Camp Tropical**	**Regional**	**G2A**	**AM04 EW**	**AM04 NS**	**Regional**
Refraction/Reflection	reflection	refraction	reflection	refraction	reflection	refraction	reflection	reflection	reflection	reflection	reflection	reflection
Instrument	Strataview	Strataview	Strataview	Strataview	Strataview	Strataview	Strataview	Strataview	Geode	Geode	Geode	Geode
Total length surveyed	1.09 km	230 m	230 m	230 m	230 m	230 m	3.34 km	230 m	1.07 km	2.03 km	590 m	230 m
Line bearing (°mag)	085°-090°	085°	085°	166°	166°	086° & 176°	170-172°	176°	170	141°	051°	086?°
Line bearing (°true)	009°-014°	009°	009°	090°	090°	010° & 100°	094°-096°	100°	094°	065°	155°	010°
No.of Channels	24	24	24	24	24	24	48	24	24	24	24	24
Channel Spacing	10 m	10 m	10 m	10 m	10 m	10 m	10 m	10 m	10 m	10 m	10 m	10 m
Phone or Group	4	4	4	4	4	4	1	4	1	1	1	4
Recording Length	2048 ms	2048 ms	256 ms	256 ms	2048 ms	2048 ms	2048 ms	2048 ms	4096 ms	4096 ms	4096 ms	4096 ms
Sampling Rate	250 µs	250 µs	250 µs	250 µs	250 µs	250 µs	250 µs	250 µs	250 µs	250 µs	250 µs	250 µs
Acquisition Filters	None	None	None	None	None	None	None	None	None	None	None	None

TABLE 3.1 Acquisition values and Survey line orientations for all seismic surveys in 2002/03, and 2004-2006.

named G2A (Figure 1.1, Figure 3.1). The original survey geometry setup and results can be seen in McMahon & Lackie (2006) (Appendix A). Hereafter in this thesis this seismic line will be referred to as G2A0203.

This G2A site was reoccupied by both AMISOR and by the seismic project in 2005/06, however the G2A 2002/03 site had shifted northwards with the normal movement of the AIS. The new location of the "same ice" was decided upon in consultation with Mike Craven (ACE-CRC), calculated from the measured surface ice velocity of this area of the AIS (Budd et al., 1982; Young & Hyland, 2002). The ice of the original G2A seismic survey was re-occupied and drilled by AMISOR in December 2005; this they named the AM03 borehole. A seismic survey was repeated nearby the AM03 site soon after drilling ceased in the same season.

The G2A 2005/06 seismic survey was not carried out directly over the AM03 borehole site. The dataloggers, cables and mooring equipment left down through the AM03 hole by AMISOR created noise interference in the seismic records, and at the time the seismic survey was commenced (although not by the time it was finished) the AMISOR camp was still setup around the AM03 hole, including the drill tent right over the site. Regardless of signal interference from AMISOR downhole moored equipment, it would not be possible to use explosives near the campsite, and camp noise would have degraded the seismic signal even further. Hence, the G2A 2005/06 seismic line was located approximately 1.5 km south of the actual AM03 drill site. This distance was sufficient to remain out of range of the noise from the AMISOR equipment.

The benefit to the seismic program of surveying nearby an AMISOR drillsite was to have access to constrained physical property values at the same locations. In some cases, such as here at G2A, the data was collected in the same summer season as well – allowing for a realistic comparison of data. AMISOR collected multiple conductivity-temperature-density (CTD) casts at each drillhole; these data and the physically measured depths of ice and seafloor can be compared with the seismic records.

Ideally seismics would precede the drilling to avoid the interference and any noise introduced into the data, but the seismic program in 2005/06 followed AMISOR onto the AIS and we could only occupy and survey the sites after AMISOR had finished.

Noise is present in a number of shot records for the 2005/06 G2A Line. Nearby ground vehicle (skidoos) and aircraft activity (light planes and helicopters) noise was inadvertently included in the seismic data. Attempts were made to exclude noise or reduce noise by firing shots when aircraft were absent and vehicles were not in visible motion, however some noise was still introduced into the data.

The G2A 2005/06 seismic line (which henceforth will be referred to as G2A0506 in this thesis) was a 2 km east-west CDP reflection survey. The survey geometry is displayed in Figure 3.2. Walk-on shots were carried out every 20 m from 45 m offset to the centre of the first 24-channel spread, after which both shot and seismic spread were rolled along by 20 m – maintaining a centrally-located shot between Channel 12 and 13. On the last spread, walk-off shots were carried out every 20 m up to 45 m offset from the end of line. (See Table 3.1. for further information.) The line was surveyed in the E-W direction to cut perpendicularly across the ice shelf foliation with the aim of discovering any visible features associated with profiling perpendicular to flow, e.g. if there was any variance in ice stream thickness (ice shelf base “topography”). Setting up the survey in this direction took no extra effort but could possibly provide more information than the same length N-S survey line which would be profiling through a single stream of ice.

3.1.2 AM04

The AM04 AMISOR drill site was also seismically surveyed in the 2005/06 season. Two CDP reflection lines were surveyed here, a 2 km line in an east-west direction (named AM04EW) and a shorter intersecting north-south line (named AM04NS). The survey geometry for AM04 is displayed in Figure 3.3. For the same reasons as at AM03, the AM04 seismic lines were located approximately 1.5 km south of the actual drill site to remain outside of range of the noise produced by the mooring equipment left downhole at AM04.

The AM04 lines were surveyed using a 24-Channel spread, with 10 m channel spacing (see Table 3.1 for further information). The first walk-on shot was located 45 m offset from the start of line and the shot spacing was 20 m throughout the survey. Once the shot was located between Channel 12 and 13, both shot and the spread were rolled

along by 20 m each time, maintaining the shot in the centre of the spread. For AM04EW walk-off shots were carried out to 45 m off the end of line. AM04NS Line was terminated early at 590 m length due to adverse weather bringing a close to the field season. The final day of surveying that was required to complete the AM04NS line and the walk off shots was not able to be completed, hence the last shot for the AM04NS line is the centre shot for the spread between Station location 10360 (Channel 1) and 10590 (Channel 24).

The AM04 seismic line was surveyed after AMISOR had returned to Davis Station, so there was no noise interference from vehicles or aircraft. Travel restrictions though were in place while our group occupied the AM04 campsite, since the area had not been reconnoitred to define a crevasse-free work area beyond a radius of a few kilometres around camp. Once the AM04EW CDP line was completed, there was still both time and explosives to continue surveying but we were not able to travel much further away from camp. The decision was made to begin an intersecting N-S CDP line perpendicular to AM04EW. AM04NS was aligned approximately inline with the flowline heading directly towards the AM04 drill site.

3.1.3 AM01

The first AMISOR drill site, AM01 (which was drilled in the 2001/02 season), was also surveyed as part of this seismic project. This was undertaken just prior to New Years Eve in the 2004/05 summer season, three years after the hole was drilled. Time available at this site was limited to one evening, and limited explosives and equipment were able to be transported to the site; consequently the seismic line was limited in length to one cable spread and the CDP profile had a low fold coverage. (See Figure 3.4 for AM01 survey geometry.)

3.1.4 Camp Tropical – CT Line

The largest CDP line collected on the AIS was surveyed in 2004/05 and was named the Camp Tropical (CT) Line after the nearby “Camp Tropical” field campsite used that season. It shall be referred to hereafter as the CT Line.

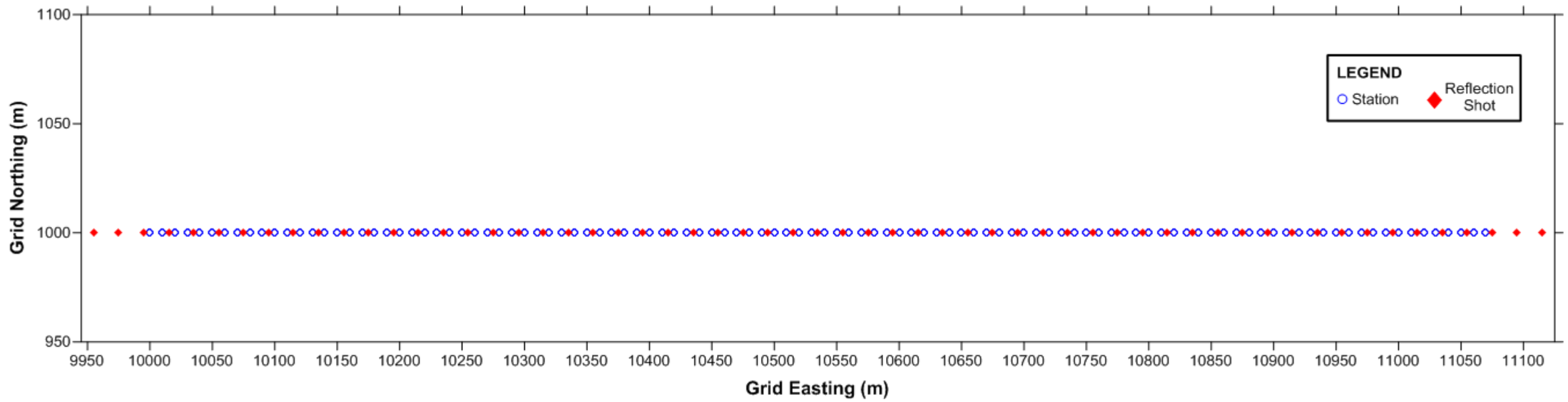

Fig 3.2 – G2A0506 survey geometry (North is up)

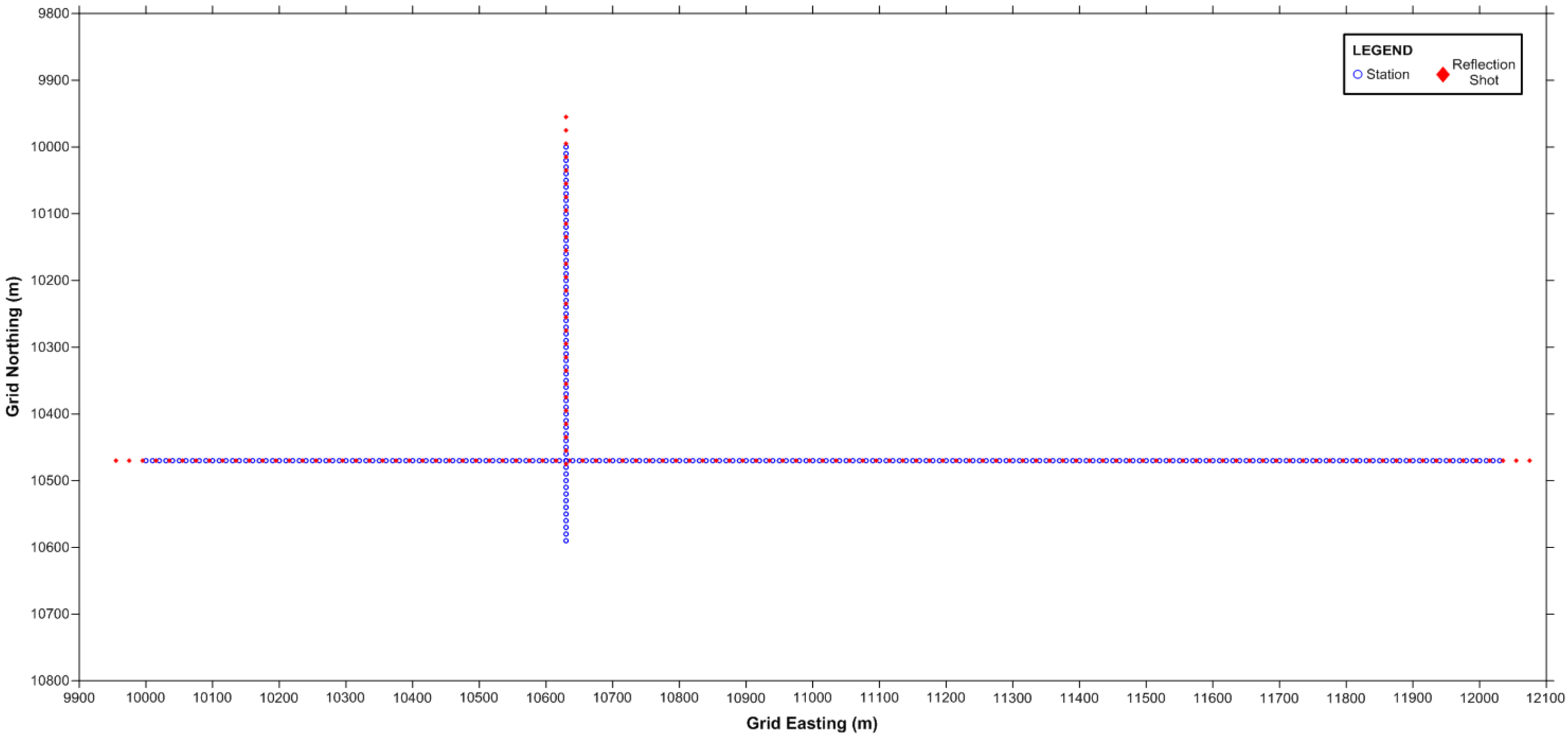

Fig 3.3 – AM04 survey geometry, for both the AM04EW and AM04NS lines (North is up)

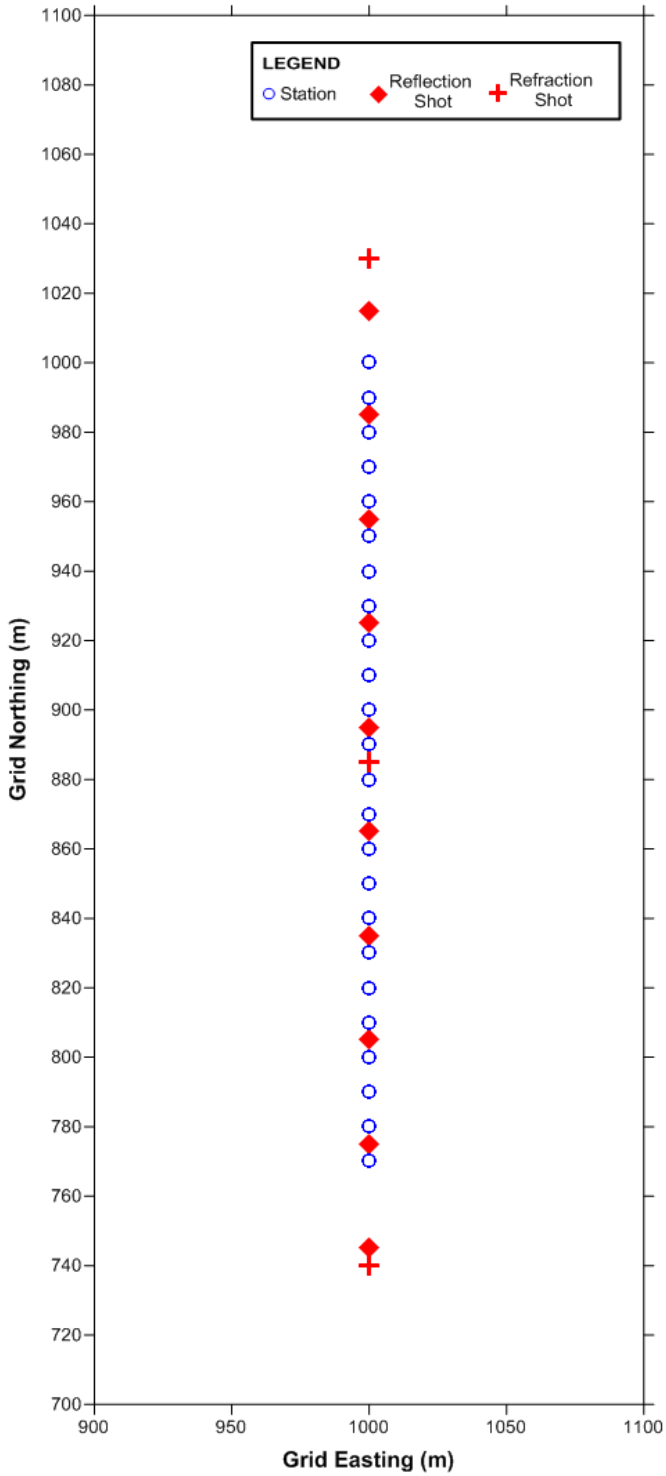

Figure 3.4 – AM01 survey geometry for the CDP survey line (North is up).

For the survey at Camp Tropical in January 2005, the aim was to detect any horizontal differences in the ice on either side of one of the flowlines visible at the surface of the

ice shelf. We located the line over a flowline visible in satellite imagery that appeared to show a low amount of strain, the same flowline over which we had earlier in the 2004/05 season surveyed for anisotropic ice fabric (see Section 3.2. for further information about these anisotropy refraction surveys).

The CT Line began at the central cross-over point of the LME-2E survey lines, and continued along a bearing of 172° magnetic towards the west. The CT Line passed about 1 km north of the LME-2W site. (See Figure 3.5 for a map view of these survey locations and lines).

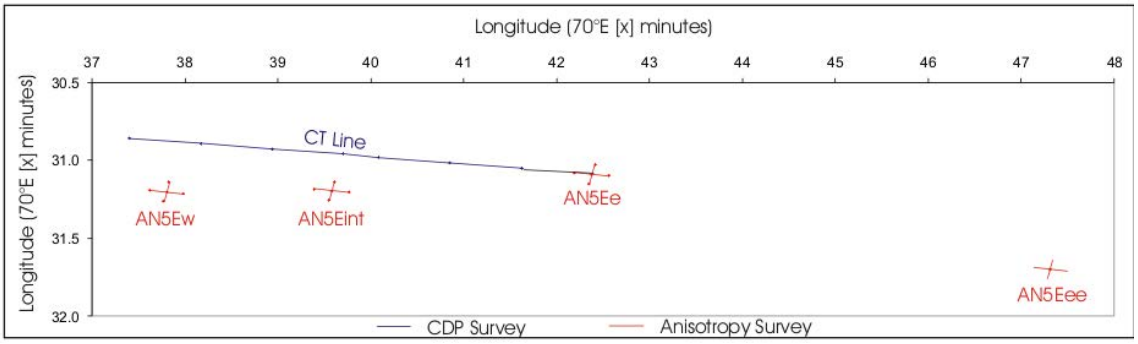

Figure 3.5 – The location and position of the Camp Tropical line (CT Line) with respect to nearby anisotropy survey sites.

The CT Line was surveyed starting in the east with Station location 20000 as Channel 1 of the first spread, with station location values decreasing to the west in the direction that the survey progressed. A total of 183 shots were fired, every 20 m, covering a distance of approximately 3 km. Walk-on shots were continued at 20 m intervals until the shot location was situated at 5 m east of the first geophone, i.e. 5 m outside the spread. From then on a roll-along switch was used to maintain the same relative shot position to the spread, until the end of the line was reached and walk off shots were carried out. The last shot was at Station location 16895 and the last geophone spread was located between 16660 (Channel 24) and 17130 (Channel 1). The full CT Line geometry is displayed in Figure 3.6.

3.2 Refraction surveys for measuring anisotropy

During the 2004/05 season, a series of refraction surveys were carried out with the aim of investigating anisotropic ice fabric; if it was present, how anisotropic the ice was, and at what depths this anisotropic fabric began or extended to (if a lower boundary appeared in the data). These were carried out on the eastern side of the ice shelf, west of Gillock Island.

Anisotropic ice was expected to be present in ice downstream of ice streams or glaciers merging as they entered the AIS; in ice that had previously undergone strain and possibly is still under some strain. A remnant anisotropic fabric was expected to remain in ice at a certain depth below the new strain-free surface ice, accreted from ongoing snow accumulation and compaction. If anisotropic fabric was strong enough, it should be measurable as an azimuthal difference in seismic velocity at a location. To test for this, a cross-line refraction survey was designed to measure seismic velocities in the surface 200 m of the ice shelf in the direction of flow and perpendicular to it – the two directions which should show the clearest results with the greatest change in velocity if there was a difference to be measured. Surveys were grouped as sets of three cross-line surveys: one within “anisotropic” ice on a flowline that appeared under relative strain, and two approximately 1 km away to the east and west of this central “anisotropic” site – to be outside the mapped strained area and hence be in “isotropic” ice. The general idea is shown in Figure 3.7.

The location where anisotropic ice was predicted to be present was picked using a strain image of the AIS produced by Neal Young (UTas). A similar map is published in Young & Hyland (2002). This strain image is shown in Figure 3.8 overlying a satellite image of the AIS. The red areas are those of high strain, and they are clearly concentrated along particular flowlines, especially along ice entering from the Mawson Escarpment Ice Stream and the east side of the AIS – these are ice streams that must change direction relatively rapidly to flow north with the shelf, as opposed to glaciers and ice streams that originated in the south that were generally already flowing north

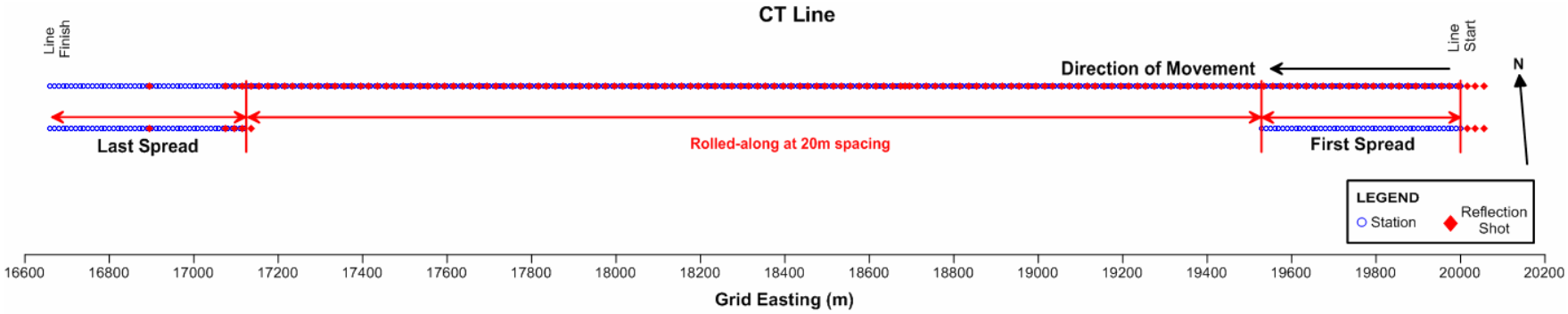

Figure 3.6 – Survey geometry plan and methodology of rollalong survey for CT Line.

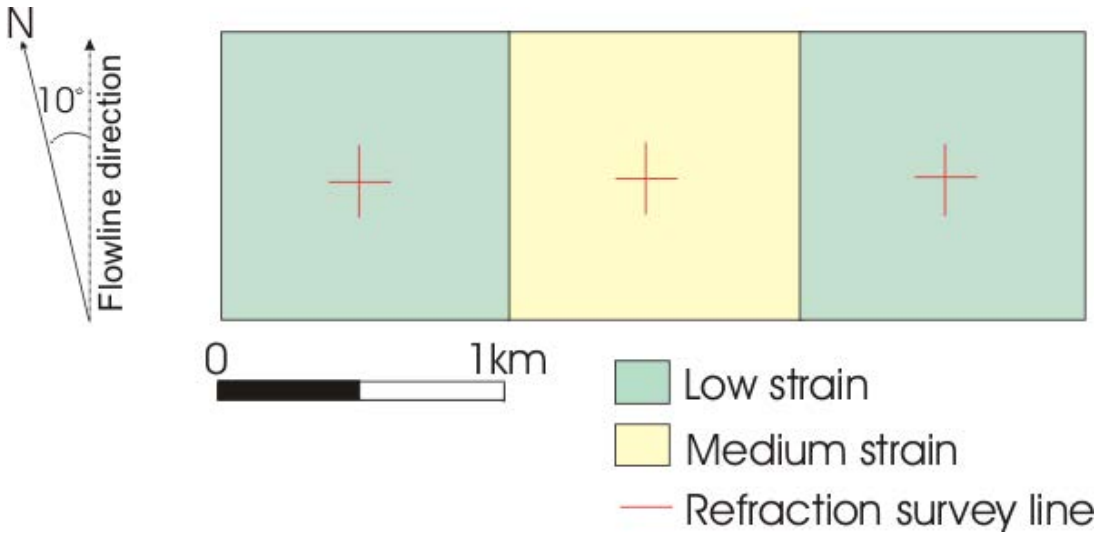

Figure 3.7 – Survey plan for an Anisotropy survey set. Crossline surveys give us seismic velocities parallel to and perpendicular to the flow direction. Survey locations were picked such that one was within suspected anisotropic ice (medium strain) and two were either side in isotropic ice (low strain).

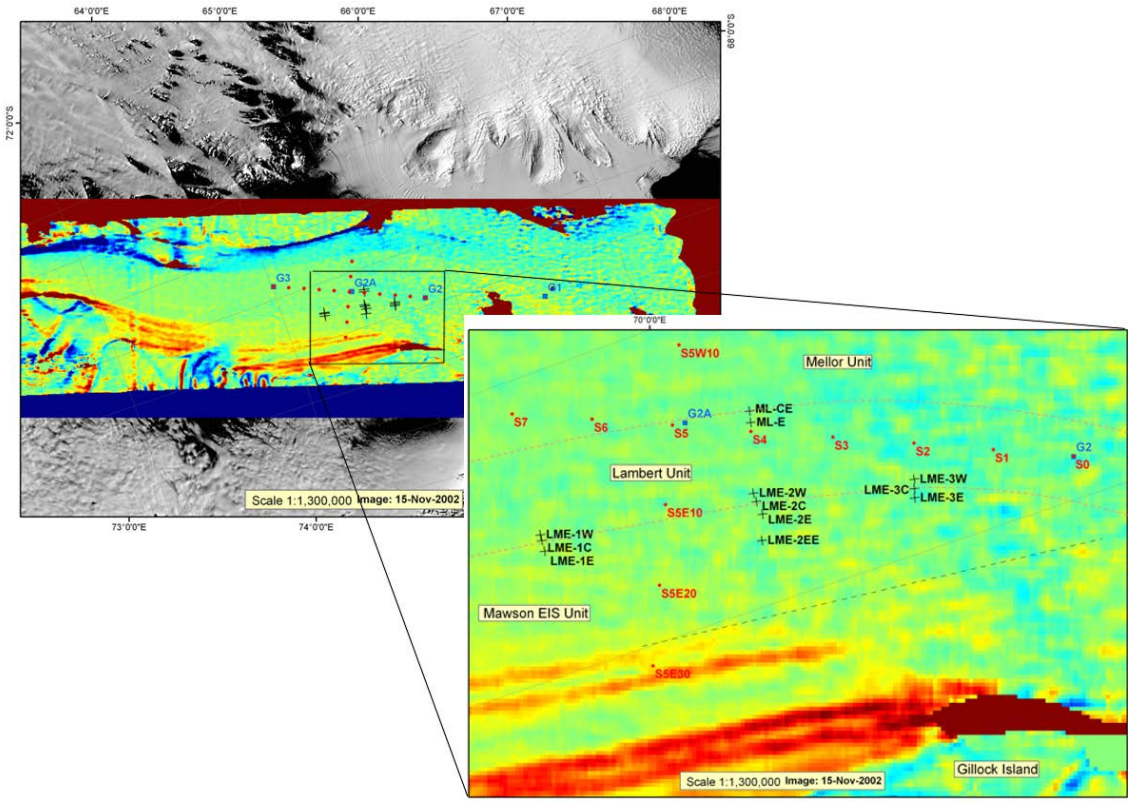

Figure 3.8 – Satellite image of the AIS overlain by strain image (Neal Young) [red = higher strain, blue = lower strain] with highlighted area showing anisotropy survey locations in relation to Flow Units (- - - line indicates reconnoitred "Safe Work" line – ground work was not permitted east of that line).

before they joined the AIS. The flowlines that displayed high strain were traced north into our season's field area, and survey locations were picked at the intersection of these strain lines and previously flown radar surveys over the Gillock Island area (for possible future data comparison of ice depths between these two datasets). The strain sites were picked based on the assumption that the strain upstream would have created an anisotropic fabric that would be preserved in the deeper ice at the downstream survey sites.

Due to safety and logistical reasons the areas of highest strain near Gillock Island, which were also situated in a heavily crevassed area, were deemed unsafe for work. The radar lines along which sites were chosen were followed west from the original proposed sites until they again crossed another flowline of higher strain amongst lower strain ice according to the strain map. These sites did not display as high a strain as the originally chosen sites, and they were located further downstream from an area where they were mapped to have undergone a similarly high rate of strain, hence any anisotropic ice present should then be at a greater depth (according to our original suppositions about burial of the strained ice under accreted unstrained ice).

Table 3.2 shows the survey sets and names for all sites surveyed for anisotropy. Each anisotropy refraction survey set was picked as three cross-line surveys (as mentioned above and displayed in Figure 3.7), except for the ML set (see Figure 3.8 for location). Due to a spreading/splitting of the flowlines here, this survey set was picked as four sites rather than three. Due to an early end to the field season in 2004/05 however, only the eastern two ML cross-line surveys were able to be completed. Earlier in the season, an extra site (LME-2EE) was added to the LME-2 survey set.

The naming protocol for the lines is as follows: A *prefix* to indicate what major flow unit boundary the surveys were located over – ML for the Mawson Glacier-Lambert Glacier flow unit boundary and LME for the Lambert Glacier-Mawson Escarpment Ice Stream flow unit boundary. This is followed by a *number* to differentiate between survey sets along the same flow boundary – LME-1 is the southern-most set, to LME-3 in the north. ML was the only set along that boundary so these survey sites did not require a number.

TABLE 3.2. List of the names of Anisotropy cross-line surveys that were completed in the 2004/05 field season.

Survey Set Name	LME-1	LME-2	LME-3	ML
List of site names for completed surveys	LME-1E LME-1C LME-1W	LME-2EE LME-2E LME-2C LME-2W	LME-3E LME-3C LME-3W	ML-E ML-CE

This is followed by an *E, C or W* identifier to show the survey's location within the set: "E" for the eastern survey, "W" for the western survey, and "C" for the central (and possibly anisotropic) site. In the case of the LME-2 set, the site LME-2EE was named as such because it was situated further east than LME-2E. For ML where two "C" sites where chosen instead of one, they were named ML-CE and ML-CW (this latter site remains unsurveyed). Each seismic line was further named with an *orientation* whether it was EW or NS.

To reach the maximum depth possible using a refraction survey, far offset shots were fired to the maximum extent of the firing cables, and the maximum spread length possible was used. Ideally, even further offset shots would have been recorded, but neither a longer firing cable nor sufficient field time existed to undertake what would be a lengthier survey. As it was, each cross-line survey took a full day to complete. The maximum spread length was 230 m, with 24 channels at 10 m spacing. The Channel and Station numbering protocol for these lines is shown in Table 3.3. The same numbering is used for all anisotropy refraction surveys.

TABLE 3.3 Numbering protocol used for all anisotropy surveys.

Line direction	N-S (parallel to flow: 176° mag)		E-W (perpendicular to flow: 086°mag)	
Channel	1	24	1	24
Station Location	1000	770	770	1000
Line end location (compass direction)	South	North	East	West

The bearing for the surveys (Table 3.1, Figure 3.7) were chosen based on the AIS flowlines in the area having an average true bearing of 010°. The lines bisected at the survey Station location 885, at the mid-point of the spread.

The same shot locations were used for each line: reciprocal shots at 1 m, 50 m, 100 m, and 250 m off the end of the line, and a centre shot, at Station location 885. The E-W line was surveyed first, and due to the centre shot that was needed for the N-S line having already been blasted in the E-W survey, the centre shot for this line was instead placed 2 m online in the southern direction, at Station location 887.

Figure 3.9 shows the survey geometry for the first anisotropy survey completed in the season, LME-2E, which was used as a test site to design how the cross-line survey could be completed in one day while gaining the longest possible offset shot data. It was also used to test the configuration of the centre shot, and how much explosive was required for the centre shot. Figure 3.10 shows the geometry for all subsequent anisotropy surveys. There were two exceptions to this due to misfires. For the LME-3W EW line the 100 m offset shot at Station location 1100 fired but did not trigger the seismograph, and it was re-shot at 1105. The same problem occurred at ML-CE EW at the 50 m offset shot at Station location 1050, and this shot was repeated at 1052 and 1048.

3.3 Regional surveys – refraction and reflection

Over all the field seasons, including the 2003/04 season, a number of regional seismic surveys were conducted in a 10 x 10 km grid (aligned to G1, G2 and G3) in the central-northern part of the AIS. S0 was located at G1, through to S10 at G3, 100 km south. Sites to the east and west of these points were affixed with E10 to denote 10 km east or W20 for 20 km to the west. E.g. the site S8E20 is 80 km south of G1 and 20 km east. By the end of the 2005/06 summer, this investigation (including those surveyed by Tassell) amounted to 45 individual survey sites, covering an area approximately 3,400 km^2 over a 110 km length of the AIS. The sites surveyed in 2002/03 had seismic lines oriented N-S; in all subsequent years the surveys were oriented E-W.

These surveys consisted of a few refraction shots, and five reflection shots per line. The length of the record was consistent to be able to use refraction shots as reflection data, but the difference was classed by the location of the shots in relation to the spread and they were treated as two separate lines of data – the reflection used to map the thickness of the ice shelf and the depth to the seafloor, and the refraction used to define near surface P wave velocities and maximum velocities for ice to be used to convert reflection times to depths. These were simple 230 m length surveys, and the fold of the reflection data was low. The geometry for these surveys is shown in Figure 3.11.

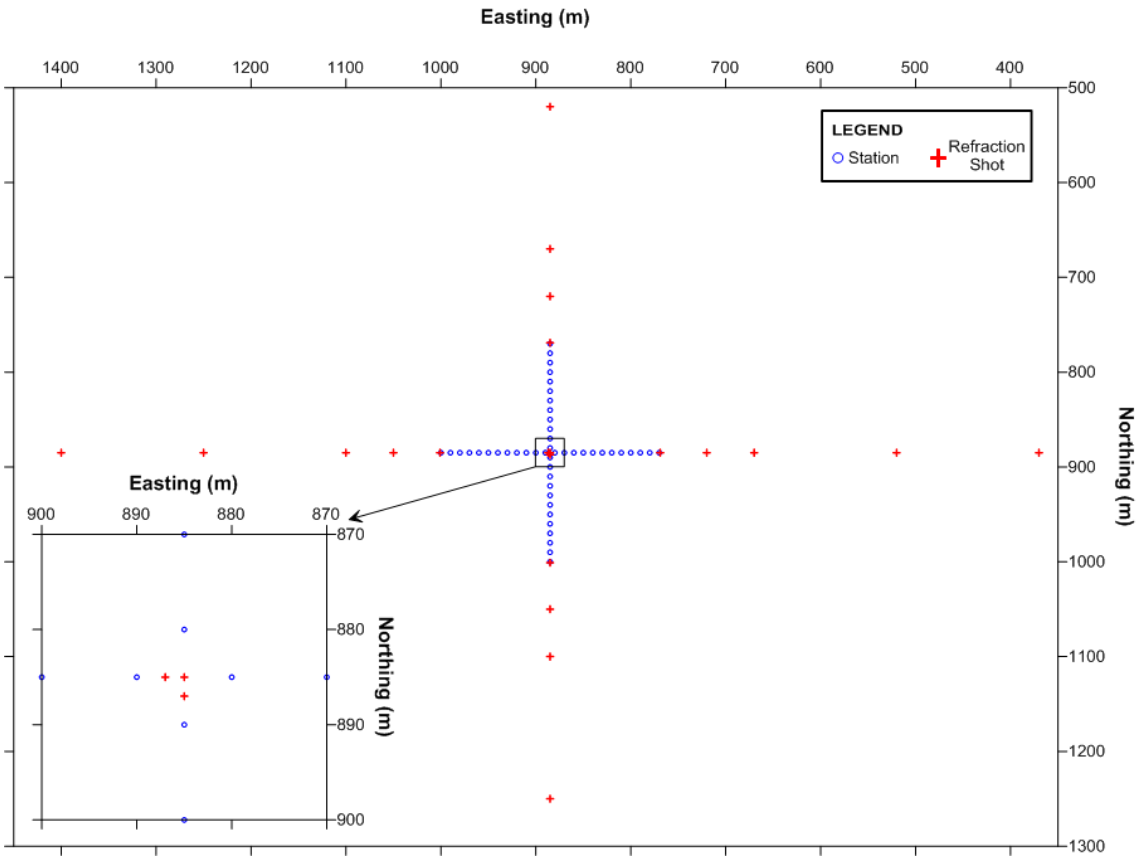

Figure 3.9 – Survey geometry for line LME-2E, the trial anisotropy survey location.

3.4 Seismic source

The seismic source used for all seismic surveys were explosive boosters with an electrical detonation system. The detonators used were Orica #8 Instantaneous Seismic Detonators (Class 1.1B). Two sizes of boosters were used, either separately or in various combinations to make different sized shots: the Orica Pentex G Booster (110 g) and the Orica Pentex H Booster (150 g) (Class 1.1D). For central refraction shots, only a single detonator at 40 cm depth was required. For anisotropy surveys only single H or G Boosters were required, at 1.5 m depth. Beyond 50 m from the end of the line, multiple boosters (H &/or G) were used at 2 m depth. For regional surveys and other CDP surveys, generally one H Booster at 1.5 m was sufficient, and where more energy was required multiple boosters (H and/or G) were used at 2 m depth.

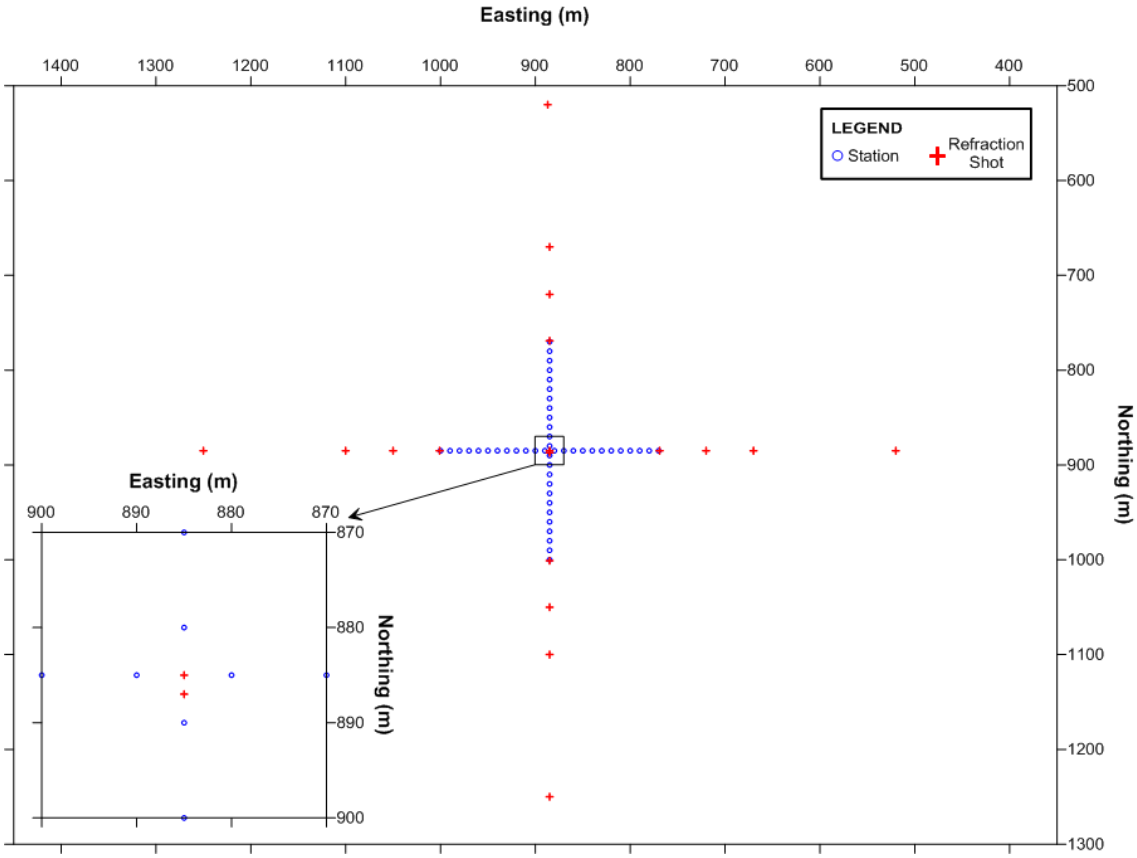

Figure 3.10 – Survey geometry plan for all anisotropy surveys (except LME-2E).

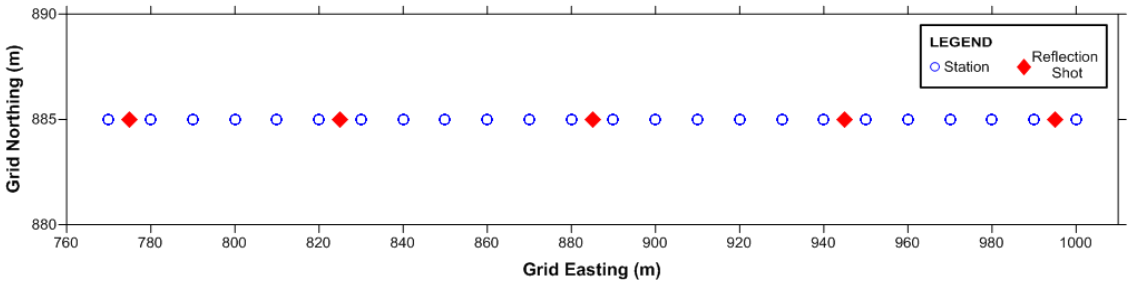

Figure 3.11 – Example survey geometry for regional sites S8E20, S8E10 and S6E10.

Chapter 4

G2A: A THREE YEAR CASE STUDY

G2A, half way between G2 and G3 on the AIS, has been the site of repeat seismic surveys spanning three years. The first CDP seismic line as part of this project was surveyed north of G2A in January 2003, the G2A0203 Line. In December 2005, G2A hosted both an AMISOR drill site (AM03) and a second CDP seismic survey, the G2A0506 Line. None of these sites are in exactly the same location, due to movement of the ice shelf and the need to survey away from established camps. The orientation of the seismic lines is also different – G2A0203 being a ~N-S line and G2A0506 an ~E-W (perpendicular to flow) line. The relative location of these surveys is shown in Figure 4.1.

The purpose of the G2A0203 survey line was to measure the thickness of the water column and to delineate between meteoric and marine ice layers at the base of the ice shelf. The results are published as McMahon & Lackie (2006) (Appendix A). Subsequently, AMISOR chose to drill at G2A. This was originally proposed for the 2004/05 season and drilling equipment had been cached at the G2A site at the end of the 2003/04 season to await the following summer. However, due to logistical issues, the site was not drilled until the 2005/06 season, by which time the cached equipment had moved downstream with the ice shelf. This allowed for a measurement of an approximate rate of ice movement for this area, which can be measured off Figure 4.1. The distance between G2A and AM03 is approximately 740 m, resulting in an annual surface ice velocity of approximately 370 ma^{-1}, comparable to the annual ice velocity value modelled by Young & Hyland (2002). G2A was resurveyed with seismics in December 2005; to both compare the two seismic datasets and to be able to compare G2A0506 seismic data with physical data collected by AMISOR.

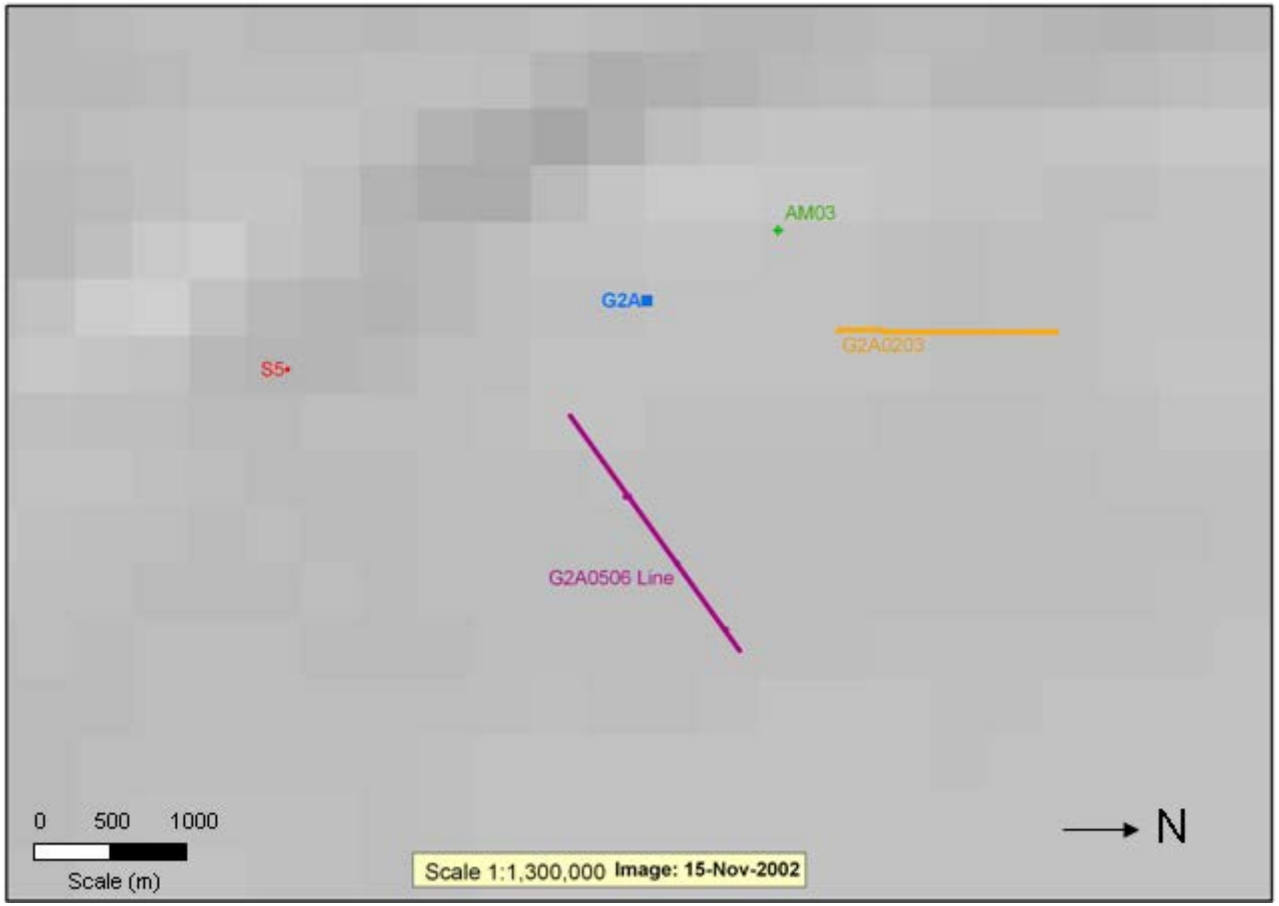

Figure 4.1 – G2A0203 (—) and G2A0506 (—) Lines on satellite image of the AIS (darker grey zone is the Mellor-Lambert Flow unit boundary), showing G2A location, AM03 drill site (in 2005/06 season) and the S5 regional site.

4.1 G2A0203 Line

The G2A0203 CDP profile processed using GLOBE Claritas© V3.3.0 (Claritas) is shown in Figure 4.2. This CDP profile was used for publication in McMahon & Lackie (2006). These data was later reprocessed using Disco Focus v5.2 (Disco Focus) at Geoscience Australia, shown in Figure 4.3. This was carried out so that all datasets were processed using the same software, allowing for an unbiased comparison of data.

4.1.1 Claritas processed data

Processing Sequence

The processing sequence used is outlined in McMahon & Lackie (2006) given in Appendix A. In summary:

- All data was converted from raw seg2 format to Seismic Unix (SU) seg-y format using SU scripts. Header locations were altered by a factor of 100 to match field grid locations. This SU seg-y file was then converted to Claritas© seg-y format in Claritas, which also merged all shots into one file. Processing continued in Claritas hereafter.
- Field geometry was applied to the 89 shot records using .sur, .obl and .geom files
- Data quality control were applied to the data via trace editing. Front muting, surgical muting and trace kill (deletion) were applied to remove refracted arrivals, to create subsets of data for separate processing, and to remove individual noisy traces.
- A spectral analysis was performed upon the data to find the frequency range of the data and to provide frequencies for later filtering. Most data occurred within the range 30-80 Hz and 160-188 Hz. The Nyquist frequency was calculated and it was determined no aliasing was present within the data.
- Bandpass frequency domain filtering was applied to remove high-frequency noise. This was defined by 30, 80, 160, 188 Hz. Further noise and some multiple reflections were removed with the application of a second bandpass filter: 10, 30, 60, 90 Hz.

- NMO Velocity analysis was performed for a pre-stack NMO correction. A velocity of 2500 ms^{-1} was determined to be suitable to apply to the data.
- The six-fold data was sorted by CDP number (numbered 100–301 going from south to north) and CDP geometry was applied via the cdp.geom file
- Stacking
- Post-stack NMO and velocity analysis was performed. Optimal stacking velocities were found to be 3300 ms^{-1} for ~400 ms reflection and 3080 ms^{-1} for ~1245 ms reflection
- Stacking using final optimal NMO velocities.
- Automatic gain control (AGC) and balancing were tested, however they did not produce an improvement in the data (in particular the AGC had a detrimental effect on the visibility of reflections) and neither were used for the final stack (Figure 4.2)

Results

The reflections at the base of the ice are visible at ~ 400 ms in the record as two definite reflections (at 397 ms and 404-411 ms) and possibly two more reflections above and below these (at 390 ms and 413 ms) (Figure 4.2, McMahon & Lackie, 2006, Figure 4b). These were interpreted by McMahon & Lackie (2006) as the base of the meteoric ice and a thin layer of marine ice, calculated to be at 754 m and 773 m depth below the surface, giving a marine ice layer of ~19 m in thickness. Other reflections occur at 800 ms, 1200ms, 1210-1220 ms (the seafloor), 1650 ms and 2030 ms. The water column was calculated to be 595 m thick, placing the seafloor at a depth of 1369 m below the surface. The ice velocity for the upper ~ 50 m was modelled from refraction data collected along the same line, and processed with Seismic Refraction Interpretation Programs (SIP) v4.1 (Rimrock Geophysics) and RAYINVR (Zelt & Smith, 1992) programs, resulting in a modelled maximum of 3720 ms^{-1} at ~ 48 m depth. An overall velocity for ice shelf ice of 3800±50 ms^{-1} – taking into account further consolidation of ice and corresponding increase in density and velocity below 50 m depth – was used to calculate ice depths. The water velocity of 1440 ms^{-1} was derived from the measured water P-wave velocity under the Ross Ice Shelf (Beaudoin et al., 1992), which was the best approximation of sub-Antarctic ice shelf water P-wave velocity at the time of publication. For more information on these results, refer to Appendix A.

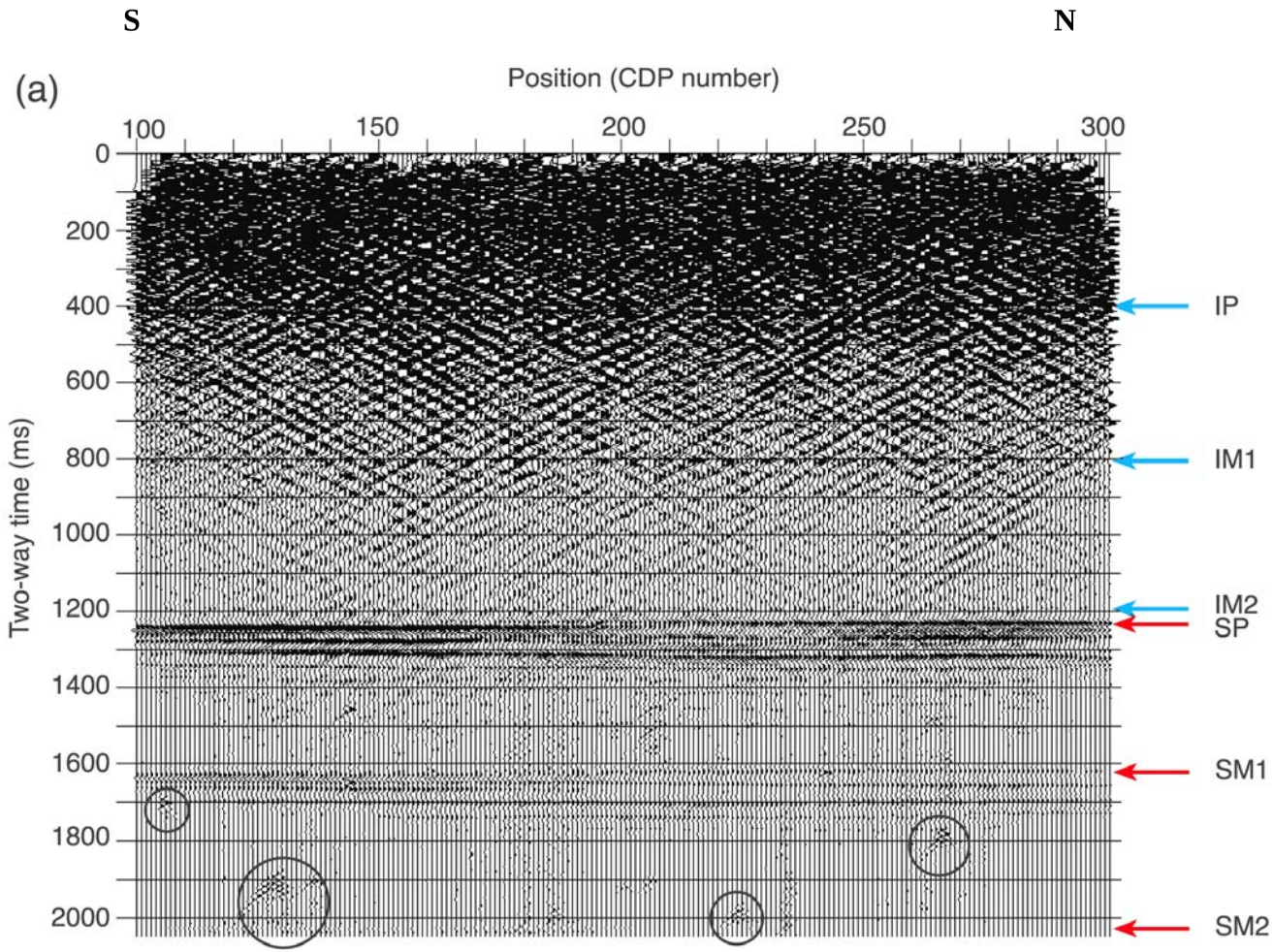

Figure 4.2 – G2A0203 Line CDP Profile (processed using Claritas) (adapted from McMahon & Lackie, 2006, Fig 4a). Reflections: IP = Ice primary, IM1 and IM2 = Ice multiples, SP = seafloor primary, SM1 and SM2 = seafloor multiples

4.1.2 Disco Focus reprocessed data

Processing Sequence

The Disco Focus-reprocessed data was performed following these steps:

- Create input files for Disco Focus (seg2 to seg-y conversion and apply geometry via line, pattern, and source files)
- Combine seg-y files to create one Disco Focus seg-y file
- Spectral analysis to determine frequency content of the data
- Resampling data to 1 ms to reduce spatial aliasing (Tassell, 2004)
- Bandpass filter (at frequencies 30, 80, 160, 188 Hz)
- Trace removal of noisy traces
- Front end muting to remove groundroll and refracted arrivals
- Surgical muting to remove deep hyperbolic features
- Deconvolution (single trace predictive) – this reduces the source wavelet to a spike and also helps remove reflection multiples
- CDP sorting
- Velocity analysis using an interactive velocity definition model (VELDEF). Velocities are picked and stored in the Disco Focus database to be applied in the NMO correction. Moveout velocities were selected for each reflection.
- Pre-stack NMO correction applied
- Stacking
- Runmix on 3 traces with weight 1, 2, 1

The reprocessed G2A0203 CDP profile is displayed in Figure 4.3. Other processing steps were tested on the data. These included f-k filtering, coherency enhancement, and spectral equalisation.. F-k filtering was attempted, however the filtering aliased the groundroll and made it difficult to design a reject zone for the data. F-k filtering was not employed. Coherency calculated across the record can be added to the original seismic data with a weighting factor, called a cohernacy enhancement. This was not applied pre-stack as it destroys natural amplitude, but was tested post-stack. Runmix was applied to serve a similar function and for model smoothing, using a 3 trace group and applying a weight of 1, 2 and 1 respectively. The improvements in the processing sequence were influenced by the work of Tassell (2004), and by discussions with Leonie Jones and

Hugh Tassell of Geoscience Australia. Further information regarding specific processing steps can be read in Tassell (2004).

Results

The notable difference between the G2A0203 data processed using Claritas and Disco Focus is the reflection appearing at 580 ms in the Disco Focus-stack (labelled as PP in Figure 4.3) that was not visible in the Claritas-stack. This reflection occurs within the water column, and is interpreted as a pycnocline – a boundary within a body of water where there is a rapid change in salinity and/or temperature. Refer to Chapter 6 for more information regarding pycnoclines.

For comparison, the processing sequence that was used in Claritas was run in Disco Focus, without the further filtering and processing steps that were applied to produce the stack in Figure 4.3. Figure 4.4 shows the difference between these two processing sequences for the PP reflection at 580 ms. The extra filtering and post-stack processing that was applied has improved the quality of the final stack and revealed this reflection.

The ice reflection and its multiples are also much more evident in the Disco Focus-stack. The characteristic of the reflections appears more continuous across the profile, mainly due to the application of the post-stack runmix smoothing processing step applied to the data in Disco Focus,. This explains why the seafloor sediment reflections are more continuous across the profile in Figure 4.3.

The IM2 multiple occurs at the same time as a pycnocline-surface-pycnocline multiple (PM1) could arrive, if the latter exists in the data. The PP reflection is weaker than the other reflections, and does not seem to have produced a pycnocline-surface-ice base (or ice-surface-pycnocline) multiple, so the likelihood of the PM1 multiple existing is questionable, since this is the ray path of all other multiples present in the data. It cannot be ruled out however that the multiple reflections at 1170-1180 ms are due to the IM2 and PM1 multiple, rather than just the IM2 multiple.

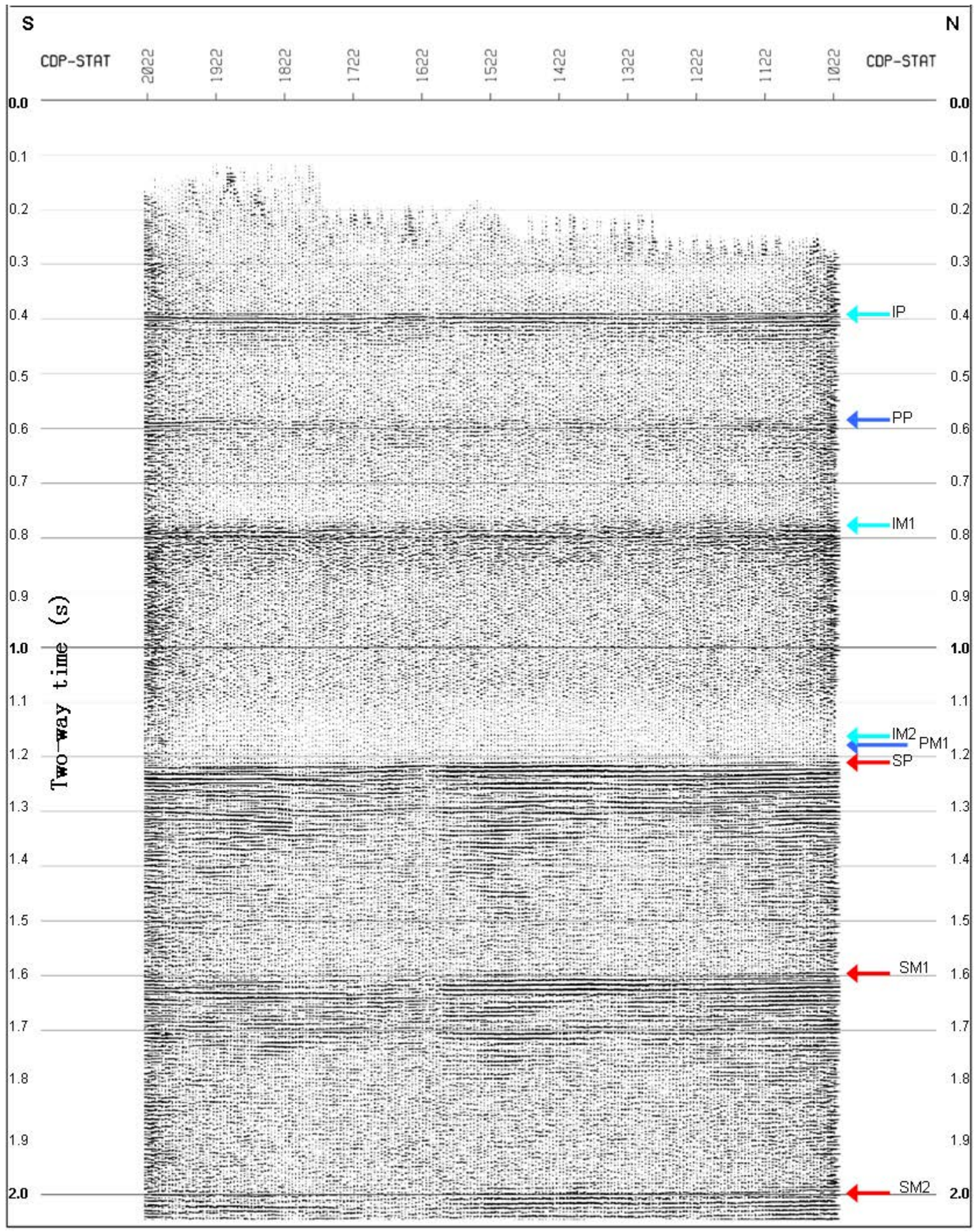

Figure 4.3 – G2A0203 Line CDP Profile (processed using Disco Focus). Reflections: IP = Ice primary, IM1 and IM2 = Ice multiples, PP= Pycnocline primary, PM1=Possible Pycnocline multiple, SP = Seafloor primary, SM1 and SM2 = Seafloor multiples

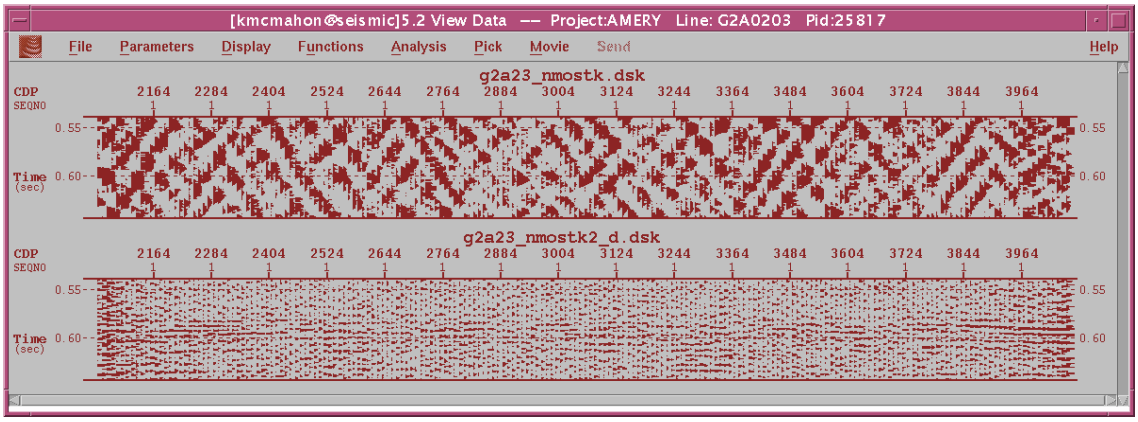

Figure 4.4 – Screen shot of Disco Focus data display window, highlighting the time 550-650 ms. Top: Previous Claritas processing sequence employed to produce Figure 4.2; no reflection evident. Bottom: Improved processing sequence used to produce Figure 4.3; reflection observed at 580 ms.

4.2 G2A0506 Line

The G2A0506 Line data was collected in December 2005, just after AMISOR had finished drilling the AM03 hole. The line was located between Station location 10000 in the west and Station location 11070 in the east (these being an arbitrarily assigned grid location value). The total line length is 1.07 km. The first shot was located at 9955; the last at 11115. The dataset consists of 59 shot records, collected with a 20 m spacing. Walk-on shots were carried out until the shot was at the centre of the 24-geophone spread, and the spread was subsequently rolled along by 20 m for each shot thereafter until walk-off shots began. This gave a maximum fold coverage of six, the same as the G2A0203 data.

Two example raw seismic records for the G2A0506 Line are given in Figure 4.5. Shot record 5010 was collected on a normal field day, with good weather. Shot record 5020 was collected on a day with intermittent noise from vehicles and aircraft (as discussed in Chapter 3). Refracted arrivals can be seen in the early times of both records, and a

clear reflection at ~1250 ms is visible in both records. Shot 5010 displays other reflections at ~400 ms, ~800 ms and ~2200 ms. Only the ~2200 ms reflection is clearly evident in Shot 5020. Shot 5020 is also more erratic, displaying spikes throughout the record.

The seismic refraction arrivals (primary event in the seismic records) and groundroll within Shot 5010 and Shot 5020 seismic records are displayed in Figure 4.6. Figure 4.7 displays the same section of these records with an increased gain applied. The refraction and groundroll content extends to greater than 500 ms in both records. It partially obscures the ~400 ms reflection (which was noted in Figure 4.5) in at least half of the record traces. If this section of refracted and surface wave data is not removed from the record prior to CDP sorting and stacking, the 400 ms reflection will be be lost. These sections of data have been removed using front end muting to maintain the early reflection data within final stacked dataset.

Figure 4.7 also reveals the amount of noise present in records collected on that day. The 400 ms reflection which can clearly be seen in the 5010 record is obscured by longer wavelength noise in the 5020 record. Figure 4.8 displays the frequency spectrum of both these shot records. Most of the frequency content of Shot 5010 is between 40-120 Hz, whereas Shot 5020 displays most content at 40-80 Hz. The content with frequencies above 120 Hz is close to zero in Shot 5010 whereas Shot 5020 displays recurring small bands of higher frequency content, aka noise. This spectral analysis of the individual records and of groups of records allowed for the definition of appropriate bands of frequency for the “normal noise” versus “noisy” groups of data. An appropriate bandpass filter could then be designed and applied to each type of data separately before CDP sorting. This allowed for most noise to be removed from the “noisy” data and resurrecting the 400 ms reflection in these data.

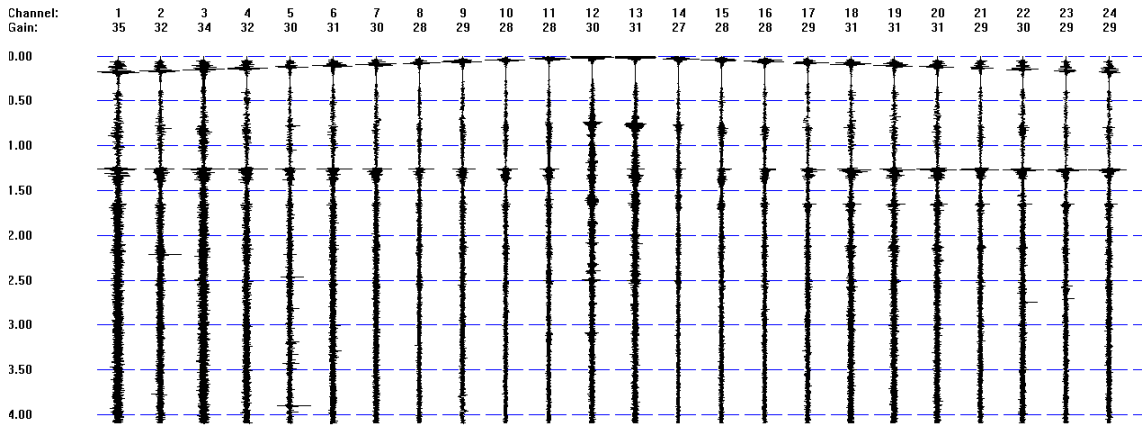

(a)

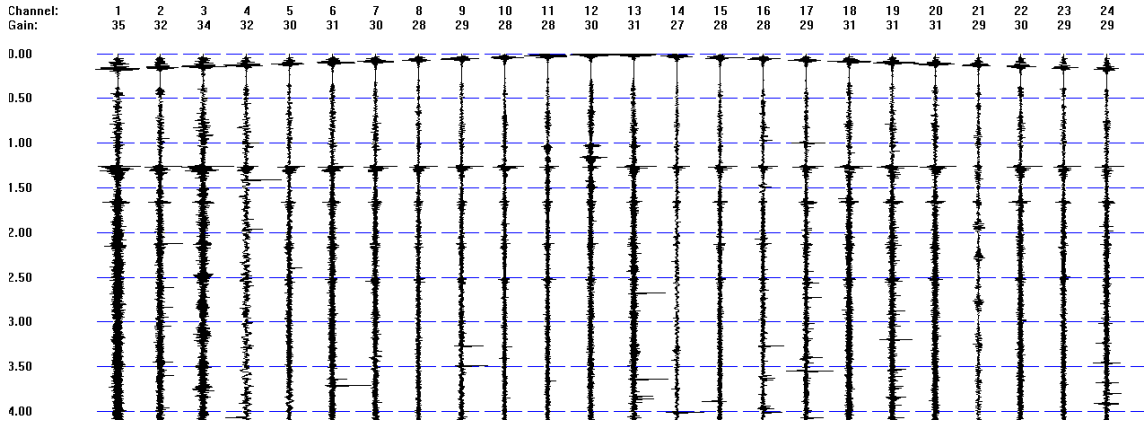

(b)

Figure 4.5 – Raw seismic records for G2A0506 shots (a) 5010.dat and (b) 5020.dat.

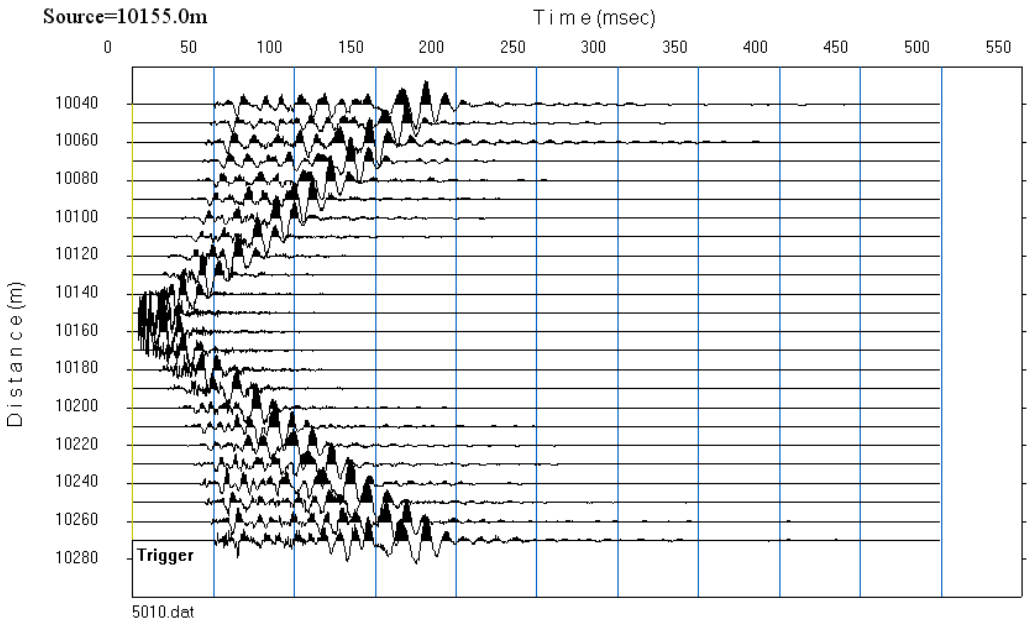

(a)

Refracted Arrivals

Groundroll

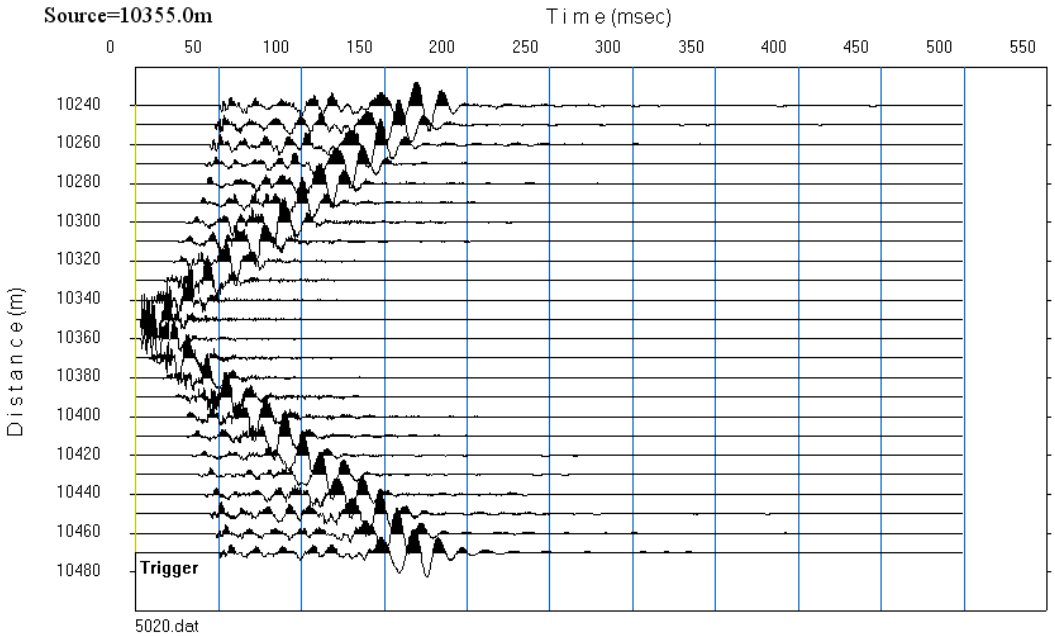

(b)

Figure 4.6 – Refracted arrivals and groundroll in the early part of the raw record of (a) 5010.dat and (b) 5020.dat

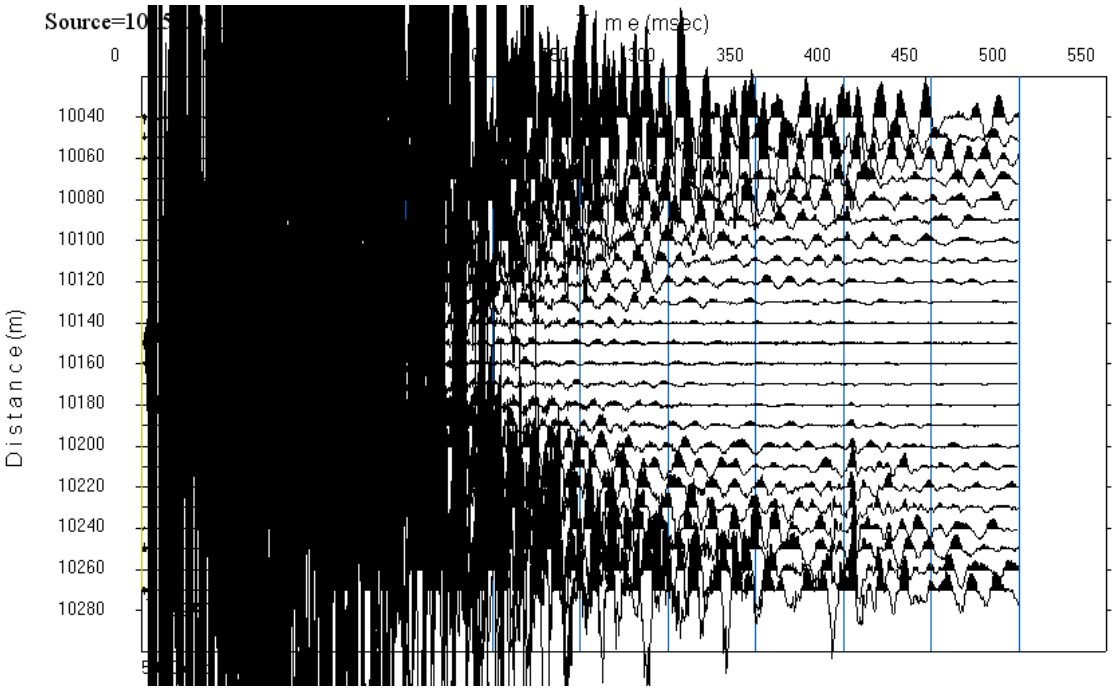

(a)

^

Reflection

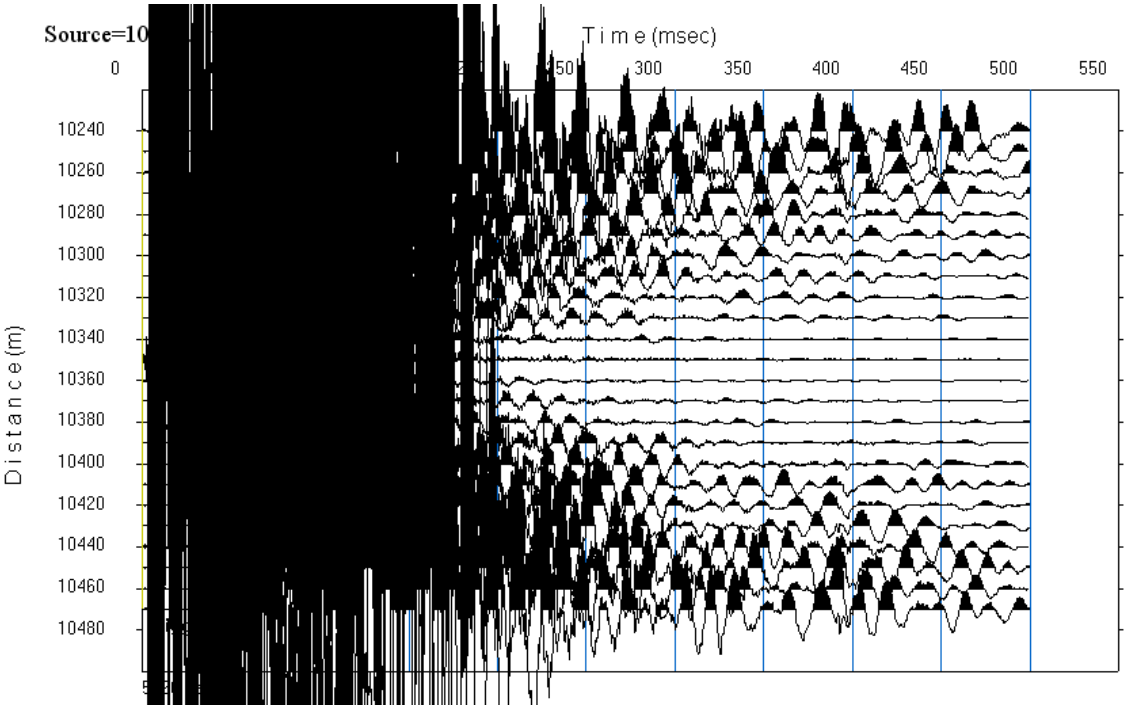

(b)

Figure 4.7 - Refracted arrivals and groundroll in the early part of the raw record of (a) 5010.dat and (b) 5020.dat displaying increased gain across the records.

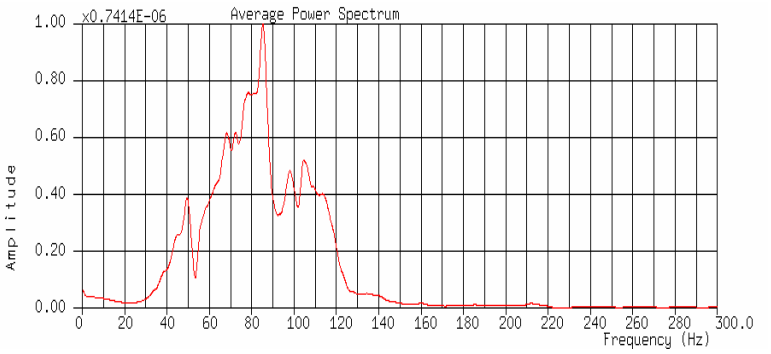

(a)

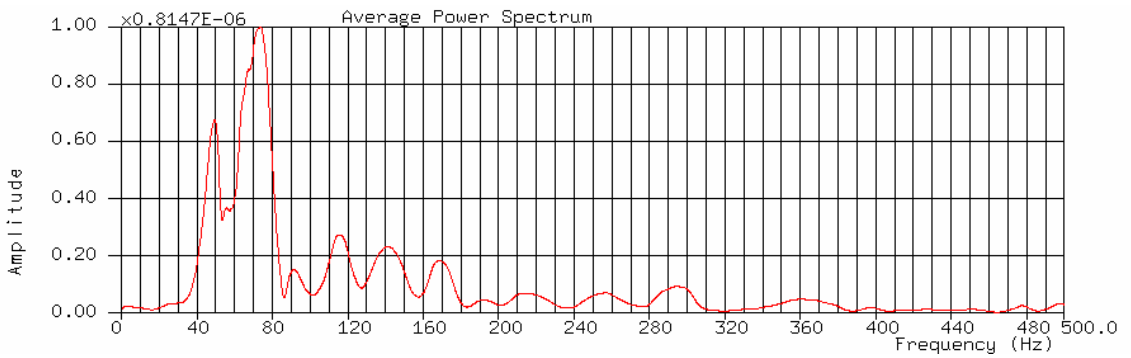

(b)

Figure 4.8 – Frequency spectrum of (a) 5010.dat and (b) 5020.dat raw records.

4.2.1 Processing sequence

The following steps were used for processing in Disco Focus:

- Create input files for Disco Focus (seg2 to seg-y conversion and apply geometry via line, pattern, and source files)
- Combine seg-y files to create one Disco Focus seg-y file
- Spectral analysis to determine frequency content of the data
- Resampling data to 1 ms to reduce spatial aliasing (Tassell, 2004)
- Bandpass filter (at frequencies 80, 88, 96, 104 Hz)
- Trace removal of noisy traces
- Front end muting to remove groundroll and refracted arrivals
- Surgical muting to remove deep hyperbolic noise
- Deconvolution (single trace predictive)
- CDP sorting

- Velocity analysis using an interactive velocity definition model (VELDEF). Velocities are picked and stored in the Disco Focus database to be applied in the NMO correction. Moveout velocities were selected for each reflection.
- Pre-stack NMO correction applied
- Stacking
- Runmix on 3 traces with weight 1, 2, 1

4.2.2 Results

The final CDP stacked profile is shown in Figure 4.9. Reflections are observed at approximately 400 ms, 578 ms, 790 ms, 1220-1240 ms and 1620-1640 ms. These are attributed to the base of the ice shelf, pycnocline within the water column, ice base multiple, seafloor and sediments, and seafloor multiple, respectively. The reflection arrival times differ somewhat from the G2A0203 data, but this is to be expected due to the difference in line orientation and location.

The PP reflection at 578 ms is discontinuous across the survey, and is strongest at the west end of the line (near station 10000). This section of strong-PP reflection data corresponds to the first day of data collection on this line, when conditions were normal. The majority of the rest of the data was collected while AMISOR were moving camp (as outlined in Chapter 3). The aircraft noise on these days has adversely affected the seismic records, reducing the signal to noise ratio (SNR).

4.3 Discussion

A full summary of the observed ice and seafloor reflection times for the G2A0203 and G2A0506 Lines and their calculated depths, including the depths measured at AM03 by AMISOR, is shown in Table 4.1. Table 4.2 shows the same calculation for the depth to the pycnocline reflection (PP).

As shown in Figure 4.2, the southern end of G2A0203 and the western end of G2A0506 are ~1.25 km apart, with G2A0506's western end almost directly south of the southern end of G2A0203. AM03 is located ~500 m west of the southern end of G2A0203. As such, the results from each of these locations cannot be expected to be exactly identical, but the results can be used for comparisons, discussion and certain deductions.

The depths in Tables 4.1 and 4.2 calculated from the P-wave velocities that were calculated from AM03 measured depths and G2A0203 arrival times would include a further uncertainty based on the distance between these two locations and whether there is a natural difference in depths between the two. The calculations were made based on the assumption that AM03 and the south end of G2A0203 had the same thickness of ice and the same depth to the seafloor; this must be considered when comparing depths calculated in this way.

4.3.1 Comparing seismic data and AMISOR depths

If we look at the seismic data, the difference in arrival time for the ice base reflection between G2A0203 and G2A0506 is 0-5 ms. For ice at 3800 ms^{-1} this is a 0-9.5 m difference, and at 3703 ms^{-1} this is 0-9.2 m difference. The difference in the arrival time of the pycnocline is -2 ms respectively, which is within the error of measurement. However if we take this difference to be true, then that corresponds to a maximum difference of 1.4-1.8 m, using water velocities of 1440 ms^{-1} and 1487 ms^{-1} respectively. If the maximum change in ice thickness over 1.25 km from south to north is +9.5 m (although the general trend is no change in time, hence no change in depth), and the maximum possible change in the pycnocline is <2 m, the depth to the pycnocline from the base of the ice should not vary by >11 m over this distance.

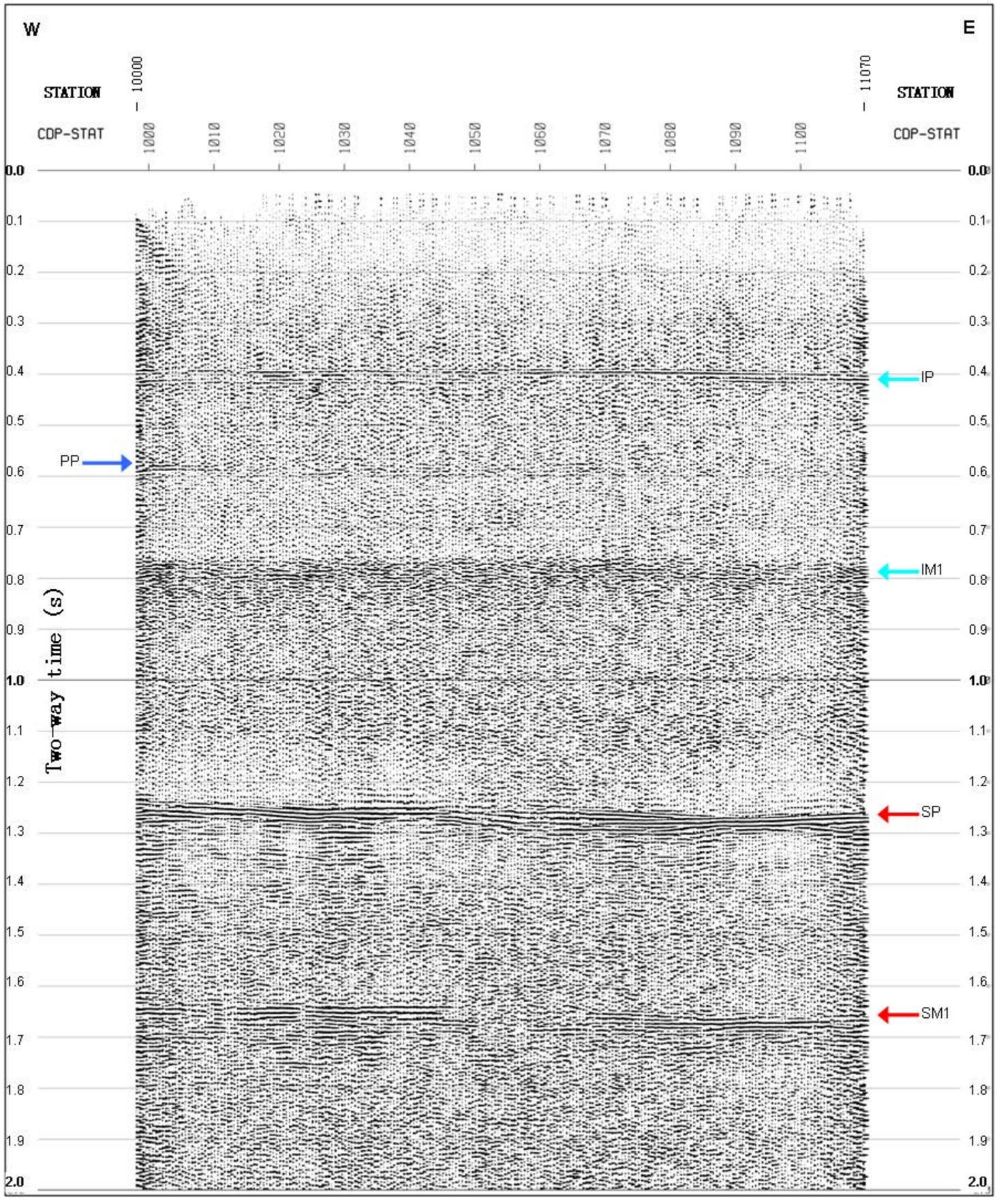

Fig 4.9 – G2A0506 Line CDP Profile (North is into the page, approximately). Reflections: IP = Ice primary, IM1 = Ice multiple, PP= Pycnocline primary, SP = Seafloor primary, SM1 = Seafloor multiple

Table 4.1 – Table of Ice & Seafloor Depths: measured depths at AM03, calculated depths for G2A seismic lines using measured reflection times and both measured and calculated P wave velocities (highlighted in grey), with depth errors based on a ± 2 ms error in reflection time. Left column P wave velocities are from refraction modelling of the G2A0203 Line and an estimated Prydz Bay seawater velocity; right column P wave velocities are calculated from AMISOR measured depths combined with seismic arrivals of 390 ms for ice base and 1220 ms for seafloor (approximated from the closest measurement at the south end of G2A0203 Line). (Note: the error on these calculated velocities is ± 19 ms^{-1} for ice and ± 4 ms^{-1} for water; however this leads to an insignificant change in depth error calculated from these values.) Annotations *A to *D: seafloor depths were calculated from the corresponding ice thicknesses, with ice from *A thinnest to *D thickest.

AM03	**G2A0203**						**G2A0506**									**Error (± 2 ms)**	
Depth (m)	South end of line: depth (m)			North end of line: depth (m)			West end of line: depth (m)			Mid-line: depth (m)			East end of line: depth (m)				
722	Ice base	P velocity ms^{-1}		Ice base	P velocity ms^{-1}		Ice base	P velocity ms^{-1}		Ice base	P velocity ms^{-1}		Ice base	P velocity ms^{-1}		P velocity ms^{-1}	
	time (ms)	3800	3703	time (ms)	3800	3703	time (ms)	3800	3703	time (ms)	3800	3703	time (ms)	3800	3703	3800	3703
*A	390	741.0	722.1	390	741.0	722.1	385	731.5	712.8	390	741.0	722.1	390	741.0	722.1	3.8	3.7
*B	397	754.3	735.0	397	754.3	735.0	405	769.5	749.9	-	-	-	-	-	-	3.8	3.7
*C	411	780.9	761.0	404	767.6	748.0	410	779.0	759.1	410	779.0	759.1	410	779.0	759.1	3.8	3.7
*D	413	784.7	764.7	413	784.7	764.7										3.8	3.7
1339	Seafloor	1440	1487	Seafloor	1440	1487	Seafloor	1440	1487	Seafloor	1440	1487	Seafloor	1440	1487	1440	1487
*A	1219	1337.9	1338.4	1209	1330.7	1331.0	1240	1347.1	1348.5	1250	1360	1345.4	1265	1371.0	1372.6	2.8	2.2
*B	1219	1304.2	1285.1	1209	1294.6	1275.4	1240	1331.9	1312.9	1250	-	-	1265	-	-	2.8	2.2
*C	1219	1307.8	1280.2	1209	1288.7	1261.4	1240	1338.0	1318.8	1250	1350.3	1324.2	1265	1365.1	1345.9	2.8	2.2
*D	1219	1323.9	1304.1	1209	1314.3	1294.4										2.8	2.2

Table 4.2 – Table of Ice & Pycnocline Depths: measured ice depth at AM03, calculated depths for G2A seismic lines using measured reflection times and both measured and calculated P wave velocities (highlighted in grey), with depth errors based on a ± 2 ms error in reflection time. Left column P wave velocities are from refraction modelling of the G2A0203 Line and an estimated Prydz Bay seawater velocity; right column P wave velocities are calculated from AMISOR measured depths combined with seismic arrivals of 390 ms for ice base and 1220 ms for seafloor (approximated from the closest measurement at the south end of G2A0203 Line). (Note: the error on these calculated velocities is ± 19 ms^{-1} for ice and ± 4 ms^{-1} for water; however this leads to an insignificant change in depth error calculated from these values.) Annotations *A to *D: seafloor depths were calculated from the corresponding ice thicknesses, with ice from *A thinnest to *D thickest.

AM03	**G2A0203**						**G2A0506**						**Error (± 2 ms)**	
Depth (m)	South end of line: depth (m)			North end of line: depth (m)			West end of line: depth (m)			Middle to East end of line: depth (m)				
722	Ice base	P velocity ms^{-1}		Ice base	P velocity ms^{-1}		Ice base	P velocity ms^{-1}		Ice base	P velocity ms^{-1}		P velocity ms^{-1}	
	time (ms)	3800	3703	time (ms)	3800	3703	time (ms)	3800	3703	time (ms)	3800	3703	3800	3703
*A	390	741.0	722.1	390	741.0	722.1	385	731.5	712.8	390	741.0	722.1	3.8	3.7
*B	397	754.3	735.0	397	754.3	735.0	405	769.5	749.9	-	-	-	3.8	3.7
*C	411	780.9	761.0	404	767.6	748.0	410	779.0	759.1	410	779.0	759.1	3.8	3.7
*D	413	784.7	764.7	413	784.7	764.7							3.8	3.7
	Pycnocline	1440	1487	Pycnocline	1440	1487	Pycnocline	1440	1487	Pycnocline	1440	1487	1440	1487
*A	580	877.8	863.4	580	877.8	863.4	578	870.5	856.3	578	876.4	861.9	1.4	1.1
*B	580	834.6	814.0	580	834.6	814.0	578	844.8	823.9	578	-	-	1.4	1.1
*C	580	851.4	829.8	580	841.0	819.6	578	852.1	831.0	578	852.6	831.5	1.4	1.1
*D	580	858.0	836.8	580	858.0	836.8							1.4	1.1

The seafloor's arrival time decreases between G2A0506 to G2A0203. The difference in time is 21 ms from the west end of G2A0506 to the south end of G2A0203. This corresponds to a difference in depth of ~15-16 m (using 1440 ms^{-1} and 1487 ms^{-1} for the seismic velocity of water respectively). As shown in Table 4.1, the depth of the seafloor varies by ~+7-8 m from south to north along G2A0203, and +24 m from west to east along G2A0506.

If these are the variations over the 1.25 km between G2A0506 and G2A0203, let us consider the probable variation to AM03. AM03 is located ~500 m west of the southern end of G2A0203 and ~1.6 km downstream from the west end of G2A0506. AMISOR measured the ice shelf base at 722 m below surface, and the seafloor at 1339 m depth. The ice thickness between G2A0506 (west) and G2A0203 (south) generally is the same, or up to 9.5 m thicker, based on seismic arrival times. Since AM03 is located directly downstream of G2A0506 along the ice flowline, it could also be likely that the change in ice thickness is ±9.5 m. However, the seismic data at G2A0203 shows either no change or a maximum -7 ms TWT variation (in the 411 ms reflection) northwards in ice thickness along its 1.09 km length. 7 ms equates to a northward thinning of 13-13.3 m (3800 ms^{-1} and 3703 ms^{-1} respectively). (This is not the first reflection though, and this shall be discussed more later). G2A0506 displays an increase in ice base arrival time of 5 ms from west to east. As calculated earlier, this is a 9.2-9.5 m change in thickness. Across these three ~1 km sections of the AIS, there is an ice thickness variation of ~13 m. With AM03 ~500 m from G2A0203, then it is probable that the ice here would only vary in depth by half that thickness, meaning the 390 ms measured at the south end of G2A0203 should be within ~7.5 m of 722 m, which is ~3.7 m greater than the error in the seismic-derived depths. Hence, it can be valid to use the AMISOR AM03 ice thickness as an equivalent for depth at the southern end of G2A0203, and the derived ice velocities and thicknesses.

4.3.2 Seismic results with CTD data

In terms of water velocities, the AM03 CTD data is the best source of data to calculate a P-wave velocity for the water at this location. Depths were calculated from information given in the CTD data report for the 2005/06 season (Rosenberg, 2006). Figure 4.10

displays the salinity versus depth, and Figure 4.11 displays temperature versus depth; both showing the full dataset and the data for the base of the ice to the base of the CTD cast (at 43 m above the seafloor).

Taking a selection of these data points, densities and P-wave velocities were calculated using the equations outlined in Appendix B. The results are plotted in Figure 4.12 and Figure 4.13. Both show a gradient, increasing with depth. The P-wave velocity increases from 1425-1460 ms^{-1}. The average value for the entire water column is 1452 ms^{-1}. Updating depth calculations with this value gives the results listed in Table 4.3.

4.3.3 Reflection coefficient

Definition: Reflection coefficient

The following seismic terms are relevant to the seismic discussion hereafter; the following section aims to give a brief explanation of the background and physics in how seismic reflections are produced.

According to Snell's Law, in different media with different densities and elastic coefficients, when waves fall upon the surface separating two media, part of the energy is reflected back into the first medium and part is transmitted or refracted into the second medium. Reflections can also occur at boundaries with free surfaces, such as a vacuum or a material of low rigidity (e.g. the atmosphere) (Rawlinson; Udías, 1999).

The **acoustic impedance** (**Z**) of a material is defined as the product of its density (ρ) and acoustic (i.e. seismic) velocity (V):

$$Z = \rho V \qquad \text{(Equation 4.1)}$$

The greater the change in Z between two materials, the greater the percentage of energy that will reflect at an interface or boundary between those two materials.

The fraction of the incident wave that is reflected at normal incidence can be derived when the acoustic impedances of the materials on both sides of a boundary are known.

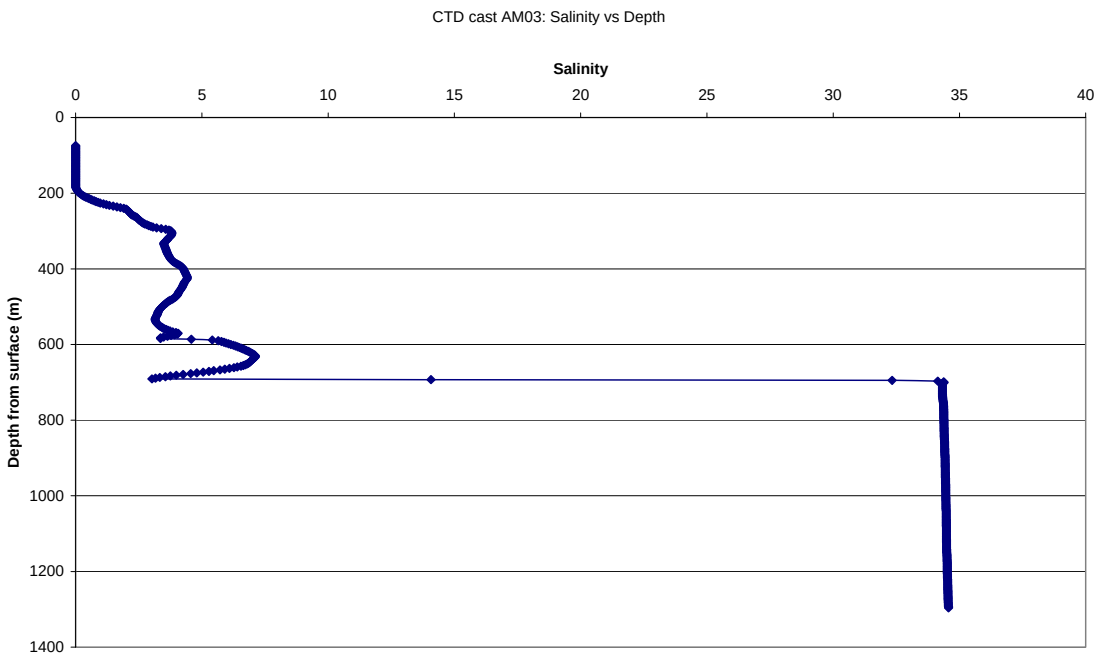

(a)

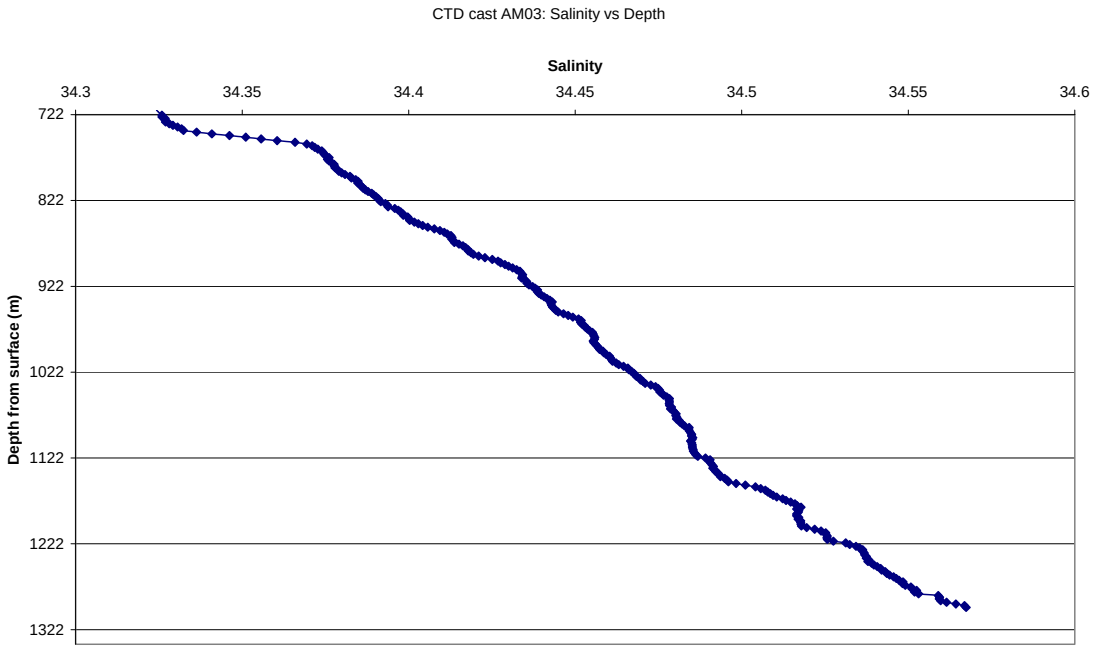

(b)

Figure 4.10 – AM03 CTD Cast 1 12/12/2005: Salinity vs depth below surface. (a) Full cast beginning at 74 m depth in borehole, where water began. (b) Data for the water column from the ice shelf base (722-1339 m depth).

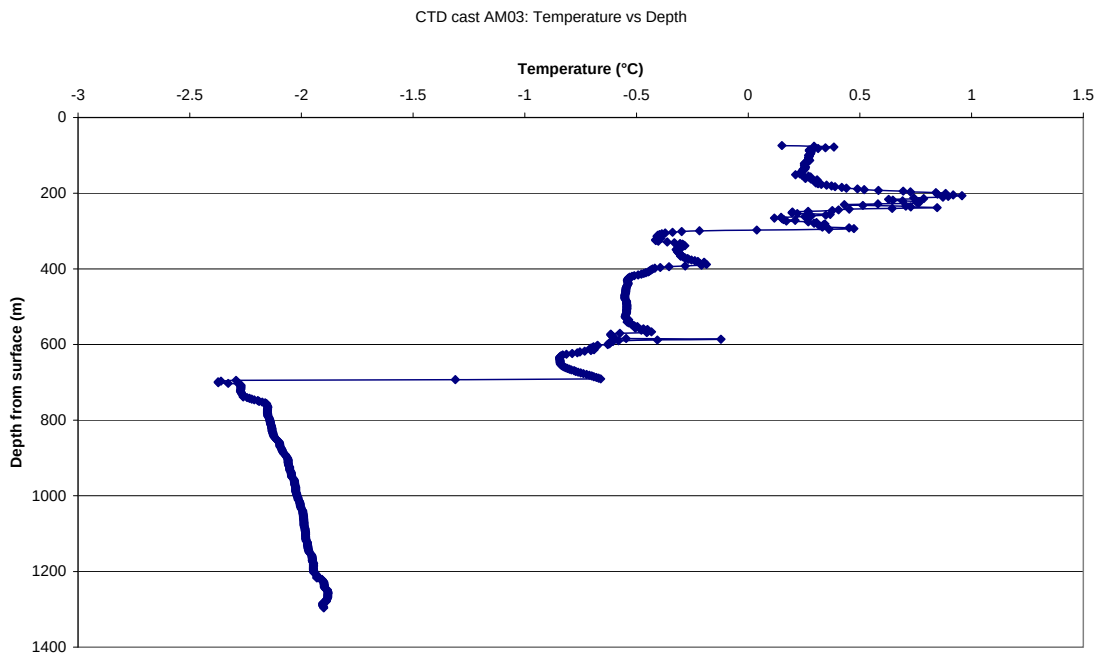

(a)

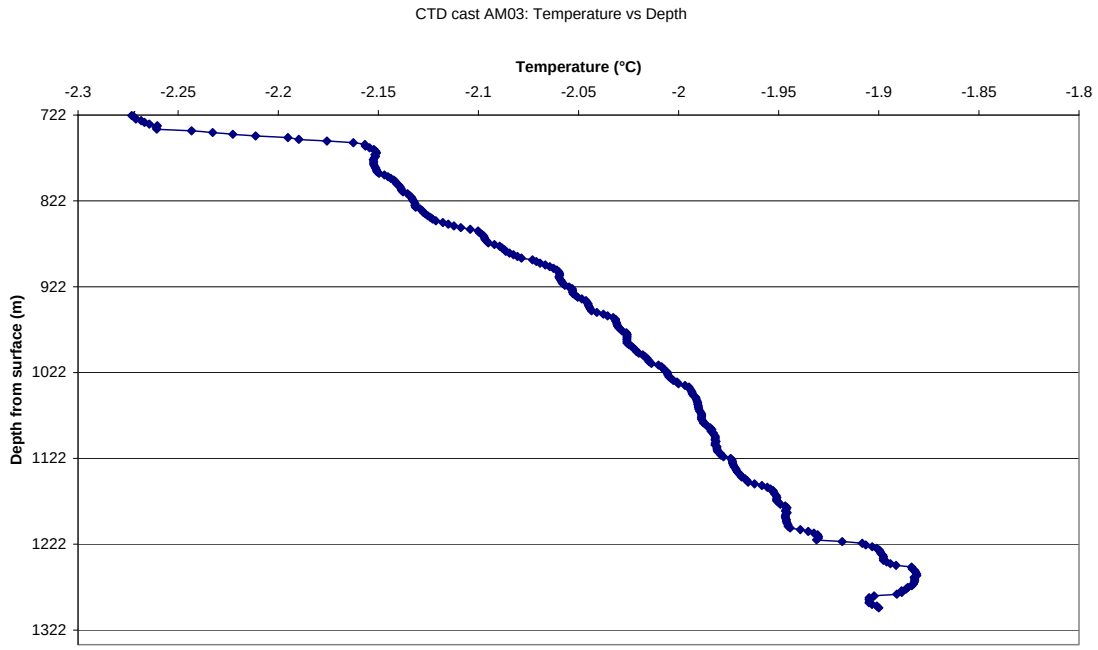

(b)

Figure 4.11 – AM03 CTD Cast 1 12/12/2005: Temperature vs depth below surface. (a) Full cast beginning at 74 m depth in borehole, where water began. (b) Data for the water column from the ice shelf base (722-1339 m depth).

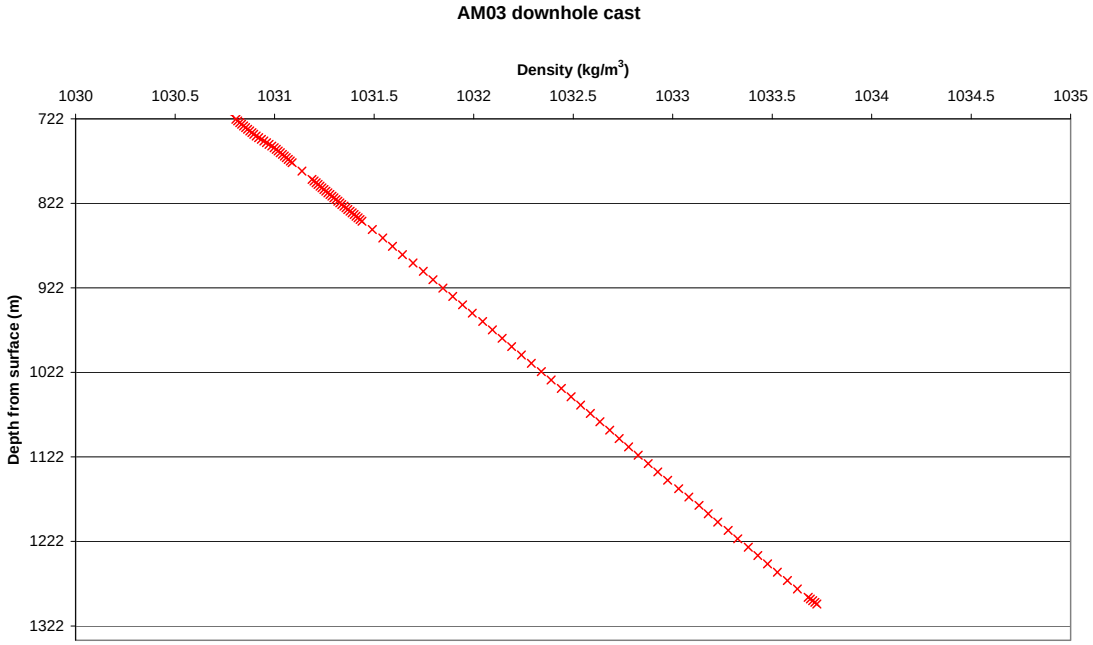

Figure 4.12 – Calculated water densities for the water column at AM03

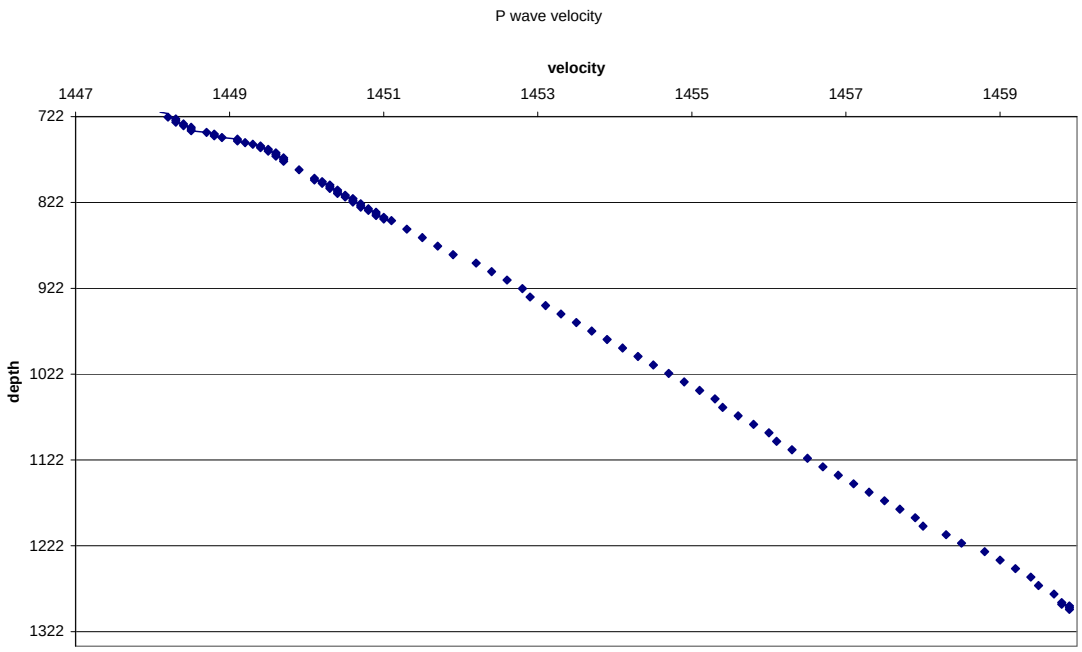

Figure 4.13 – Calculated P-wave velocities for the water column at AM03

Table 4.3 - Table of Ice, Pycnocline & Seafloor Calculated Depths: measured ice depth at AM03, calculated depths for G2A seismic lines using measured reflection times and both measured and calculated P wave velocities (highlighted in grey), with depth errors based on a ± 2 ms error in reflection time. Left column P wave velocities are from refraction modelling of the G2A0203 Line and an estimated Prydz Bay seawater velocity; right column P wave velocities are calculated from AMISOR AM03 CTD data.. (Note: the error on these calculated velocities is ± 19 ms^{-1} for ice and ± 4 ms^{-1} for water; however this leads to an insignificant change in depth error calculated from these values.) Annotations *A to *D: seafloor depths were calculated from the corresponding ice thicknesses, with ice from *A thinnest to *D thickest.

AM03	G2A0203						G2A0506									Depth Error (m) (from ± 2 ms time error)	
Depth (m)	South end of line: depth (m)			North end of line: depth (m)			West end of line: depth (m)			Mid-line: depth (m)			East end of line: depth (m)				
722	Ice base	P velocity ms^{-1}		Ice base	P velocity ms^{-1}		Ice base	P velocity ms^{-1}		Ice base	P velocity ms^{-1}		Ice base	P velocity ms^{-1}		P velocity ms^{-1}	
	time (ms)	3800	3703	time (ms)	3800	3703	time (ms)	3800	3703	time (ms)	3800	3703	time (ms)	3800	3703	3800	3703
*A	390	741.0	722.1	390	741.0	722.1	385	731.5	712.8	390	741.0	722.1	390	741.0	722.1	3.8	3.7
*B	397	754.3	735.0	397	754.3	735.0	405	769.5	749.9	-	-	-	-	-	-	3.8	3.7
*C	411	780.9	761.0	404	767.6	748.0	410	779.0	759.1	410	779.0	759.1	410	779.0	759.1	3.8	3.7
*D	413	784.7	764.7	413	784.7	764.7										3.8	3.7
	Pycnocline	1440	1452	Pycnocline	1440	1452	Pycnocline	1440	1452	Pycnocline	1440	1452	Pycnocline	1440	1452	1440	1452
*A	580	877.8	860.0	580	877.8	860.0	578	870.5	852.9	578	870.5	852.9	578	876.4	858.6	1.4	1.5
*B	580	834.6	813.7	580	834.6	813.7	578	844.8	823.6	578	-	-	578	-	-	1.4	1.5
*C	580	851.4	829.7	580	841.0	819.6	578	852.1	830.8	578	852.1	830.8	578	852.6	831.2	1.4	1.5
*D	580	858.0	836.5	580	858.0	836.5										1.4	1.5
1339	Seafloor	1440	1452	Seafloor	1440	1452	Seafloor	1440	1452	Seafloor	1440	1452	Seafloor	1440	1452	1440	1452
*A	1219	1337.9	1323.9	1209	1330.7	1316.7	1240	1347.1	1333.6	1250	1360.2	1345.4	1265	1371.0	1357.3	1.4	1.4
*B	1219	1304.2	1279.2	1209	1294.6	1269.6	1240	1331.9	1306.6	1250	-	-	1265	-	-	1.4	1.4
*C	1219	1307.8	1277.8	1209	1288.7	1259.0	1240	1338.0	1312.5	1250	1350.3	1324.2	1265	1365.1	1339.4	1.4	1.4
*D	1219	1323.9	1298.2	1209	1314.3	1288.7										1.4	1.4

The equation for the **reflection coefficient** (R), the ratio of reflected and incident amplitudes, is shown in Equation 4.2 - where Z_1 and Z_2 are the acoustic impedances of the upper and lower layers respectively. Conversely, the **transmission coefficient** (T) is an expression of the ratio of transmitted and incident amplitudes, given in Equation 4.3.

$$R = \left(\frac{Z_2 - Z_1}{Z_2 + Z_1} \right) \qquad \text{(Equation 4.2)}$$

$$T = \left(\frac{2Z_1}{Z_2 + Z_1} \right) \qquad \text{(Equation 4.3)}$$

The fraction of **reflection energy** reflected (R^2) and transmitted (T^2) are related by the equation

$$R^2 + T^2 = 1 \qquad \text{(Equation 4.4)}$$

since the amount of reflected energy plus transmitted energy must equal the total amount of incident energy (Mussett & Khan, 2000). Multiplying the reflection energy by 100 yields the amount of energy reflected as a percentage of the original energy.

Calculating these values gives an indication of the expected strength of a reflection based on measured properties. Based upon physical properties of the media, we should be able to ascertain whether or not a reflection should be seen at a certain time in the seismic record. Conversely, the calculations can also explain whether the reflection that is seen was due to properties such as temperature, salinity and density (in this case water density) or if there must be another factor contributing to a reflection as well.

Reflection coefficient of G2A0506 reflections

Looking at the AM03 CTD data in terms of an explanation for the presence of the reflections in the seismic data, in both the salinity and temperature datasets there is a highly significant change in values close to the base of the ice shelf. In the salinity data (Figure 4.10b) this is expressed as an increase in salinity from 34.332 to 34.371 over depths 740-756 m (16 m). The temperature data (Figure 4.11b) shows an increase in

temperature from -2.2607°C to -2.1565°C over depths 739-758 m (19 m). This corresponds to the change in density over this depth range that leads to the change in P wave velocity from 1448.5 to 1449.4 ms^{-1}.

To check these physical property changes against seismic reflections, reflection coefficients (R) were calculated from density and P wave velocity, shown in Figure 4.13. Due to the size of the dataset, only two sections of data were calculated using every data point, otherwise every 5th was used. Figure 4.14 shows the trends for R values calculated between adjacent data points (~2 m spacing) (RC1) and between every 5th data point (~10 m spacing) (RC2). Both trends show a significant increase in the reflection coefficient between 728 m and 758 m depth. The RC5 trend also shows a smaller increase, but still significant, at 882, 1199 and 1218 m.

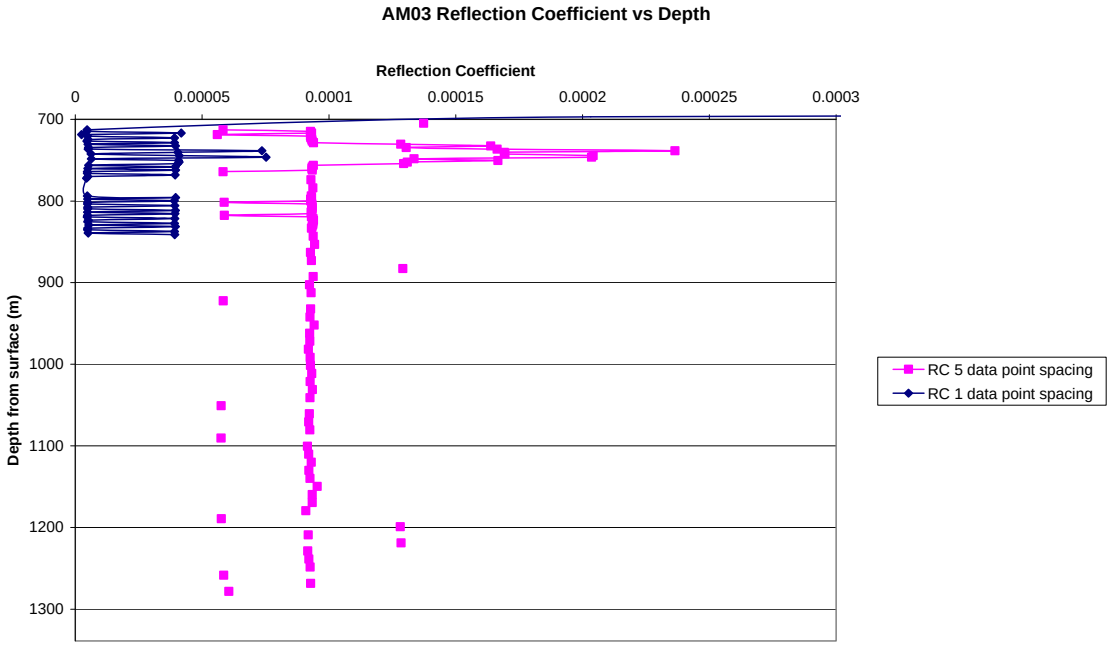

Figure 4.14 – AM03 Reflection coefficient versus depth below surface (m)

From the RC 5 base value of 9.2×10^{-5}, the maximum reflection coefficient occurs at 738 m depth, with a value of 2.3×10^{-4} – a ratio of ~1:2.8. This depth of 738 m corresponds well with the 735 m calculated for the 397 ms reflection in the G2A0203 data. The RC1 trend shows a much sharper change in R at 738 and 746 m, with an R

ratio of 1:14 and 1:11. This corresponds to the 397 ms and the 404 ms (748 m) reflection of G2A0203, and explains why they are stronger reflectors in the seismic data than 397 and 413 ms. The R ratios for 882, 1199 and 1218 m are 1:1.4, 1:2.2 and 1:1.4 respectively. The 882 m R increase could correspond to the 580 ms (860 m) reflection. The difference in depth could be partly explained by the difference in location, with AM03 being closer to a major flow unit boundary in the AIS where circulation may change, but the difference in depth is mostly due to the spacing of calculations. R values calculated between each data point would narrow down the depth; with RC5, the results do not show whether the change occurred in the previous four data points, so the error would be -8 m.

The R increases at 1199 m and 1218 m are interesting. Looking at the G2A0203 seismic profile (Figure 4.2) there appears to be no reflections at these times. The only change in the seismic data here is a decrease in amplitude (without a reflection) from ~1100 ms to the seafloor reflection. The same characteristic is displayed in the G2A0506 seismic profile. It may be that a more significant R ratio was required to produce a reflection.

4.3.4 Basal accumulation and melt rate

Looking at the basal accumulation rates given in Figure 4.15, the G2A area displays a melting rate of -1.2 to -2 m/yr (G2A is located near the boundary between these two zones in Figure 4.6). The surface ice velocity at G2A was calculated to be ~370 ma^{-1}, which equates to a “surface travel time” difference of ~4 yrs between G2A0506 and AM03. This gives a thickness of ice change of -4.8 to -8 m from G2A0506 to AM03. Since, however, there is not such a change between G2A0506 and G2A0203, it is unlikely this rate of melt is appropriate for this particular area of the AIS, or on this small a scale.

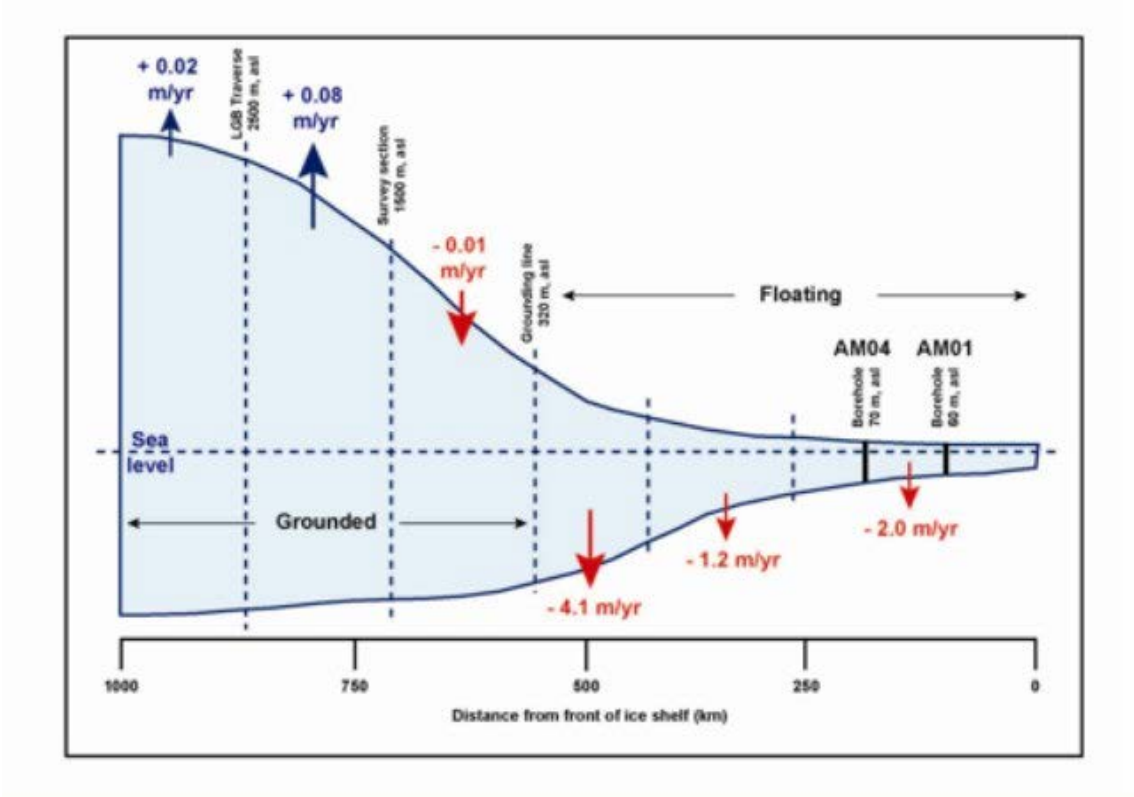

Figure 4.15 – Schematic diagram showing rates of accumulation and melt along and under the AIS from south to north (Unacknowledged, 2008).

4.4 Conclusions

G2A seismic reflection data displays three major primary reflections: the base of the AIS, a pycnocline in the upper water column, and the seafloor with sediments. The base of the ice shows four reflections in the G2A0203 profile, and 2-3 reflections in the G2A0506 profile. These reflections can be correlated to significant increases in the reflection coefficient, R, around these depths at AM03. The trend of R shows increases at 738 and 746 m, which correspond best to the 397 ms and 404 ms reflection depths measured at G2A (735 m and 748 m respectively). These R increases are definitely below the base of the ice shelf, within the upper water column, since the base of the ice was measured at 722 m by AMISOR and video was taken down the borehole which confirmed this (pers. Comm, M. Craven, 2006). The base of the ice shelf therefore relates to the upper reflection at 390 ms (385-390 at G2A0506; 712-722 m depth),

which is less strong than the 397 and 404-411 ms reflection. The question is what is then causing these strong reflections just below the ice shelf?

The answer would appear to simply be the water properties themselves due to the dynamics of the ice shelf. The base of the ice shelf is an area of water freshening as sea water mixes with basal melt, and also cooling as the ice cools the underlying layer of water. This changes to a more saline and warmer body of water between the depths ~738-758 m (as shown by the temperature and salinity data from AM03 CTD cast). These depths correspond to the 397 ms and 404-410/411 ms reflections respectively. The presence of the fourth reflection at 413 ms in G2A0203 data may be another distinct change in water properties that was present in 2002/03 but was not present in 2005/06 when the AM03 CTD cast and G2A0506 seismic data were collected. So these reflections are all real, and are due to the physical water properties. The possibility exists that a sub-ice shelf layer of frazil ice may form the first cool fresh layer under the ice shelf. This may be seasonal, and affected by the water circulation. AMISOR noted seeing frazil ice beneath the AIS in the video footage from the 2005/06 boreholes (pers. Comm, M. Craven, 2006; pers. Comm, D. Rasch, 2006).

What the AMISOR video also proved was that there was no marine ice present at AM03 in 2005/06, and hence there was unlikely to have been any in 2002/03; casting doubt upon the theory of a marine ice layer put forward by McMahon (2003) and McMahon & Lackie (2006). The AMISOR drill and CTD data have instead presented an alternative theory of a cool fresh layer of melt water at the base of the ice shelf, with a sharp enough gradient in physical properties to produce more than one strong reflection. It has shown that the base of the ice is to be measured to the upper weaker reflection, and that the second and third stronger reflections are intra-water column layers. One/some of these layers may also coincide with the presence of frazil ice within the water column.

Since the base of the ice can be identified as the 385-390 ms reflection, the calculated ice P wave velocity of 3700 ms^{-1} is valid within the scope of the seismic results and errors and the water P wave velocity can be calculated to 1452 ms^{-1} using the CTD data, the depth to the pycnocline (from surface) becomes 860 m at G2A0203 and 853-859 m at G2A0506 (west-east). This is a depth below the ice shelf base of 138 m at G2A0203 and 137-140 m at G2A0506, which are consistent. The R increase here was measured at

882 m depth, yet this could be due to a thickening of this fresh cool water body at AM03, while 8 m thickening could be due to the coarseness of the R calculations at this depth.

The seafloor then sits at a depth of 1324-1317 m at G2A0203 (south-north) and 1334-1357 m at G2A0506 (west–east), corresponding to a total water column thickness of 602 m and 621-635 m, respectively. This reveals that bathymetry increases going north, and increases to the west, although bathymetry must decrease marginally further NW from there to reach 1339 m depth at AM03. The variance in the seafloor depths while the depth to the pycnocline is almost equal reveals and supports the conclusion that the interaction of the ice shelf and the water column is what is controlling this layered water feature, rather than any seafloor-controlled circulation.

While an ice thickness increase of 9.5 m from west-G2A0506 to G2A0203 does not align with the average melt rate of -1.2 to -2 m/yr in this area, it may be due to a natural variation in ice base topography due to a variation in original ice thickness or non-uniform basal melt rather than due to a 2.8 m/yr accumulation of ice between G2A0506 and G2A0203.

The seismic results do not indicate that there is an above average or abnormally high degree of melt between the upstream younger ice of G2A0506 and the downstream older ice of G2A0203. The seismic results indicate a stable ice thickness in this area of ~712-722 m, and a stable fresh cool body of water underneath the base of the ice shelf in the summer months, between 137-140 m in thickness.